DEPARTMENT OF PHYSICS
UNIVERSITY OF JYVÄSKYLÄ
RESEARCH REPORT No. 2/2007

PHONONIC TRANSPORT IN DIELECTRIC MEMBRANES

BY
THOMAS KÜHN

Academic Dissertation
for the Degree of
Doctor of Philosophy

To be presented, by the permission of the
Faculty of Mathematics and Natural Sciences
of the University of Jyväskylä,
for public examination in Auditorium KEM-1 of the
University of Jyväskylä on April 13, 2007
at 12 o'clock noon

Jyväskylä, Finland
April 2007

ISBN 978-951-39-3181-0

URN:ISBN:978-951-39-3181-0

Preface

This work has been carried out at the Department of Physics and Nanoscience Center of the University of Jyväskylä during the years 2002-2007.

I want to thank my supervisor Professor Matti Manninen for the excellent and motivating guidance throughout the work. He has good advice for any kind of problem and like nobody else he is able to find something positive in the most irritating situations.

I also want to thank Doctor Dragoş-Victor Anghel for a good and fruitful co-operation and for the interesting research topics he came up with. It was a lot of fun to work with him and I certainly learned much. Further I want to thank Dragoş and Doctor Michael Walter for correcting my thesis.

Many thanks go to Doctor Ilari Maasilta and his group for many inspiring discussions and the whole Physics Department and Nanoscience staff for the pleasant working atmosphere.

Financial support from the NordForsk foundation for my trips to Oslo is also gratefully acknowledged.

Warm thanks go out to my parents, who always patiently listen, motivate and cheer me up. Thanks to my parents-in-law for helping out with everything, most of all taking care of the children in the long evenings and weekends that I was missing at home.

Most of all I want to thank my beloved wife Minna for all the support, understanding and patience (I know it hasn't always been easy) and my sons Oliver and Anton for all the joy and happiness they give me every moment I am able to be with them. Nothing cheers me up more than a happy voice calling "iiisiiii" and the sound of small feet running to greet me after a long working day.

Jyväskylä, April 2007

Thomas Kühn

Abstract

This thesis is a review of six publications in which we studied the thermal properties of thin amorphous dielectric membranes. For this we study the phonon modes of these membranes. In elasticity theory, these modes are divided into three groups, which we call the horizontal shear modes and the symmetric and antisymmetric Lamb modes. The Lamb waves have very complicated displacement fields and non-linear dispersion relations, which produce interesting low temperature effects.

Due to the finite thickness of the membrane, we observe a cross-over of the phonon gas from a three dimensional distribution at higher temperatures to a two dimensional distribution at lower temperatures. We study how this cross-over affects the thermal properties of the membrane. A big emphasis lies on the heat conduction in the membrane, which we study in the ballistic and the diffusive limits. For the diffusive case, we consider two different scattering mechanisms. First we treat the case where the membrane is cut into more sophisticated structures and the phonons scatter at the edges of these structures. Then we take the amorphous nature of the membranes into account, which is modeled by a distribution of two-level systems. These two-level systems are sensitive to vibrations in the membrane and thus provide a scattering mechanism for phonons.

Last we numerically calculate the operating parameters of a membrane-mounted superconducting transition-edge sensor in a temperature range that spans the whole 2D to 3D transition of the membrane phonon gas.

List of Publications

I Heat transport in ultra-thin dielectric membranes and bridges
T. Kühn, D. V. Anghel, J. P. Pekola, M. Manninen and Y. M. Galperin
Phys. Rev. B **70**, 125425 (2004)

II Ballistic phonon transport in dielectric membranes
T. Kühn and I. J. Maasilta
Nucl. Instr. and Meth. A **559**, 724 (2006)

III Interaction of two-level systems in amorphous materials with arbitrary phonon fields
D. V. Anghel, T. Kühn, Y. M Galperin, and M. Manninen
Phys. Rev. B **75**, 064202 (2007)

IV Quantization of the elastic modes in an isotropic plate
D. V. Anghel and T. Kühn
(submitted) cond-mat/0611528

V Interaction of two-level systems with phonons in amorphous nanoscopic membranes T. Kühn, D. V. Anghel, Y. M. Galperin and M. Manninen
to be submitted

VI Optimal operation of transition-edge sensors on ballistic membranes
T. Kühn and I. J. Maasilta
(submitted) cond-mat/0702542

The author has written the drafts of papers **I**, **II**, **III**, **V** and **VI**, and participated in writing **IV**. He has written all computer code needed for the numerical computations, done most of the analytical calculations and participated in the derivation of the model in paper **III**.

Contents

Chapter 1

Introduction

Science has an everlasting need for more precision in its measurements, but the higher the attempted precision of the measurement is, the more sensitive the used detectors have to be. This entails many technical complications, and their solutions occupy a great part of today's scientists. However, even if all technical difficulties were overcome and we would be able to build a "perfect" detector, the precision of our measurements would still be limited by fundamental physics. In such ultra-sensitive detectors, thermal fluctuations and the discreteness of particle and energy fluxes are seen as noise, which limits the bandwidth and energy resolution of the detector. To sufficiently reduce the thermal noise, the detectors usually are operated at sub-Kelvin temperatures. To ensure the sensitivity required for the experiments, but also for good spatial and temporal resolutions, the detectors have to be in general very small, with dimensions in the micrometer range or below.

In such ranges of size and temperature, we can no longer describe the detector as an ensemble of bulk elements, so when we calculate its physical properties and response parameters, we have to take its finite size and all the boundary effects carefully into account. The research on finite size effects in electron systems has been going on for many decades and their properties are quite well understood. On the other hand, the detailed properties of the phonon gas in mesoscopic systems have not been studied so extensively, mainly because the devices did not depend so crucially on them until the development of the ultra-sensitive detectors.

A typical ultra-sensitive detector, for example a microcalorimeter or microbolometer, consists of a thermal sensing element, which is mounted on a thin dielectric membrane. The role of the membrane is to support the only a few tens of nanometers thick thermal sensing element and to ensure a good thermal insulation, which is necessary to reach sub-Kelvin temperatures. To further increase the thermal insulation, the membrane may be cut into a self-supporting structure that consists of a wider central part holding the thermal sensing element, and narrow bridges which connect the central

part to the bulk. Usually the used membranes are made of low-stress silicon nitride (SiN_x) and can be as thin as 30 nm. At the mentioned operating temperatures typical phonon wavelengths can very well be greater than the thickness of the membrane. For example at 100 mK the dominant thermal phonon wavelength in SiN_x is about 250 µm. The phonon gas of any system with dimensions smaller than the typical phonon wavelength is not well described by simple three dimensional (3D) plane waves. Instead we have to take the geometry of the system into account when calculating its phonon modes.

The phonon modes of thin membranes (in elasticity theory they are also called plates) are superpositions of transversal and longitudinal plane waves. They are called horizontal shear and Lamb waves. The Lamb waves have very complicated displacement fields and non-linear dispersion relations. Especially the low frequency antisymmetric Lamb waves have a quadratic dispersion relation, like a massive particle. This has interesting consequences in the low temperature limit, when the phonon gas in the membrane becomes quasi-2D. One of these consequences is that the heat capacity of the membrane becomes linear in temperature [I], while a linear dispersion relation would yield a T^2 dependence. Another interesting effect is that many thermal properties of the membrane, like for instance the heat conductivity, are predicted to have a global minimum as function of the membrane thickness for a fixed temperature [II]. This behaviour can be used to optimize many device setups [VI].

In this thesis we report calculations of thermal properties of thin amorphous dielectric membranes. For this we study the phonon modes in the membranes, using elasticity theory. To fix the notations and to introduce the basic concepts, we give a brief introduction in elasticity theory in Chapter 2.

The membrane phonon modes are introduced in Chapter 3, where we also present the formal quantization of the elastic field in this geometry.

At high enough temperatures, the thermal properties of the membrane resemble the thermal properties of 3D bulk systems. As we decrease the temperature, we gradually reach a phase in which the membrane properties are qualitatively different from 3D bulk systems and correspond to a quasi-2D phonon gas distribution [1, 2, I]. We present this dimensionality cross-over in Chapter 4 and show its effects on the heat conduction in the ballistic and diffusive limits.

In order to calculate the heat conductivity in the diffusive limit, we have to include scattering mechanisms for phonons. The phonons may scatter on the disorder or impurities in the membrane and on the membrane surfaces or edges. Since the surfaces are typically smooth, the scattering on the disorder and on the edges dominate [I].

The dimensionality cross-over and some of the low temperature properties of the membranes could be obtained by considering only the scattering

of phonons on the membrane or bridge edges [I]. Nevertheless, to obtain a better qualitative agreement with experiments [3, 4, 5, 6, 7, 8] we also have to include the scattering on disorder.

The disorder in an amorphous medium is modeled by an ensemble of two-level systems [9, 10, III, V]. The scattering of phonons on two-level systems have been studied before, but only in the context of 3D bulk materials, where the phonon modes are the simple transversal and longitudinal plane waves [9]. To apply the formalism to the membrane phonons [V], we first had to generalize the model to be able to describe the interaction of two-level systems with arbitrary displacement fields [III]. The results are presented in Section 4.4.

In Chapter 5 we use the accumulated knowledge to numerically calculate the operating parameters of a membrane mounted superconducting transition-edge sensor (TES) as function of the membrane thickness and operating temperatures. These results can be used to optimize the functionality of these devices by carefully tuning the detector and substrate temperatures and the membrane thickness.

1.1 Conventions

Although the notations and conventions are described at their first use, we explain here for the reader's convenience what we consider to be the most important of them.

In our calculation we use both vector and subscript notations. Vectors are always denoted in boldface, matrices by square brackets $[\cdot]$ and fourth rank tensors by double square brackets $[[\cdot]]$. For example the phonon displacement field will be denoted by $\mathbf{u}$, the strain tensor by $[S]$ and the tensor of elastic stiffness constants by $[[c]]$. By the superscript T (i.e. $[M]^T$) we denote the transpose of a matrix or a vector, whereas unit vectors are written with a hat, for example $\hat{\mathbf{k}}$. Furthermore we have two different subscript notations. One is the usual cartesian real space notation, the other is the so called abbreviated subscript notation, which we introduce in Section 2.2 [11]. To distinguish between the two, we use lower case letters in real space notation (for example S_{ij}) and capital letters in abbreviated subscript notation (for example S_I). In calculations with subscript notation, we always sum over repeated subscripts. Furthermore we make extensive use of the dyadic product, which is in vector notation usually denoted by a colon, for example $[T] : [S]$, which in subscript notation becomes $T_{ij}S_{ij}$.

Chapter 2

Theory of elasticity and acoustics

2.1 Introduction

The theory of elasticity describes the response of solids to elastic deformation. From it evolves the field of acoustics in solids, which deals with time-varying deformations. In elasticity theory, matter is treated as if it were continuous, i.e. we deal with length scales that are much bigger than any inter-atomic distances in the material. To describe the motion within the solid, we divide it into small volume elements $\delta V = \delta x \delta y \delta z$, each containing many atoms. Within one volume element, the atoms move in unison. The vibrational motion of single atoms is not of interest. To each volume element we can assign an equilibrium position $\mathbf{r}_n$. Its motion about this equilibrium position is called the displacement $\mathbf{u}_n(t)$. If we let δV go to zero, $\mathbf{u}_n(t)$ becomes the continuous displacement field $\mathbf{u}(\mathbf{r}, t)$.

The displacement field describes all forms of motion of the material, also rigid motions, like translations or rotations of the whole medium. Material deformation is only caused by displacement of volume elements relative to each other. Hence rigid motion does not cause material deformation and because $\mathbf{u}$ is non-zero also for rigid motion, it is not a good measure for the deformation of a medium. Instead, material deformations are quantitatively described by the 3×3 component strain tensor $[S]$, which is defined as the symmetric gradient of the displacement field,

$$S_{ij} \;=\; \frac{1}{2}(\partial_i u_j + \partial_j u_i)\,. \tag{2.1}$$

The strain tensor is by definition a symmetric tensor ($S_{ij} = S_{ji}$). Anti-symmetric deformations describe rotations, which do not enter the elastic equations [11].

The response of a material to elastic deformation is called stress. The 3×3 stress tensor is usually denoted by $[T]$, but because we use that notation

for another quantity later in the thesis, we use Ezawa's notation for the stress tensor, $[T] = \rho[p]$ [12], where ρ is the mass density of the material. From the stress we can calculate the forces caused by material deformation within the medium. These forces are called traction forces, and have units of force per unit area. The traction force that acts on a surface is then given by $\rho p_{ij}\hat{n}_j$, where $\hat{\mathbf{n}}$ is the surface normal.

According to Hooke's Law, the stress is linearly proportional to the strain, which mathematically is expressed as

$$\rho p_{ij} \quad = \quad c_{ijkl} S_{kl} \,. \tag{2.2}$$

Here and everywhere else in this thesis we implicitly sum over repeated indices. In Eq. (2.2), we defined the fourth rank tensor of elastic stiffness constants $[[c]]$. In the absence of body torques, which holds for most media and which we assume throughout this thesis, the stress tensor is, like the strain tensor, symmetric. The symmetry of the stress tensor directly leads to the equality $c_{ijkl} = c_{jikl}$ and because of Eq. (2.2) and the symmetry of $[S]$, we can choose $[[c]]$ such that $c_{ijkl} = c_{ijlk}$. Furthermore it can be shown that also $c_{ijkl} = c_{klij}$ [11]. In summary, the symmetry properties of $[[c]]$ are

$$c_{ijkl} = c_{jikl} = c_{ijlk} = c_{klij} \,. \tag{2.3}$$

This means that $[[c]]$ has maximum 21 independent components in any kind of medium. For the special case of isotropic media, the number of independent parameters is only two.

2.2 Abbreviated subscripts

The symmetry of $[S]$, $[p]$ and $[[c]]$ allows us to simplify calculations by introducing the abbreviated subscript notation. A 3×3 symmetric tensor has six independent components, so the symmetric matrices $[S]$ and $[p]$ are in abbreviated subscripts written as the six component vectors

$$\mathbf{p} \quad = \quad \begin{pmatrix} p_{xx} & p_{yy} & p_{zz} & p_{yz} & p_{xz} & p_{xy} \end{pmatrix}^T \tag{2.4}$$

$$\mathbf{S} \quad = \quad \begin{pmatrix} S_{xx} & S_{yy} & S_{zz} & 2S_{yz} & 2S_{xz} & 2S_{xy} \end{pmatrix}^T \,. \tag{2.5}$$

The extra factor 2 in Eq. (2.5) ensures that we can write the dyadic product between $[p]$ and $[S]$ directly as a vector dot product, $p_{ij}S_{ij} = \mathbf{p}^T \cdot \mathbf{S} \equiv p_I S_J$. As indicated in Section 1.1, to distinguish between full and abbreviated subscript notations, we use lower case characters (for instance p_{ij}) for full subscripts and capital letters (i.e. p_I) for abbreviated subscripts.

Since the fourth rank tensor $[[c]]$ shares the same symmetries as the strain and the stress tensors, it can be written in abbreviated subscripts as well. In this notation, it becomes the 6×6 component matrix $[c]$ or c_{IJ}, where

we group the first two full subscripts into one abbreviated subscript and the last two full subscripts into another abbreviated subscript (for example c_{xxyz} becomes c_{14}). Then we can write Eq. (2.2) as $\rho p_I = c_{IJ} S_J$. For isotropic media, $[c]$ reads

$$[c] = \begin{pmatrix} c_{11} & c_{12} & c_{12} & 0 & 0 & 0 \\ c_{12} & c_{11} & c_{12} & 0 & 0 & 0 \\ c_{12} & c_{12} & c_{11} & 0 & 0 & 0 \\ 0 & 0 & 0 & c_{44} & 0 & 0 \\ 0 & 0 & 0 & 0 & c_{44} & 0 \\ 0 & 0 & 0 & 0 & 0 & c_{44} \end{pmatrix}, \tag{2.6}$$

where $c_{12} = c_{11} - 2c_{44}$, so as we stated in Section 2.1, the tensor $[c]$ in this case is composed of only two independent parameters, c_{11} and c_{44}.

As discussed in Ref. [15], the elastic stiffness constants c_{11} and c_{44} can also be expressed by Young's modulus E and Poisson's ratio σ. The relation between the constants is

$$c_{11} = \frac{(1-\sigma)E}{(1+\sigma)(1-2\sigma)} \tag{2.7}$$

$$c_{44} = \frac{E}{2(1+\sigma)}\,. \tag{2.8}$$

The parameter E is a measure of how much straining the material increases the stress, while σ describes how much a body expands (or shrinks) in the lateral directions upon compression. For normal materials, i.e. materials that expand in the lateral directions upon compression, σ takes values between 0 and 0.5.

2.3 Equation of motion and 3D plane waves

The forces that act on a volume element δV are the sum of all external forces plus the traction forces that the neighbouring volume elements apply to its surface. If there are no external forces present, the total force is given by the integrated surface force alone,

$$\rho \oint_{\partial(\delta V)} d^2\mathbf{r}\, p_{ij}\hat{n}_j = \rho \int_{\delta V} d^3\mathbf{r}\, \partial_j p_{ij}\,, \tag{2.9}$$

where we used Gauß' theorem for the integral transformation. According to Newton's law, we then have

$$\rho \int_{\delta V} d^3\mathbf{r}\, \partial_j p_{ij} = \rho \int_{\delta V} d^3\mathbf{r}\, \partial_t^2 u_i \tag{2.10}$$

Taking $\delta V \to 0$, we arrive at the translational equation of motion for elastic media,

$$\begin{aligned} \partial_t^2 u_i &= \partial_j p_{ji} \\ &= \rho^{-1} \partial_j c_{jikl} \frac{1}{2} (\partial_k u_l + \partial_l u_k) \\ &= \rho^{-1} c_{ijkl} \partial_j \partial_k u_l \\ &\equiv \tilde{L}_{il} u_l \,. \end{aligned} \tag{2.11}$$

Here we defined the operator $\tilde{L}_{il} \equiv \rho^{-1} c_{ijkl} \partial_j \partial_k$ and used the symmetry of c_{ijkl} (2.3) in the second step of the calculation. In the case of isotropic media, $\tilde{L}$ can be written in the more intuitive form

$$\tilde{L}\mathbf{u} = c_l^2 \nabla(\nabla \cdot \mathbf{u}) + c_t^2 \nabla \times \nabla \times \mathbf{u} \,. \tag{2.12}$$

If no boundaries are present (i.e. the system is infinite in size), Eq. (2.12) gives rise to three independent plane wave solutions, one longitudinally polarized wave with the sound velocity $c_l \equiv \sqrt{c_{11}/\rho}$ and two transversally polarized waves with the sound velocity $c_t \equiv \sqrt{c_{44}/\rho}$. All three solutions have linear dispersion relations,

$$\omega_{l,t} = c_{l,t} k \,, \tag{2.13}$$

where k is the absolute value of the wave vector $\mathbf{k}$.

As a consequence of Eqs. (2.7) and (2.8) and the range of values that Poisson's ratio can take ($0 \leq \sigma \leq 0.5$), the longitudinal sound velocity is always bigger than the transversal one and in particular we have

$$c_l^2 \geq 2 c_t^2 \,. \tag{2.14}$$

2.4 Free boundaries

Until now we have treated matter as if it was infinite. As long as the system we describe is very big, this is usually a good approximation. As a measure of what is "big" and what is "small", we usually compare the dimensions of the system to the wavelength of the vibrations we want to describe. If this characteristic wavelength is much smaller than all system dimensions, our system is big and we can treat it as if it was infinite. We then talk about three-dimensional (3D) bulk systems. In the opposite limit however, where the characteristic wavelength is much bigger than the system dimensions, we have to take the boundaries into account. This leads to the coupling of the 3D bulk waves into new, more complicated waves. To motivate this, we will study the reflection of a 3D plane wave at a system surface, which we also call a free boundary.

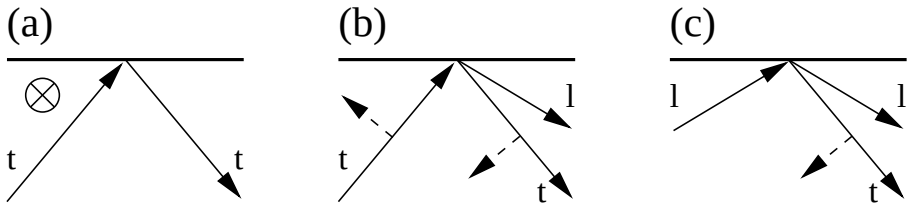

Figure 2.1: Reflection of a plane wave incident on a free surface. The horizontal shear wave (a), which is polarized perpendicular to the plane of incidence (indicated by the $\otimes$), is reflected into a pure horizontal shear wave. The vertical shear (b) and the longitudinal (c) waves are reflected into a superposition of vertical shear and longitudinal waves. Wave vectors are indicated by solid lines and the polarization vectors of the horizontal shear waves are indicated by the dashed lines. The polarization vectors of the longitudinal waves are parallel to the wave vectors.

The traction forces that act on free boundaries are zero. If we denote the surface of a solid of volume V by ∂V and its normal by $\hat{\mathbf{n}}$, we can write the boundary condition as

$$(\hat{n}_i p_{ij})(\mathbf{r} \in \partial V) \quad = \quad 0\,. \tag{2.15}$$

In general, a plane wave incident on a free boundary will be reflected into a superposition of longitudinal and transversal plane waves. To show this, we study the interaction of a plane wave,

$$\hat{\mathbf{u}} e^{i(\mathbf{k}\cdot\mathbf{r}-\omega t)} \quad = \quad \hat{\mathbf{u}} e^{i((\mathbf{k}_\parallel+\mathbf{k}_\sigma)\cdot\mathbf{r}-\omega t)}\,, \tag{2.16}$$

with a free, plane surface. In Eq. (2.16) we decomposed the wave vector $\mathbf{k}$ into the component $\mathbf{k}_\parallel$ pointing along the surface and the perpendicular component $\mathbf{k}_\sigma$, where $\sigma = t$ for transversal waves and l for longitudinal waves. By $\hat{\mathbf{u}}$ we denote the polarization of the wave. It is parallel to the wave vector for longitudinal waves, or perpendicular to it for transversal waves. As the boundary condition (2.15) has to be fulfilled at every point on the boundary and at every instant in time, the incident and reflected waves have to have the same $\mathbf{k}_\parallel$ and ω, while the perpendicular parts of the wave vector are different for different polarizations. This leads to Snell's law of acoustics

$$c_t^2(k_t^2 + k_\parallel^2) \quad = \quad c_l^2(k_l^2 + k_\parallel^2)\,. \tag{2.17}$$

A transversal wave can in general be polarized into any direction within the plane that is perpendicular to the wave vector. We can describe this

general transversal polarization as a superposition of two polarization vectors which are perpendicular to each other and each perpendicular to the wave vector. For the problem at hand it will prove useful to choose these two polarizations such that one of the waves will be polarized parallel to the surface and perpendicular to the plane of incidence, while the second wave will be polarized within the plane of incidence. We call the former wave horizontal shear and the latter vertical shear. This way of choosing the polarizations has the advantage that the horizontal shear mode can be treated separately in the reflection problem. The other two modes (i.e. the vertical shear and the longitudinal mode) will always couple to each other when being reflected at a surface (See Fig. 2.1).

For simplicity, we place the surface parallel to the xy plane, cutting the z axis at z_0, where the medium fills all the space below the surface (i.e. $z < z_0$), and choose the xz plane to be the plane of incidence. This means that the horizontal shear mode is polarized in the y direction and its displacement vector has only one component, u_y. To avoid ambiguity, we denote the perpendicular part of the wave vector for the horizontal shear mode by k_h rather than k_t. Then the displacement field of a horizontal shear wave incident on the surface is

$$u_y^i = e^{i(k_\parallel x + k_h z - \omega t)}, \tag{2.18}$$

while the reflected wave is described by

$$u_y^r = r_h e^{i(k_\parallel x - k_h z - \omega t)}. \tag{2.19}$$

Calculating the stress that is caused by the wave, we use the boundary condition (2.15) (the traction forces are zero on the surface) to determine the reflection coefficient r_h to be $r_h = \exp(2ik_h z_0)$ and the horizontal shear eigenmode of an infinite half-space becomes

$$u_y = \cos(k_h(z - z_0))e^{i(k_\parallel x - \omega t)}. \tag{2.20}$$

A vertical shear wave incident on the surface will, except for two special cases, always be reflected into a superposition of a vertical shear wave and a longitudinal wave. Similarly, a longitudinal wave incident on the surface will always be reflected into a superposition of a longitudinal and a vertical shear wave. Using a superposition of a vertical shear wave and a longitudinal wave as incident wave on the surface at $z = z_0$, we can write the incident (i) and reflected (r) waves as

$$\begin{aligned}
u_x^i &= I_l k_\parallel e^{i(k_\parallel x + k_l z - \omega t)} - I_t k_t e^{i(k_\parallel x + k_t z - \omega t)} \\
u_z^i &= I_l k_l e^{i(k_\parallel x + k_l z - \omega t)} + I_t k_\parallel e^{i(k_\parallel x + k_t z - \omega t)} \\
u_x^r &= R_l k_\parallel e^{i(k_\parallel x - k_l z - \omega t)} - R_t k_t e^{i(k_\parallel x - k_t z - \omega t)} \\
u_z^i &= -R_l k_l e^{i(k_\parallel x - k_l z - \omega t)} - R_t k_\parallel e^{i(k_\parallel x - k_t z - \omega t)}.
\end{aligned}$$

Here k_t and k_l are chosen such that they comply to Snell's law (2.17). Applying the boundary condition (2.15) we get a matrix equation connecting the coefficients I_l, I_t, R_l and R_t,

$$\mathbf{r} \;=\; [M](z_0)\cdot\mathbf{i}\,, \tag{2.21}$$

where $\mathbf{r}\equiv(R_t,R_l)^T$, $\mathbf{i}\equiv(I_t,I_l)^T$ and

$$[M](z_0) \;\equiv\; \begin{pmatrix} -Ae^{2ik_tz_0} & -k_lBe^{i(k_t+k_l)z_0} \\ -k_tBe^{i(k_t+k_l)z_0} & Ae^{2ik_lz_0} \end{pmatrix}. \tag{2.22}$$

The coefficients A and B are given by

$$A \;=\; \frac{4k_tk_lk_\parallel^2-(k_t^2-k_\parallel^2)^2}{4k_tk_lk_\parallel^2+(k_t^2-k_\parallel^2)^2} \tag{2.23}$$

$$B \;=\; \frac{4k_\parallel(k_t^2-k_\parallel^2)}{4k_tk_lk_\parallel^2+(k_t^2-k_\parallel^2)^2} \tag{2.24}$$

and fulfil the relation $A^2+k_tk_lB^2=1$. Equation (2.21) gives the freedom to choose one of the reflection coefficients freely. We choose $R_t=\pm I_t$ and get two sets of modes, one with a symmetric x component vs. $z-z_0$, the other one with an antisymmetric x component. The symmetric mode is given by

$$u_x \;=\; -k_t\left(2k_\parallel^2\cos(k_l(z-z_0))+(k_t^2-k_\parallel^2)\cos(k_t(z-z_0))\right)e^{ik_\parallel x} \tag{2.25}$$

$$u_z \;=\; ik_\parallel\left(-2k_tk_l\sin(k_l(z-z_0))+(k_t^2-k_\parallel^2)\sin(k_t(z-z_0))\right)e^{ik_\parallel x}, \tag{2.26}$$

while the antisymmetric mode is

$$u_x \;=\; k_\parallel\left((k_t^2-k_\parallel^2)\sin(k_l(z-z_0))-2k_tk_l\sin(k_t(z-z_0))\right)e^{ik_\parallel x} \tag{2.27}$$

$$u_z \;=\; -ik_l\left((k_t^2-k_\parallel^2)\cos(k_l(z-z_0))+2k_\parallel^2\cos(k_t(z-z_0))\right)e^{ik_\parallel x}\,. \tag{2.28}$$

Here we omitted the time dependence of the modes for brevity.

2.5 Elastic energy

At the end of this chapter, we want to calculate the total energy that is stored in an elastic medium. For this, we multiply the equation of motion (2.11) with $\partial_t\mathbf{u}$ and integrate over V.

$$\int_V d^3\mathbf{r}\,\rho(\partial_tu_i)(\partial_t^2u_i) \;=\; \rho\int_V d^3\mathbf{r}\,(\partial_tu_i)(\partial_jp_{ij})\,. \tag{2.29}$$

The integrand on the left hand side can be rewritten as $\partial_t \left[\rho(\partial_t u_i)^2/2\right]$, while we convert the integral on the right hand side by partial integration,

$$\begin{aligned} \rho \int_V d^3\mathbf{r}\,(\partial_t u_i)(\partial_j p_{ij}) &= \rho \oint_{\partial V} d^2\mathbf{r}\,(\partial_t u_i)(\hat{n}_j p_{ij}) \\ &\quad -\rho \int_V d^3\mathbf{r}\,(\partial_t \partial_j u_i) p_{ij} \\ &= -\int_V d^3\mathbf{r}\,(\partial_t S_{ij}) c_{ijkl} S_{kl}\,, \end{aligned} \tag{2.30}$$

where the surface integral is zero because of the free boundary condition (2.15) and we used Eqs. (2.2) and (2.1) in the second step of the calculation. Then Eq. (2.29) becomes

$$\partial_t \int_V d^3\mathbf{r}\,\frac{1}{2}\rho(\partial_t u_i)^2 + \int_V d^3\mathbf{r}\,(\partial_t S_{ij}) c_{ijkl} S_{kl} = 0 \tag{2.31}$$

The first term on the left hand side is of the form $\partial_t m v^2/2$ and we identify it as the rate of change of kinetic energy. As there is no power flow into the system (we assumed that there are no external forces applied), the second integral must be the rate of change of stored elastic energy. Because of the symmetry of $[[c]]$, we can write the integrand in (2.31) as $(\partial_t S_{ij}) c_{ijkl} S_{kl} = S_{ij} c_{ijkl} (\partial_t S_{kl}) = \partial_t (S_{ij} c_{ijkl} S_{kl})/2$ and have thus obtained an expression for the total energy in the system,

$$U = \frac{1}{2}\int_V d^3\mathbf{r}\,\left(\rho(\partial_t u_i)^2 + c_{ijkl}(\partial_i u_j)(\partial_k u_l)\right)\,. \tag{2.32}$$

Here we have again used Eq. (2.1) to express U as function of $\mathbf{u}$ alone.

Chapter 3

The elastic eigenmodes of a membrane

The acoustic eigenmodes of a free standing infinite plate or membrane are, like the eigenmodes of half spaces, superpositions of the plane wave solutions of 3D bulk materials. They are divided into three independent groups or sets of solutions, the horizontal shear modes (h) and the symmetric (s) and antisymmetric (a) Lamb modes [11]. We call these groups of modes polarizations and denote them by $\sigma = \{h, s, a\}$.

To derive an expression for these modes, we assume a plate of thickness d and area $A = l_x \times l_y$, with $l_x, l_y \gg d$. The volume of the membrane is denoted by $V = A \times d$. The parallel membrane surfaces are perpendicular to the z direction and cut the z axis at $\pm d/2$. In Fig. 3.1 we show a schematic picture of such a membrane.

3.1 Derivation of the eigenmodes

Like in Section 2.4, we choose the plane of incidence to be the xz plane. This allows us to directly use the results for the single free surface in the derivation of the eigenmodes. The horizontal shear modes of the membrane, which we call h modes, are all the modes (2.20) with $z_0 = d/2$ that also fulfil the boundary condition (2.15) at the lower surface at $z = -d/2$. This gives us a condition for k_h,

$$k_h = \frac{m\pi}{d}, \tag{3.1}$$

where m is an integer that takes all values between 0 and ∞. This result is very similar to the quantum mechanical problem of a particle in a box, only that here m can also be zero. The reason for this extra zero originates from the different boundary condition, which demands that one of the partial derivatives of the wave function is zero, rather than the wave function itself.

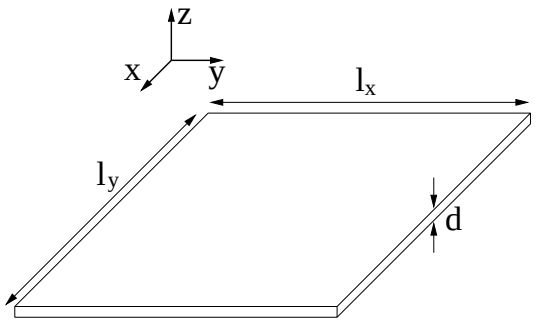

Figure 3.1: A typical membrane as it is used in many experiments. The thickness d of the membrane is usually of the order of 100 nm, but the discussion in this chapter is valid for any length scale, as long as $l_x, l_y \gg d$ and elasticity theory can be applied. The two membrane surfaces are perpendicular to $\hat{\mathbf{z}}$ and cut the z axis at $\pm d/2$.

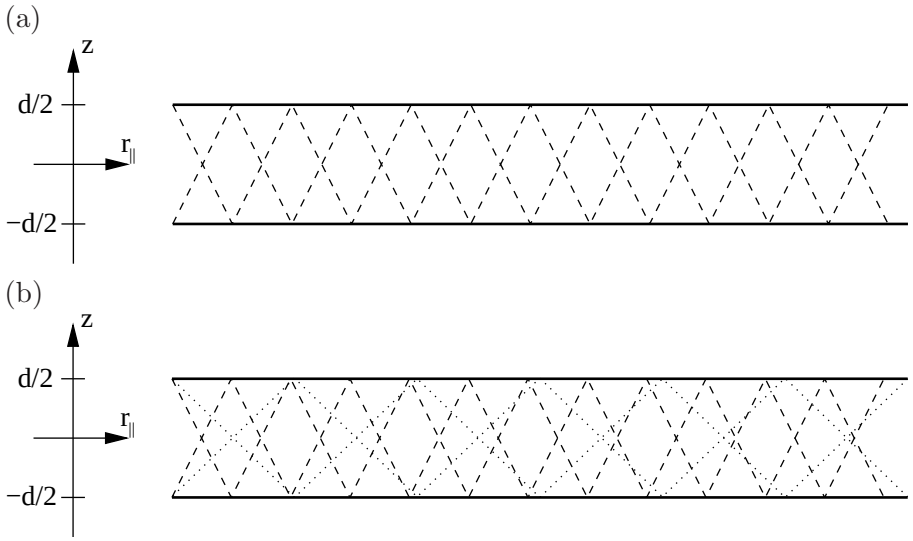

Figure 3.2: Partial wave pattern for (a) the horizontal shear modes and (b) the Lamb modes of an infinite isotropic membrane. The membrane surfaces are situated at $z = \pm d/2$ (solid lines), the dashed lines indicate the directions of the wave vectors of the transversal partial waves while the dotted lines indicate the directions of the wave vectors of the longitudinal partial waves.

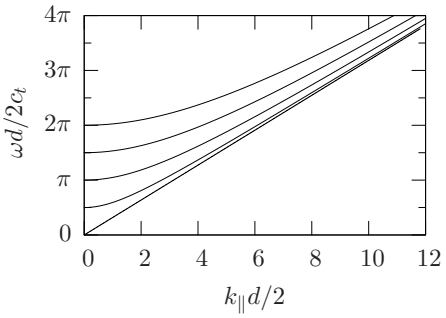

Figure 3.3: The first five branches of the horizontal shear modes.

From Eq. (3.1) directly follows the dispersion relation for the h modes,

$$\omega_{h,m}(k_\parallel) \;=\; c_t\sqrt{k_\parallel^2+(m\pi/d)^2}\,. \tag{3.2}$$

We call the functions $\omega_{h,m}(k_\parallel)$ branches. Different branches are identified by the number m, which we therefore call branch number. The first five branches of the horizontal shear modes are shown in Fig. 3.3. The displacement field of the h modes can be written as

$$\mathbf{u}_h \;=\; N_h\cos(k_h(z-d/2))(\hat{\mathbf{k}}_\parallel\times\hat{\mathbf{z}})e^{i(\mathbf{k}_\parallel\cdot\mathbf{r}-\omega t)}\,, \tag{3.3}$$

where we dropped the restriction of the plane of incidence being the xz plane and instead allow for an arbitrary direction of propagation along the plate. The normalization constant N_h is

$$N_h \;=\; \begin{cases} \sqrt{1/V} & \text{for} \quad m=0 \\ \sqrt{2/V} & \text{for} \quad m>0 \end{cases}\,. \tag{3.4}$$

The s and a modes, which originate from the vertical shear and the longitudinal mode of the last section, are derived in a similar manner. Equation (2.21) with $z_0 = d/2$ describes the reflection at the upper surface of the membrane. Similarly the reflection at the lower surface is described by the equation

$$\begin{aligned} \mathbf{i} &= [M'](-d/2)\cdot\mathbf{r} \\ &= [M](d/2)\cdot\mathbf{r}\,. \end{aligned} \tag{3.5}$$

To avoid having to introduce new notations, we used the same definitions for $\mathbf{i}$ and $\mathbf{r}$ as in Section 2.4, i.e. $\mathbf{r}$ denotes downwards moving waves, which are incident on the lower surface and $\mathbf{i}$ denotes upwards moving waves, which are reflected from it. Inserting (2.21) into (3.5), we get

$$\mathbf{i} \;=\; [M]^2(d/2)\mathbf{i}\,. \tag{3.6}$$

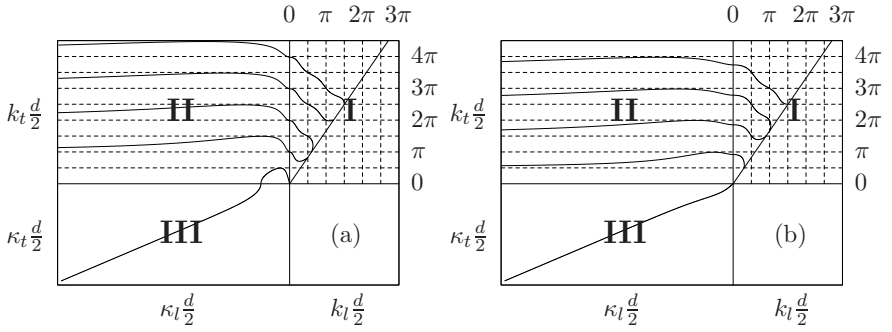

Figure 3.4: The curves $(k_l(k_\parallel), k_t(k_\parallel))$ for (a) the s modes and (b) the a modes. The curves start out in the upper right quadrant at the straight line, where $k_\parallel = 0$ and $c_t k_t = c_l k_l$.

This equation only has solutions if its characteristic determinant is zero ($\mathrm{Det}([M]^2 - [I]) = 0$), which yields two transcendental equations, each defining the dispersion relation for one of the two sets of Lamb modes. The s modes comply with the equation

$$\frac{4k_t k_l k_\parallel^2}{(k_t^2 - k_\parallel^2)^2} = -\frac{\tan(k_t d/2)}{\tan(k_l d/2)}, \tag{3.7}$$

while for the a modes we have

$$\frac{4k_t k_l k_\parallel^2}{(k_t^2 - k_\parallel^2)^2} = -\frac{\tan(k_l d/2)}{\tan(k_t d/2)}. \tag{3.8}$$

Together with Snell's law (2.17) we can extract from (3.7) and (3.8) the curves $(k_t(k_\parallel), k_l(k_\parallel))$, from which in turn we can calculate the dispersion relations $\omega(k_\parallel)$. In general, k_t and k_l can have complex values, but because of Snell's law (2.17) and the constraint that ω must be real, this would mean that also $k_\parallel$ becomes complex, which would lead to displacement fields that are not normalizable on infinite membranes. Therefore, k_t and k_l are always *either* real *or* imaginary, and $k_\parallel$ is always real, which ensures propagating modes along the surface. Nevertheless, the later discussion becomes somewhat more compact, if we replace k_t and k_l by the complex quantities $\bar{k}_t \equiv k_t + i\kappa_t$ and $\bar{k}_l \equiv k_l + i\kappa_l$, where $k_{t,l}$ and $\kappa_{t,l}$ are real and positive. This enables us to treat three different combinations of $\bar{k}_t$ and $\bar{k}_l$ being real or imaginary at once. In particular the combinations are $\bar{k}_t$ and $\bar{k}_l$ both real, $\bar{k}_t$ real and $\bar{k}_l$ imaginary and $\bar{k}_t$ and $\bar{k}_l$ both imaginary. The combination $\bar{k}_t$ imaginary and $\bar{k}_l$ real does not occur.

Like the h modes, the s and a modes are cut into branches, but the branch number m for the s and a modes does not follow quite as readily as for the h modes. We want to find m such that for a fixed value of $k_\parallel$ a higher

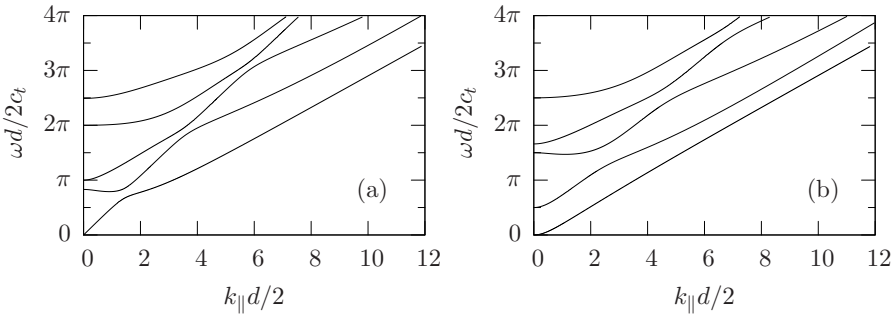

Figure 3.5: First five branches of the (a) the s modes and (b) the a modes.

value of m always yields a higher value for ω as well, i.e. we want to use m to order the branches by frequency. For the h modes that is automatically the case, for the s and a modes we need to have a closer look. If we set $k_\parallel = 0$, Eq. (3.7) yields together with Snell's law for the s modes

$$\omega_{s,n}(k_\parallel = 0) = 2n\pi c_t/d \quad \text{or} \quad (2n+1)\pi c_l/d \quad . \tag{3.9}$$

By the integer n, the branches of the s modes are well distinguished, but because the even values $2n$ are multiplied with a different constant than the odd values $2n+1$ ($c_t \neq c_l$), ordering the branches by n will not order them by frequency. Nevertheless, branches of the same polarization never cross and by ordering the values from (3.9) by frequency, we can define the branch number m in such a way that $m_1 < m_2$ always yields $\omega_{s,m_1}(k_\parallel) < \omega_{s,m_2}(k_\parallel)$. For the a modes the situation is similar. From Eq. (3.8) with $k_\parallel = 0$ follows

$$\omega_{a,n}(k_\parallel = 0) = (2n+1)\pi c_t/d \quad \text{or} \quad 2n\pi c_l/d \quad , \tag{3.10}$$

and we choose m in the same way as for the s modes.

In Figure 3.4, the curves $(k_t(k_\parallel), k_l(k_\parallel))$ are shown for the first branches of the s and a modes. The curves start out for $k_\parallel = 0$ in the upper right quadrant (Quadrant I), where both $\bar{k}_t$ and $\bar{k}_l$, are real (i.e. $\bar{k}_t = k_t$ and $\bar{k}_l = k_l$). In this quadrant, k_t increases with increasing $k_\parallel$, while k_l decreases. Upon reaching the value zero, $\bar{k}_l$ takes on the imaginary values $i\kappa_l$ (Quadrant II). κ_l then increases monotonically with increasing $k_\parallel$, while, except for the respective lowest branch, k_t is bounded, $m\pi < k_t \leq (2m+1)\pi/2$ for the s modes and $(2m-1)\pi/2 < k_t \leq m\pi$ for the a modes, where m again is the branch number. For the lowest branch of the s modes, $\bar{k}_t$ becomes zero for a finite value of $k_\parallel$ and turns imaginary thereafter, κ_t increasing monotonically with increasing $k_\parallel$ (Quadrant III). For the lowest branch of the a modes, $\bar{k}_l$ and $\bar{k}_t$ are both imaginary for *all* values of $k_\parallel$, which leads to the interesting effect of a quadratic dispersion relation for small $k_\parallel$ (shown in Section 3.2). The dispersion relations for the first five branches of the s and a modes are shown in Fig. 3.5.

The displacement field of the s modes is given by

$$\begin{aligned}\mathbf{u}_s \;=\; N_s \Big\{ i\bar{k}_t \Big(2k_\parallel^2 \cos(\bar{k}_t d/2)\cos(\bar{k}_l z) \;+ (\bar{k}_t^2 - k_\parallel^2)\cos(\bar{k}_l d/2)\cos(\bar{k}_t z) \Big)\, \hat{\mathbf{k}}_\parallel \\ - \; k_\parallel \Big(2\bar{k}_t\bar{k}_l \cos(\bar{k}_t d/2)\sin(\bar{k}_l z) - (\bar{k}_t^2 - k_\parallel^2)\cos(\bar{k}_l d/2)\sin(\bar{k}_t z) \Big)\, \hat{\mathbf{z}} \Big\}\, e^{i\mathbf{k}_\parallel\cdot\mathbf{r}},\end{aligned} \tag{3.11}$$

while the displacement field of the a modes is

$$\begin{aligned}\mathbf{u}_a \;=\; N_a \Big\{ i\bar{k}_t \Big(2k_\parallel^2 \sin(\bar{k}_t d/2)\sin(\bar{k}_l z) \;+ (\bar{k}_t^2 - k_\parallel^2)\sin(\bar{k}_l d/2)\sin(\bar{k}_t z) \Big)\, \hat{\mathbf{k}}_\parallel \\ + \; k_\parallel \Big(2\bar{k}_t\bar{k}_l \sin(\bar{k}_t d/2)\cos(\bar{k}_l z) - (\bar{k}_t^2 - k_\parallel^2)\sin(\bar{k}_l d/2)\cos(\bar{k}_t z) \Big)\, \hat{\mathbf{z}} \Big\}\, e^{i\mathbf{k}_\parallel\cdot\mathbf{r}}.\end{aligned} \tag{3.12}$$

Like the h modes, the s and a modes are standing waves along the z direction and propagate along the $\hat{\mathbf{k}}_\parallel$ direction. Unlike the h modes however, their functional dependence on the z coordinate is not the same along the whole branch, but depends on the value of $k_\parallel$. The normalization constants N_s and N_a will be given in Appendix A.

3.2 Low energy expansion

In many problems, we are interested in the behaviour of phonons of very low energies. These are the phonons of the lowest branch of each polarization in the limit $\omega \ll \omega_{\sigma,1}(k_\parallel = 0)$, i.e. the energies of the phonons of interest are much smaller than the zero-$k_\parallel$ energy of any of the higher branches. In this limit we can give analytic expressions for the functions $\omega_{\sigma,0}(k_\parallel)$ by expanding equations (3.2), (3.7) and (3.8) in $k_\parallel$.

3.2.1 h mode

For the lowest branch of the h phonons, ω is linear in $k_\parallel$ for all values of $k_\parallel$ and the low energy expansion for that mode takes the simple form

$$\omega_{h,0,k_\parallel} \;=\; c_t k_\parallel \tag{3.13}$$

3.2.2 s mode

For the lowest branch of the s phonons, $\bar{k}_l$ takes the imaginary values $i\kappa_l$, while $\bar{k}_t$ is real ($\bar{k}_t = k_t$) and we write Eq. (3.7) as

$$\frac{4k_t\kappa_l k_\parallel^2}{(k_t^2 - k_\parallel^2)^2} \;=\; \frac{\tan(k_t d/2)}{\tanh(\kappa_l d/2)}\,. \tag{3.14}$$

Expanding Eq. (3.14) to the leading order in $k_\parallel$, we get

$$\begin{aligned} \omega_{s,0,k_\parallel} &= 2\frac{c_t}{c_l}\sqrt{c_l^2 - c_t^2}k_\parallel \\ &\equiv c_s k_\parallel \,, \end{aligned} \tag{3.15}$$

where with (2.14) one can show that $c_s \geq c_t$.

3.2.3 a mode

The low energy expansion of the lowest a mode branch is a little bit more tricky to calculate. Here both $\bar{k}_t$ and $\bar{k}_l$ take the respective imaginary values $i\kappa_t$ and $i\kappa_l$ and we thus write Eq. (3.8) as

$$\frac{4\kappa_t\kappa_l k_\parallel^2}{(\kappa_t^2 + k_\parallel^2)^2} = \frac{\tanh(\kappa_l d/2)}{\tanh(\kappa_t d/2)} \,. \tag{3.16}$$

We need to expand this equation to the second leading order to get a non-zero result, which gives us a quadratic dispersion relation for very small $k_\parallel$ [13, 14, 15],

$$\begin{aligned} \omega_{a,0,k_\parallel} &= dc_t\sqrt{\frac{c_l^2 - c_t^2}{3c_l^2}}k_\parallel^2 \\ &\equiv \frac{\hbar}{2m^\star}k_\parallel^2 \,. \end{aligned} \tag{3.17}$$

This means that for $k_\parallel d \ll 1$, the lowest a mode branch behaves like a massive particle with the effective mass $m^\star$, which increases with decreasing membrane thickness.

When calculating the expansion of the normalization constant of the lowest a mode (A.5), it is not enough to expand to the second leading order, as all the terms cancel to zero. In order to get a non-zero expression, we have to expand (A.5) to third leading order. This includes the dispersion relation (3.8), leading to a second term that is proportional to $k_\parallel^4$,

$$\omega_{a,0,k_\parallel} = \frac{\hbar}{2m^\star}\left(k_\parallel^2 - d^2\frac{27c_l^2 - 20c_t^2}{90c_l^2}k_\parallel^4\right) \,. \tag{3.18}$$

3.3 Quantization of the modes

To be able to do any further calculations with the set of eigenmodes we derived for the membrane, we have to make sure that it is orthonormal and complete. For the proof of completeness we show that the operator $\tilde{L}$, which we defined in Eq. (2.11), is self-adjoint on an arbitrary volume V with boundary ∂V. We then use the hermiticity of the operators $\tilde{L}$ and

$\tilde{\mathbf{k}}_{\|} \equiv i(\hat{\mathbf{x}}\partial_x + \hat{\mathbf{y}}\partial_y)$ and the symmetry of the eigenmodes to show that the latter are orthogonal to each other. The normalization constants (3.4), (A.4) and (A.5) were chosen such that the norm of the mode $||\mathbf{u}|| = 1$. In the end of the chapter, we will formally quantize the phonon eigenmodes of the membrane.

3.3.1 Self-adjointness of the operator $\tilde{L}$

We are going to show that $\tilde{L}$ is a self-adjoint operator on an arbitrary volume V with the smooth border ∂V. The Hilbert space $\mathcal{H}$, that $\tilde{L}$ acts on, consists of all square-integrable 3D vector functions that are defined on V. The scalar product on $\mathcal{H}$ is defined as usual,

$$\langle \mathbf{v}|\mathbf{u}\rangle \;=\; \int_V d^3\mathbf{r}\, \mathbf{v}^\dagger(\mathbf{r}) \cdot \mathbf{u}(\mathbf{r})\,, \tag{3.19}$$

and the norm is

$$||\mathbf{u}|| \;\equiv\; \sqrt{\langle \mathbf{u}|\mathbf{u}\rangle}\,. \tag{3.20}$$

Furthermore, in this section we will understand the derivatives in a generalized sense. If $f(\mathbf{r})$ is an arbitrary function on V, then we define $\partial_i f$ as the function that satisfies

$$\int_V d^3\mathbf{r}\, g(\mathbf{r})\partial_i f(\mathbf{r}) \;=\; \int_{\partial V} d^2\mathbf{r}\, f(\mathbf{r})g(\mathbf{r})\hat{n}_i - \int_V d^3\mathbf{r}\, f(\mathbf{r})\partial_i g(\mathbf{r})\,, \tag{3.21}$$

for any function $g(\mathbf{r})$ of class C^1 on V, i.e. functions that are derivable and have continuous first derivatives, and all the integrals on the right hand side of Eq. (3.21) exist and are finite.

The domain $\mathcal{D}(\tilde{L})$ of $\tilde{L}$ is formed of all functions $\mathbf{u}(\mathbf{r}) \in \mathcal{H}$ that obey the boundary conditions (2.15) and for which $\tilde{L}\mathbf{u}$ exists and is contained in $\mathcal{H}$. Since $\mathcal{D}(\tilde{L})$ includes the space $C^2(V)$ of functions that are twice derivable and have continuous, integrable second derivatives on V, and $C^2(V)$ is dense in $\mathcal{H}$, $\mathcal{D}(\tilde{L})$ is dense in $\mathcal{H}$ as well. Therefore, $\tilde{L}$ is a symmetric operator. Let now $\mathbf{u}$ and $\mathbf{v}$ be functions in $\mathcal{D}(\tilde{L})$, then

$$\begin{aligned}
\rho\langle \mathbf{v}|\tilde{L}\mathbf{u}\rangle \;&=\; \int_V d^3\mathbf{r}\, v_i^\star c_{ijkl}\partial_j\partial_k u_l \\
&=\; \int_{\partial V} d^2\mathbf{r}\, v_i^\star c_{ijkl} n_j \partial_k u_l - \int_V d^3\mathbf{r}\, (\partial_j v_i^\star) c_{ijkl}\partial_k u_l \\
&=\; -\int_{\partial V} d^2\mathbf{r}\, (\partial_j v_i^\star) c_{ijkl} n_k u_l + \int_V d^3\mathbf{r}\, (\partial_k\partial_j v_i^\star) c_{ijkl} u_l \\
&=\; \rho\langle \tilde{L}\mathbf{v}|\mathbf{u}\rangle\,,
\end{aligned} \tag{3.22}$$

where we used the symmetry condition (2.3) for $[[c]]$. The surface integrals in Eq. (3.22) are zero because both $\mathbf{u}$ and $\mathbf{v}$ fulfil the boundary condition (2.15). But (3.22) for $\mathbf{u}, \mathbf{v} \in \mathcal{D}(\tilde{L})$ means that $\tilde{L}$ is hermitian [12].

To show that $\tilde{L}$ is also self-adjoint, let $\mathbf{v}$ be a function in $\mathcal{H}$ (i.e. possibly outside $\mathcal{D}(\tilde{L})$), such that $\langle \mathbf{v}|\tilde{L}\mathbf{u}\rangle$ is a continuous linear functional in $\mathbf{u} \in \mathcal{D}(\tilde{L})$. This means that we can find an $M_{\mathbf{v}} > 0$ for which

$$\langle \mathbf{v}|\tilde{L}\mathbf{u}\rangle \quad \leq \quad M_{\mathbf{v}}||\mathbf{u}|| \tag{3.23}$$

for any $\mathbf{u} \in \mathcal{D}(\tilde{L})$ and, by the Riesz-Fréchet theorem [16], a function $\mathbf{v}' \in \mathcal{H}$ exists that fulfils $\langle \mathbf{v}|\tilde{L}\mathbf{u}\rangle = \langle \mathbf{v}'|\mathbf{u}\rangle$ for any $\mathbf{u} \in \mathcal{D}(\tilde{L})$. We then define the adjoint operator $\tilde{L}^\dagger$ that acts on all the functions $\mathbf{v}$ that satisfy (3.23) and the relation $\tilde{L}^\dagger \mathbf{v} = \mathbf{v}'$. These functions $\mathbf{v}$ form the domain $\mathcal{D}(\tilde{L}^\dagger)$ of $\tilde{L}^\dagger$.

By the hermiticity of $\tilde{L}$ it follows that, if $\mathbf{v}, \mathbf{u} \in \mathcal{D}(\tilde{L})$, $\langle \mathbf{v}|\tilde{L}\mathbf{u}\rangle = \langle \tilde{L}\mathbf{v}|\mathbf{u}\rangle$ is a linear functional, so any function from $\mathcal{D}(\tilde{L})$ is included in $\mathcal{D}(\tilde{L}^\dagger)$, i.e. $\mathcal{D}(\tilde{L}) \subset \mathcal{D}(\tilde{L}^\dagger)$. To prove that $\tilde{L}$ is self-adjoint, we have to show that also $\mathcal{D}(\tilde{L}^\dagger) \subset \mathcal{D}(\tilde{L})$, which would imply that $\mathcal{D}(\tilde{L}^\dagger) = \mathcal{D}(\tilde{L})$ and thus $\tilde{L} = \tilde{L}^\dagger$.

For this we investigate again the product $\langle \mathbf{v}|\tilde{L}\mathbf{u}\rangle$, but now for $\mathbf{u} \in \mathcal{D}(\tilde{L})$ and $\mathbf{v} \in \mathcal{D}(\tilde{L}^\dagger)$. Then, with (3.22),

$$\begin{aligned} \rho\langle \mathbf{v}|\tilde{L}\mathbf{u}\rangle &= -\int_{\partial V} d^2\mathbf{r}\,(\partial_j v_i^\star) c_{ijkl} n_k u_l + \rho\langle \tilde{L}\mathbf{v}|\mathbf{u}\rangle \\ &\equiv \rho\langle \tilde{L}^\dagger \mathbf{v}|\mathbf{u}\rangle\,, \end{aligned} \tag{3.24}$$

where now the surface integral does not necessarily vanish, because $\mathbf{v}$ does not necessarily fulfil the boundary condition (2.15). In other words, we have to show that $(\partial_j v_i^\star) c_{ijkl} n_k u_l = 0$ for all $\mathbf{v} \in \mathcal{D}(\tilde{L}^\dagger)$, which we are going to prove by contradiction.

First we rewrite Eq. (3.24) as

$$\rho\langle (\tilde{L} - \tilde{L}^\dagger)\mathbf{v}|\mathbf{u}\rangle \quad = \quad \int_{\partial V} d^2\mathbf{r}\,(\partial_j v_i^\star) c_{ijkl} n_k u_l\,, \tag{3.25}$$

which is true for any $\mathbf{u} \in \mathcal{D}(\tilde{L})$. In other words, if $(\partial_j v_i^\star) c_{ijkl} n_k u_l \neq 0$ on ∂V, we can find a $\mathbf{u} \in \mathcal{D}(\tilde{L})$ for which $\rho\langle (\tilde{L} - \tilde{L}^\dagger)\mathbf{v}|\mathbf{u}\rangle \neq 0$. This means that $\mathbf{v} \neq 0$ on a set of measure larger than zero in the interior of V, which we denote as $V^\circ \equiv V - \partial V$. Then we can find a nonempty compact set $S \subset V^\circ$ and a twice derivable function $\mathbf{u}'$ that is zero outside S and satisfies

$$\langle (\tilde{L} - \tilde{L}^\dagger)\mathbf{v}|\mathbf{u}'\rangle \quad \neq \quad 0\,. \tag{3.26}$$

Since $\mathbf{u}'$ is zero outside of $S \subset V^\circ$, this means that $\mathbf{u}'$ as well as any of its derivatives are zero on ∂V. Therefore $\mathbf{u}' \in \mathcal{D}(\tilde{L})$ and

$$\begin{aligned} \langle (\tilde{L} - \tilde{L}^\dagger)\mathbf{v}|(\mathbf{u} + \mathbf{u}')\rangle &= \int_{\partial V} d^2\mathbf{r}\,(\partial_j v_i^\star) n_k c_{ijkl} (u_l + u_l') \\ &= \int_{\partial V} d^2\mathbf{r}\,(\partial_j v_i^\star) n_k c_{ijkl} (u_l) \end{aligned} \tag{3.27}$$

By Eqs. (3.25) and (3.27) we have

$$\langle (\tilde{L} - \tilde{L}^\dagger)\mathbf{v}|(\mathbf{u} + \mathbf{u}')\rangle \quad = \quad \langle (\tilde{L} - \tilde{L}^\dagger)\mathbf{v}|\mathbf{u}\rangle\,, \tag{3.28}$$

whereas Eqs. (3.25) and (3.26) imply that

$$\langle(\tilde{L}-\tilde{L}^\dagger)\mathbf{v}|(\mathbf{u}+\mathbf{u}')\rangle \quad \neq \quad \langle(\tilde{L}-\tilde{L}^\dagger)\mathbf{v}|\mathbf{u}\rangle\,, \tag{3.29}$$

This is a contradiction and therefore we must have $(\partial_j v_i^\star)n_k c_{ijkl}=0$ on ∂V. This in turn means that

$$\langle\mathbf{v}|\tilde{L}\mathbf{u}\rangle \quad = \quad \langle\tilde{L}^\dagger\mathbf{v}|\mathbf{u}\rangle \tag{3.30}$$

and by the definition of $\mathcal{D}(\tilde{L}^\dagger)$ and the Riesz-Fréchet theorem $\mathbf{v}\in\mathcal{D}(\tilde{L})$, which means that $\mathcal{D}(\tilde{L})=\mathcal{D}(\tilde{L}^\dagger)$ and $\tilde{L}=\tilde{L}^\dagger$. Therefore the operator $\tilde{L}$ is self-adjoint on an arbitrary volume V, so we can form a complete, orthonormal set of its eigenfunctions.

To find a complete orthonormal set of eigenfunctions of $\tilde{L}$ in the membrane, we use the operator

$$\tilde{\mathbf{k}}_\parallel \quad \equiv \quad i(\hat{\mathbf{x}}\partial_x+\hat{\mathbf{y}}\partial_y)\,. \tag{3.31}$$

This operator is self-adjoint as well, if it acts on wave functions that are defined on an infinite rectangular plate, or on a finite plate with periodic boundary conditions. Since $\tilde{L}$ and $\tilde{\mathbf{k}}_\parallel$ are both combinations of partial spatial derivatives, they commute. Hence there is a complete set of eigenfunctions common to $\tilde{L}$ and $\tilde{\mathbf{k}}_\parallel$. But these functions are the ones given in Eqs. (3.3), (3.11) and (3.12), with real $k_\parallel$ and k_h, k_t and k_l respectively satisfying (3.2), (3.7) and (3.8).

3.3.2 Orthogonality of the elastic eigenmodes

In this section we will show that the eigenfunctions that are common to the commuting operators $\tilde{L}$ and $\tilde{\mathbf{k}}_\parallel$ are orthogonal to each other and therefore will, after normalization, form a complete, orthonormal set of functions. These are the functions $\mathbf{u}_{\sigma,m,k_\parallel}$ from Section 3.1. For the purpose of this derivation, we rewrite the displacement field as

$$\mathbf{u}_{\sigma,m,\mathbf{k}_\parallel} \quad = \quad \mathbf{u}_{\sigma,m}(z)e^{i\mathbf{k}_\parallel\cdot\mathbf{r}}\,. \tag{3.32}$$

As $\mathbf{k}_\parallel$ is perpendicular to the z axis, we have thus split the z dependence from the x and y dependence. The functions $\exp(i\mathbf{k}_\parallel\cdot\mathbf{r})$ are eigenfunctions of the operator $\tilde{\mathbf{k}}_\parallel$ with the non-degenerate eigenvalues $\mathbf{k}_\parallel$. For a finite, rectangular membrane of area A and with periodic boundary conditions

$$\langle e^{i\mathbf{k}_\parallel\cdot\mathbf{r}}|e^{i\mathbf{k}'_\parallel\cdot\mathbf{r}}\rangle \quad = \quad \delta_{\mathbf{k}_\parallel,\mathbf{k}'_\parallel} \tag{3.33}$$

and the scalar product of $\mathbf{u}_{\sigma,m,\mathbf{k}_\parallel}$ with $\mathbf{u}_{\sigma',m',\mathbf{k}'_\parallel}$ is

$$\begin{aligned}\langle\mathbf{u}_{\sigma,m,\mathbf{k}_\parallel}|\mathbf{u}_{\sigma',m',\mathbf{k}'_\parallel}\rangle &= \delta_{\mathbf{k}_\parallel,\mathbf{k}'_\parallel}\int_{-b/2}^{b/2}dz\,\mathbf{u}^\dagger_{\sigma,m}(z)\cdot\mathbf{u}_{\sigma',m'}(z)\\ &\equiv \delta_{\mathbf{k}_\parallel,\mathbf{k}'_\parallel}\langle\mathbf{u}_{\sigma,m}(z)|\mathbf{u}_{\sigma\prime,m'}(z)\rangle\,.\end{aligned} \tag{3.34}$$

As explained in Section 2.4, the h modes are polarized perpendicular to the plane of incidence and parallel to the membrane surfaces, while the s and a modes are polarized within the plane of incidence. This means that the displacement fields of the h modes are perpendicular to the displacement fields of the s and a modes, so the scalar product $\langle \mathbf{u}_h | \mathbf{u}_{a,s} \rangle$ is trivially zero. The displacement fields of the s and a modes have opposite symmetries, which means for the scalar product $\langle \mathbf{u}_s | \mathbf{u}_a \rangle$ that the integrand in Eq. (3.34) is odd and therefore the integral is zero as well. Collecting the results, we obtain

$$\langle \mathbf{u}_{\sigma,m}(z) | \mathbf{u}_{\sigma',m'}(z) \rangle \quad \propto \quad \delta_{\sigma,\sigma'} \, . \tag{3.35}$$

All that we are left to show is that the scalar product between phonons from different branches is zero, i.e. phonon modes with different branch number m are orthogonal to each other. This follows directly from the hermiticity of $\tilde{L}$,

$$\begin{aligned} 0 &= \langle \mathbf{u}_{\sigma,m,\mathbf{k}_\parallel} | \tilde{L} \mathbf{u}_{\sigma,m',\mathbf{k}_\parallel} \rangle - \langle \tilde{L} \mathbf{u}_{\sigma,m,\mathbf{k}_\parallel} | \mathbf{u}_{\sigma,m',\mathbf{k}_\parallel} \rangle \\ &= (\omega^2_{\sigma,m,\mathbf{k}_\parallel} - \omega^2_{\sigma,m',\mathbf{k}_\parallel}) \langle \mathbf{u}_{\sigma,m,\mathbf{k}_\parallel} | \mathbf{u}_{\sigma,m',\mathbf{k}_\parallel} \rangle \, . \end{aligned} \tag{3.36}$$

Since the eigenvalues of $\tilde{L}$ for different m but same σ and $\mathbf{k}_\parallel$ are non-degenerate, Eq. (3.36) directly implies

$$\langle \mathbf{u}_{\sigma,m,\mathbf{k}_\parallel} | \mathbf{u}_{\sigma,m',\mathbf{k}_\parallel} \rangle \quad \propto \quad \delta_{m,m'} \, , \tag{3.37}$$

which completes our proof of orthogonality. Inserting the normalization constants from (3.4), (A.4) and (A.5) into the respective expressions for the eigenfunctions (3.3), (3.11) and (3.12), we obtain

$$\langle \mathbf{u}_{\sigma,m,\mathbf{k}_\parallel} | \mathbf{u}_{\sigma',m',\mathbf{k}'_\parallel} \rangle \quad = \quad \delta_{\sigma,\sigma'} \delta_{m,m'} \delta_{\mathbf{k}_\parallel,\mathbf{k}'_\parallel} \, . \tag{3.38}$$

3.3.3 Quantization of the elastic field

To quantize the elastic field, we use the classical Hamiltonian (2.32). First we note that the displacement field $\mathbf{u}$, and any other field in the elastic body, is a function of the position $\mathbf{r}$ in the undeformed body and the time t. Since $\mathbf{r}$ does not change in time, the partial time derivative $\partial_t \mathbf{u}$ is identical to the total time derivative, which we denote by $\dot{\mathbf{u}}$. Therefore, to write the equations in the standard form, we will replace ∂_t everywhere with the total time derivative. With this substitution, Eq. (2.32) becomes

$$H_{\mathrm{ph}} \quad = \quad \frac{1}{2} \int_V d^3\mathbf{r} \, \Big(\rho (\dot{u}_i)^2 + c_{ijkl} (\partial_i u_j)(\partial_k u_l) \Big) \, . \tag{3.39}$$

The canonical variables are the field $\mathbf{u}$ and the conjugate momentum $\boldsymbol{\pi} = \rho\dot{\mathbf{u}}$, which satisfy the Hamilton equations

$$\dot{\mathbf{u}} = \frac{\delta H_{\rm ph}}{\delta \boldsymbol{\pi}}\,, \tag{3.40}$$

$$\dot{\boldsymbol{\pi}} = -\frac{\delta H_{\rm ph}}{\delta \mathbf{u}}\,. \tag{3.41}$$

Equation (3.41) is nothing but the dynamic equation (2.11).

In the second quantization, $\mathbf{u}$ and $\boldsymbol{\pi}$ become the field operators $\tilde{\mathbf{u}}$ and $\tilde{\boldsymbol{\pi}}$, respectively. If we use $\tilde{b}^\dagger_\mu$ and $\tilde{b}_\mu$ to denote the creation and annihilation operators of a phonon with quantum numbers $\mu = \sigma, m, \mathbf{k}_\parallel$, then the *real* displacement and generalized momentum field operators, $\tilde{\mathbf{u}}(\mathbf{r}) = \tilde{\mathbf{u}}^\dagger(\mathbf{r})$ and $\tilde{\boldsymbol{\pi}}(\mathbf{r}) = \tilde{\boldsymbol{\pi}}^\dagger(\mathbf{r})$, are

$$\tilde{\mathbf{u}}(\mathbf{r}) = \sum_\mu \left[\mathbf{f}_\mu(\mathbf{r})\tilde{b}_\mu + \mathbf{f}^\star_\mu(\mathbf{r})\tilde{b}^\dagger_\mu\right] \tag{3.42}$$

$$\begin{aligned}\tilde{\boldsymbol{\pi}}(\mathbf{r}) &= \rho\sum_\mu \left[\dot{\mathbf{f}}_\mu(\mathbf{r})\tilde{b}_\mu + \dot{\mathbf{f}}^\star_\mu(\mathbf{r})\tilde{b}^\dagger_\mu\right] \\ &= -i\rho\sum_\mu \omega_\mu \left[\mathbf{f}_\mu(\mathbf{r})\tilde{b}_\mu - \mathbf{f}^\star_\mu(\mathbf{r})\tilde{b}^\dagger_\mu\right]\,,\end{aligned} \tag{3.43}$$

where $\mathbf{f}_\mu(\mathbf{r}) \equiv C_\mu \mathbf{u}_\mu(\mathbf{r})$ and C_μ is a real constant which we shall determine from the commutation relations of the $\tilde{b}_\mu$ operators.

From Eqs. (3.42) and (3.43) we can extract the operators $\tilde{b}_\mu$ and $\tilde{b}^\dagger_\mu$ in terms of $\tilde{\mathbf{u}}$ and $\tilde{\boldsymbol{\pi}}$. In order to do this, we first note from (3.3), (3.11) and (3.12) that

$$[\mathbf{u}_{h,m,\mathbf{k}_\parallel}(\mathbf{r})]^\star = \mathbf{u}_{h,m,-\mathbf{k}_\parallel}(\mathbf{r}), \tag{3.44}$$

whereas

$$[\mathbf{u}_{s,m,\mathbf{k}_\parallel}(\mathbf{r})]^\star = \alpha_{s,m,\mathbf{k}_\parallel}\mathbf{u}_{s,m,-\mathbf{k}_\parallel}(\mathbf{r})\,, \tag{3.45}$$

with $\alpha_{s,m,\mathbf{k}_\parallel} \equiv \bar{k}_t^2/|\bar{k}_t|^2$, i.e. $\alpha_{s,m,\mathbf{k}_\parallel} = 1$, if $\bar{k}_t$ is real, and $\alpha_{s,m,\mathbf{k}_\parallel} = -1$, if $\bar{k}_t$ is imaginary. Similarly

$$[\mathbf{u}_{a,m,\mathbf{k}_\parallel}(\mathbf{r})]^\star = \alpha_{a,m,\mathbf{k}_\parallel}\mathbf{u}_{a,m,-\mathbf{k}_\parallel}(\mathbf{r})\,, \tag{3.46}$$

where $\alpha_{a,m,\mathbf{k}_\parallel} \equiv \bar{k}_l^2/|\bar{k}_l|^2$. To make the notation general, we define $\alpha_{h,m,\mathbf{k}_\parallel} \equiv 1$ and then, by denoting $\bar{\mu} \equiv \sigma, m, -\mathbf{k}_\parallel$, we write

$$\int_V \mathbf{f}^T_\mu(\mathbf{r})\cdot\mathbf{f}_{\mu'}(\mathbf{r})\,d^3\mathbf{r} = \alpha_{\mu'}C^2_\mu\delta_{\mu,\bar{\mu}'}\,. \tag{3.47}$$

Multiplying (3.42) and (3.43) by $\mathbf{f}^\dagger_\mu(\mathbf{r})$ and integrating over V, we get

$$\int_V \mathbf{f}^\dagger_\mu(\mathbf{r})\tilde{\mathbf{u}}(\mathbf{r})\,d^3\mathbf{r} = C^2_\mu[\tilde{b}_\mu + \alpha_\mu\tilde{b}^\dagger_{\bar{\mu}}]\,, \tag{3.48}$$

$$\int_V \mathbf{f}^\dagger_\mu(\mathbf{r})\tilde{\boldsymbol{\pi}}(\mathbf{r})\,d^3\mathbf{r} = -i\rho\omega_\mu C^2_\mu\left[\tilde{b}_\mu - \alpha_\mu\tilde{b}^\dagger_{\bar{\mu}}\right]\,. \tag{3.49}$$

Solving the system we obtain

$$\tilde{b}_\mu = \frac{1}{2C_\mu^2}\left[\int_V \mathbf{f}_\mu^\dagger(\mathbf{r})\tilde{\mathbf{u}}(\mathbf{r})\,d^3\mathbf{r} + \frac{i}{\rho\omega_\mu}\int_V \mathbf{f}_\mu^\dagger(\mathbf{r})\tilde{\boldsymbol{\pi}}(\mathbf{r})\,d^3\mathbf{r}\right] \quad (3.50)$$

and

$$\begin{aligned}\alpha_\mu\tilde{b}_\mu^\dagger &= \frac{1}{2C_\mu^2}\left[\int_V \mathbf{f}_\mu^\dagger(\mathbf{r})\tilde{\mathbf{u}}(\mathbf{r})\,d^3\mathbf{r} - \frac{i}{\rho\omega_\mu}\int_V \mathbf{f}_\mu^\dagger(\mathbf{r})\tilde{\boldsymbol{\pi}}(\mathbf{r})\,d^3\mathbf{r}\right] \\ \Rightarrow \tilde{b}_\mu^\dagger &= \frac{1}{2C_\mu^2}\left[\int_V \mathbf{f}_\mu^T(\mathbf{r})\tilde{\mathbf{u}}(\mathbf{r})\,d^3\mathbf{r} - \frac{i}{\rho\omega_\mu}\int_V \mathbf{f}_\mu^T(\mathbf{r})\tilde{\boldsymbol{\pi}}(\mathbf{r})\,d^3\mathbf{r}\right]. \quad (3.51)\end{aligned}$$

Using the canonical commutation relations, $[\tilde{\mathbf{u}}(\mathbf{r}), \tilde{\mathbf{u}}(\mathbf{r}')] = [\tilde{\boldsymbol{\pi}}(\mathbf{r}), \tilde{\boldsymbol{\pi}}(\mathbf{r}')] = 0$ and $[\tilde{\mathbf{u}}(\mathbf{r}), \tilde{\boldsymbol{\pi}}(\mathbf{r}')] = i\hbar\delta(\mathbf{r}-\mathbf{r}')$, we obtain the commutation relations for the operators $\tilde{b}$ and $\tilde{b}^\dagger$,

$$[\tilde{b}_\mu\,, \tilde{b}_{\mu'}] = [\tilde{b}_\mu^\dagger\,, \tilde{b}_{\mu'}^\dagger] = 0 \quad (3.52)$$

and

$$[\tilde{b}_\mu\,, \tilde{b}_{\mu'}^\dagger] = \frac{\hbar}{2\rho\omega_\mu C_\mu^2}\delta_{\mu,\mu'}\,, \quad (3.53)$$

which implies that

$$C_\mu = \sqrt{\frac{\hbar}{2\rho\omega_\mu}}\,. \quad (3.54)$$

Using Eqs. (3.42) and (3.43) with the proper normalization of $\mathbf{f}$, we can write $H_{\rm ph}$ from Eq. (3.39) in operator form,

$$\begin{aligned}H_{\rm ph} &= \frac{\rho}{2}\int_V d^3\mathbf{r}\sum_{\mu,\mu'}\left(\dot{\mathbf{f}}_\mu^\dagger(\mathbf{r})\tilde{b}_\mu^\dagger + \dot{\mathbf{f}}_\mu^T(\mathbf{r})\tilde{b}_\mu\right)\cdot\left(\dot{\mathbf{f}}_{\mu'}(\mathbf{r})\tilde{b}_{\mu'} + \dot{\mathbf{f}}_{\mu'}^\star(\mathbf{r})\tilde{b}_{\mu'}^\dagger\right) \\ &+\frac{1}{2}\int_V d^3\mathbf{r}\sum_{\mu,\mu'}\left(\partial_i[\mathbf{f}_\mu^\star(\mathbf{r})]_j\tilde{b}_\mu^\dagger + \partial_i[\mathbf{f}_\mu(\mathbf{r})]_j\tilde{b}_\mu\right)c_{ijkl}\left(\partial_k[\mathbf{f}_\mu(\mathbf{r})]_l\tilde{b}_\mu + \partial_k[\mathbf{f}_\mu^\star(\mathbf{r})]_l\tilde{b}_\mu^\dagger\right) \\ &= \sum_\mu \hbar\omega_\mu[\tilde{b}_\mu^\dagger\tilde{b}_\mu + 1/2]\,. \quad (3.55)\end{aligned}$$

As expected, the Hamiltonian of the elastic body can be written as a sum of Hamiltonians of harmonic oscillators. These oscillators are the phonon modes of the plate.

Chapter 4

Thermal properties of thin membranes

For better thermal insulation, nanoscale detectors like microcalorimeters and microbolometers are often mounted on top of thin dielectric membranes. The thermal properties, like the heat capacity and conductivity of these membranes, directly influence the operating parameters of the mounted detector.

Due to the finite thickness of the membrane, its phonons behave like a three dimensional (3D) phonon gas only at high enough temperatures. At lower temperatures the phonon gas will "condense" into a quasi two dimensional (2D) state. We will discuss this dimensionality cross-over in Section 4.1 at the example of the heat capacity of the membrane and we will introduce the cross-over temperature T_C and cross-over thickness d_C. In Section 4.2 we will discuss ballistic phonon transport in the membrane, while in Sections 4.3 to 4.5 we will investigate diffusive heat transfer and discuss two different phonon scattering mechanisms in the membrane.

4.1 Dimensionality cross-over of the phonon gas

In isotropic 3D bulk systems, the phonon dispersion relation is a linear function of the wave vector, $\omega_\sigma = c_\sigma k$. If the temperature is low enough, the optical modes are not excited and the thermal properties of the system are determined only by the acoustic phonons. The dimensionality of the phonon gas has a big influence on these properties. For instance the heat capacity c_V follows at low temperatures (i.e. $T < \Theta_D$) the Debye law and is proportional to T^3 in 3D bulk systems [17]. In a hypothetical 2D system on the other hand, where motion is restricted into a plane and thus only one transversal and one longitudinal mode exist and all dispersion relations are linear, c_V would be proportional to T^2.

In systems of finite size the phonon dispersion relation splits into branches.

In the limit of low temperatures or very small system sizes, where the dominant thermal phonon wavelength λ_T becomes comparable to the system size, the phonon gas becomes lower dimensional. For instance in the case of the membranes we study, the dimensionality of the phonon gas is 3D, if λ_T is much shorter than the membrane thickness d. In the opposite limit, where $\lambda_T \gg d$, the phonon gas is 2D, the dimensionality cross-over happening when $\lambda_T \approx d$. This change in dimensionality can be seen in the temperature dependence of quantities like the heat capacity and the heat conductance of the membrane.

To illustrate this dimensionality cross-over, we calculate the heat capacity of an infinite membrane, where the phonon gas becomes quasi-2D below the cross-over temperature T_C. We will also show that the heat capacity of this quasi-2D system is proportional to T, rather than to T^2 as would be the case in a "real" 2D system.

The phononic heat capacity can in general be written as [18]

$$c_V = \frac{\hbar^2}{4k_BT^2}\sum_{\mu}\frac{\omega_\mu^2}{\sinh^2(\beta\hbar\omega_\mu/2)}\,, \tag{4.1}$$

where $\beta = (k_BT)^{-1}$ and μ denotes a set of quantum numbers that describe the phonon modes of the system in question (similar as in Section 3.3.3). Expressing c_V in terms of the phonon modes of the membrane, where $\mu = \sigma, m, k_\parallel$, we get

$$\begin{aligned} c_V &= \frac{\hbar^2 A}{8\pi k_BT^2}\sum_{\sigma,m}\int_0^\infty dk_\parallel\, k_\parallel \frac{\omega_{\sigma,m}^2(k_\parallel)}{\sinh^2(\beta\hbar\omega_{\sigma,m}(k_\parallel)/2)} \\ &= \frac{\hbar^2 A}{8\pi k_BT^2}\sum_{\sigma,m}\int_{\omega_{\sigma,m}(0)}^\infty d\omega\,\frac{dk_{\parallel,\sigma,m}}{d\omega}k_{\parallel,\sigma,m}(\omega)\frac{\omega^2}{\sinh^2(\beta\hbar\omega/2)} \\ &= \frac{k_BA}{8\pi}\sum_{\sigma,m}\int_{x_{\sigma,m}(0)}^\infty dx\left(\frac{d}{dx}\frac{k_{\parallel,\sigma,m}^2}{2}\right)\frac{x^2}{\sinh^2(x/2)}\,. \end{aligned} \tag{4.2}$$

Here we defined $x \equiv x_{\sigma,m}(k_\parallel) = \beta\hbar\omega_{\sigma,m}(k_\parallel)$. The lower limits $x_{\sigma,m}(0)$ of the integration in (4.2) are proportional to $1/T$, hence at very low temperatures we get that $x_{\sigma,m}(0) \to \infty$ for all $m > 0$ and $x_{\sigma,m=0} = 0$, which means that only the lowest branch of each polarization contributes to the heat capacity. In this low temperature limit, we can use the low energy expansions (3.13), (3.15) and (3.17) and get

$$\begin{aligned} c_V &= \frac{k_BA}{8\pi\hbar^2}\int_0^\infty dx\left(\left(\frac{1}{c_t^2}+\frac{1}{c_s^2}\right)x(k_BT)^2 + m^\star k_BT\right)\frac{x^2}{\sinh^2(x/2)} \\ &= \pi k_BA\left(\left(\frac{1}{c_t^2}+\frac{1}{c_s^2}\right)3\zeta(3)\left(\frac{k_BT}{\pi\hbar}\right)^2 + \frac{m^\star}{\pi\hbar}\zeta(2)\left(\frac{k_BT}{\pi\hbar}\right)\right)\,. \end{aligned} \tag{4.3}$$

The contributions of the lowest h and s modes lead to the expected T^2 dependence of the heat capacity in the limit of the phonon gas in the membrane being 2D. Due to its quadratic dispersion relation, the contribution of the lowest a mode, on the other hand, yields a term that is linear in T. For low enough temperatures this linear term will always dominate and the heat capacity becomes proportional to T rather than to the more intuitive T^2.

In the high temperature limit, the difference $\delta x_m = x_{\sigma,m+1} - x_{\sigma,m} \to 0$, which means that in principle we can convert the sum over m in (4.2) into an integral. In practice, however, we run into difficulties, as we do not have an explicit expression for the dispersion relations of the Lamb modes. To motivate the cross-over temperature in the membrane, we will thus only use the contribution of the h modes to the heat capacity, which we denote by $c_{V,h}$. Here the dispersion relation are explicitly given by Eq. (3.13) and Eq. (4.2) becomes

$$c_{V,h} = \frac{\pi k_B A}{8} \left(\frac{k_B T}{\pi \hbar}\right)^2 \sum_m \int_{\beta\hbar c_t m\pi/d}^{\infty} dx \, \frac{x^3}{\sinh^2(x/2)} \,. \tag{4.4}$$

For the h modes, the quantity δx_m is given by $\delta x_{m,h} = \beta\hbar c_t \pi/d$, which is small if $Td \gg \hbar c_t/k_B$. In this high temperature limit, we have a 3D phonon gas and recover the Debye law,

$$\begin{aligned} c_{V,h} &= \frac{\pi k_B A}{8} \left(\frac{k_B T}{\pi \hbar}\right)^2 \int_0^{\infty} dx' \, \frac{k_B T d}{\hbar \pi} \int_{x'}^{\infty} dx \, \frac{x^3}{\sinh^2(x/2)} \\ &= \frac{\pi k_B V}{8} \left(\frac{k_B T}{\pi \hbar}\right)^3 \int_0^{\infty} dx \int_0^{x} dx' \, \frac{x^3}{\sinh^2(x/2)} \\ &= 12\pi k_B V \zeta(4) \left(\frac{k_B T}{\pi \hbar}\right)^3 . \end{aligned} \tag{4.5}$$

In numerical calculations we can show that the Lamb modes have the same high temperature behaviour. We thus conclude that the phonon gas in the membrane is purely 2D if $Td \ll \hbar c_t/k_B$ and becomes 3D in the limit $Td \gg \hbar c_t/k_B$. Accordingly we define the cross-over temperature T_C as

$$T_C \equiv \frac{\hbar c_t}{2 k_B d} \,. \tag{4.6}$$

As the dominant thermal phonon frequency is of the order $k_B T/\hbar$, we can also formulate a cross-over condition by comparing the dominant thermal wavelength λ_T with the membrane thickness d. If λ_T is much larger than d, the phonon gas is 2D, while for $\lambda_T \ll d$ we work in the 3D limit. This

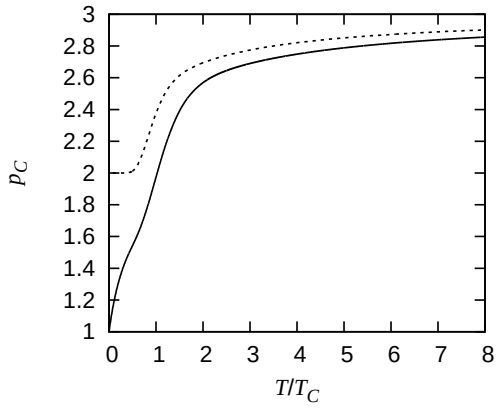

Figure 4.1: Logarithmic slope p_C of a thin membrane as function of temperature. T_C is the cross-over temperature, $T_C \equiv (\hbar c_t/2k_B) \times d^{-1}$. The dashed curve shows p_C for only the h modes, corresponding to the hypothetical case that longitudinal and transversal modes stay uncoupled in the membrane.

means that, even for a fixed temperature, the dimensionality of the phonon gas still depends on the membrane thickness. By rearranging Eq. (4.6) we thus define the cross-over thickness d_C as

$$d_C \equiv \frac{\hbar c_t}{2k_B T}\,. \tag{4.7}$$

As the heat capacity follows a power law in both the 2D and the 3D limit, the dimensionality of the phonon gas is easily made visible through the logarithmic slope of c_V, $p_C \equiv d\ln(c_V)/d\ln(T)$. In case of a given power law behaviour $c_V \propto T^\alpha$, p_C becomes equal to the exponent α. In Fig. 4.1, we plot p_C for a thin membrane as function of temperature. We also plot p_C for the h modes separately, as it shows very well the intuitively expected behaviour, i.e. p_C asymptotically approaches the value 3 for high temperatures and the value 2 for low temperatures.

4.2 Radiative heat transfer

In some experiments, it has been observed that the phonon transport in thin membranes is ballistic [7, 19]. In this limit, a device mounted on top of a membrane emits phonons similar to a photon black-body radiator, effectively being cooled in the process. In this section we call the device the heater and the part of the membrane below it the radiator. The electrons in the heater interact with the phonons in the heater and the radiator, which, if the electron-phonon coupling is strong enough, have a thermal distribution. A schematic drawing of the system is shown in Fig. 4.2. The arbitrarily

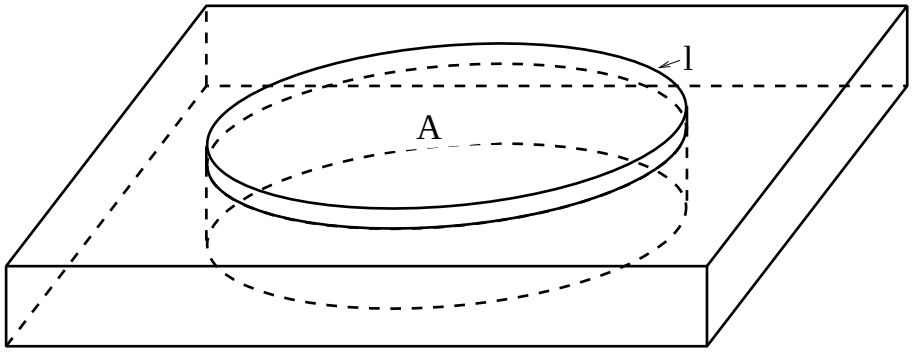

Figure 4.2: Schematic drawing of an electronic heat source with area A and circumference l mounted on a thin membrane. The membrane area directly below the heater (indicated by dashed lines) is assumed to be the radiating volume analog to a black body radiator. The area of the heater is much smaller than the total area of the membrane.

shaped heater is assumed to be 2D and has the area A and the circumference l. The radiator then has the same shape and a volume $V = Ad$, where d is the thickness of the membrane. The radiating surface is the part of the radiator surface that does not coincide with the membrane surfaces and is thus given by ld. To be precise, the following argumentation is only valid for concave radiator shapes, but if the radiator shape is not concave, an effective radiating surface can be found that fulfils this condition.

The heat flux $\dot{\mathbf{Q}}$ of the phonon field is given by [20]

$$\dot{\mathbf{Q}} = \frac{1}{V}\sum_{\mu}\hbar\omega_{\mu}\mathbf{v}_{\mu}n_{\mu}\,, \tag{4.8}$$

where $\mathbf{v}_{\mu}$ is the phonon group velocity, which in the membrane is $\partial\omega_{\mu}/\partial\mathbf{k}_{\|}$, and n_{μ} is the phonon distribution function. As we assume a thermal distribution, $n_{\mu} = n_{\mu,0}$ is equal to the Bose-Einstein distribution $1/(\exp(\beta\hbar\omega_{\mu})-1)$. The total radiated power can be calculated by integrating the heat flux of the phonon field over the emitting part of the radiator surface.

$$P = \int_{S} d\mathbf{s}\cdot\dot{\mathbf{Q}}_{\mathrm{out}}\,. \tag{4.9}$$

In our assumption, phonons are generated inside the radiator and propagate outwards through the radiator surface. Hence there is no flux into the radiator, which we indicated by the subscript *out* in Eq. (4.9). As the emitting surface is always perpendicular to the membrane surfaces, our surface integral becomes an integral over the circumference of the radiator,

$$P = \frac{d}{V}\oint_{l} dl\sum_{\mu}\hbar\omega_{\mu}n_{\mu}\hat{\mathbf{n}}_{l}\cdot\mathbf{v}_{\mu}\Theta(\hat{\mathbf{n}}_{l}\cdot\mathbf{v}_{\mu}/v_{\mu})$$

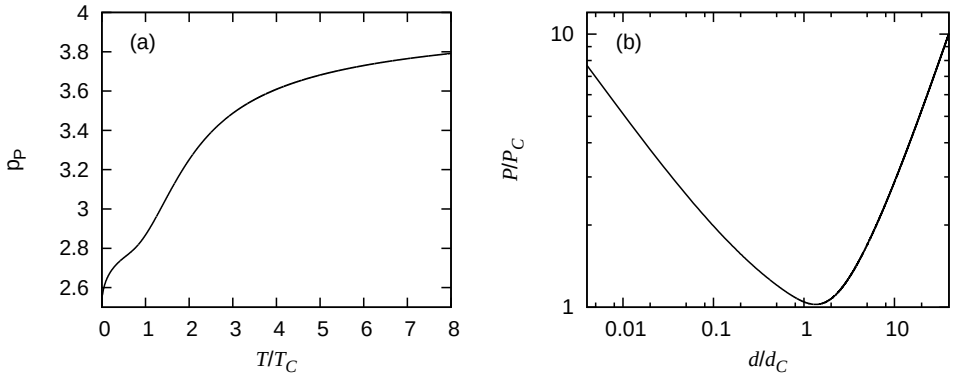

Figure 4.3: (a) Logarithmic slope $p_P \equiv d\ln(P)/d\ln(T)$ as function of temperature. (b) Radiated power as function of membrane thickness for a fixed temperature. Here we defined $P_C \equiv c_t l\hbar/\pi \times (k_B T/\hbar c_t)^3$.

$$= \frac{d}{V}\oint_l dl \sum_\mu \hbar\omega_\mu n_\mu |v_\mu| \cos(\vartheta)\Theta(\cos(\vartheta))\,. \tag{4.10}$$

The Θ-function assures that power can only flow out of the system, not into it. The unit vector $\hat{\mathbf{n}}_l$ is the surface normal on the area element $dl \times d$ and $|v_\mu|\cos(\vartheta)$ is the part of the group velocity that is perpendicular to the surface. Performing the summation over the phonon modes and remembering that $V = Ad$, the radiated power becomes

$$\begin{aligned} P &= \frac{1}{(2\pi)^2}\oint_l dl \sum_{\sigma,m} \int_{-\pi/2}^{\pi/2} d\vartheta\, \cos(\vartheta) \int_0^\infty dk_\parallel\, k_\parallel \hbar\omega_\mu |v_\mu| n_\mu \\ &= \frac{l}{2\pi^2}\sum_{\sigma,m}\int_0^\infty dk_\parallel \left|\frac{\partial\omega_\mu}{\partial k_\parallel}\right| \frac{k_\parallel\hbar\omega_\mu}{\exp(\beta\hbar\omega_\mu)-1}\,. \end{aligned} \tag{4.11}$$

Note that this result differs from the one we gave in Ref. [II] by a factor $4/\pi$, there we did not take the geometry of the problem properly into account.

Again, P can only be calculated numerically in the general case, but we can calculate analytic expressions for the 2D and 3D limits to get a qualitative picture. In the 3D limit the effect of the surfaces on the phonon modes becomes negligible. We therefore assume for this case that the bulk modes are decoupled and all have dispersion relations like the h modes, i.e. $\omega_{\sigma'} = c_{\sigma'}\sqrt{k_\parallel^2 + (m\pi/d)^2}$, with $\sigma' = t$ or l. Then the radiated power becomes

$$P_{3\mathrm{D}} = \frac{ld\hbar}{8\pi^2}\left(\frac{2}{c_t^2}+\frac{1}{c_l^2}\right)\left(\frac{k_B T}{\hbar}\right)^4 \Gamma(4)\zeta(4)\,. \tag{4.12}$$

$$\tag{4.13}$$

This is the classical 3D result [18], the radiated power is proportional to T^4 and is linearly proportional to the radiating surface, which means that $P_{3\mathrm{D}} \propto d$.

For the 2D limit, we use again the low energy expansions (3.13), (3.15) and (3.17), which leads to

$$\begin{aligned} P_{2\mathrm{D}} &= \frac{l\hbar}{2\pi^2}\left[\left(\frac{1}{c_t}+\frac{1}{c_s}\right)\Gamma(3)\zeta(3)\left(\frac{k_BT}{\hbar}\right)^3\right. \\ &\quad \left.+\sqrt{\frac{2m^\star}{\hbar}}\Gamma\left(\frac{5}{2}\right)\zeta\left(\frac{5}{2}\right)\left(\frac{k_BT}{\hbar}\right)^{5/2}\right]. \end{aligned} \tag{4.14}$$

This means that at low temperatures the radiated power becomes proportional to $T^{5/2}$. As function of the membrane thickness, $P_{2\mathrm{D}}$ is proportional to $1/\sqrt{d}$. This is somewhat surprising at first, as for a real 2D system one would expect that the thermal properties of the membrane are independent of d. The origin of this behaviour lies in the dispersion relation of the lowest a mode. As already stated, this mode behaves like a massive particle with the effective mass $m^\star$, which increases with decreasing membrane thickness.

In conclusion, if we decrease the membrane thickness starting from the 3D limit, the radiated power will decrease until it reaches a minimum at about the cross-over thickness d_C. If the membrane thickness is decreased further, the radiated power will increase again. In Fig. (4.3) we show the logarithmic slope $p_P \equiv d\ln(P)/d\ln(T)$ as function of temperature and the radiated power P as function of membrane thickness. As can be seen, for a fixed temperature, P has a minimum near the cross-over thickness d_C.

4.3 Diffusive heat transfer

Phenomenologically, the diffusive heat transfer, or heat conduction, is described by the equation [20]

$$\dot{\mathbf{Q}} = -\kappa\boldsymbol{\nabla}T\,, \tag{4.15}$$

where $\dot{\mathbf{Q}}$ is the heat flux per unit area and κ is called the heat conductivity. Thermodynamics usually only deals with systems of a single temperature T. Heat conduction, on the other hand, is a non-equilibrium effect that only occurs in the presence of a temperature gradient, which makes its treatment somewhat difficult. One therefore has to assume the variations in T to be small, such that we can have *local* equilibrium, where the temperature is considered to be homogeneous over sufficiently large areas and thus the phonon number n_μ can be defined. Neighbouring regions then have slightly different temperatures and n_μ becomes a function of position. As in Section 4.2, the heat flux is given by

$$\dot{\mathbf{Q}} = \frac{1}{V}\sum_\mu \hbar\omega_\mu \mathbf{v}_\mu n_\mu\,, \tag{4.16}$$

where $\mathbf{v}_\mu = \partial\omega_\mu/\partial\mathbf{k}$ is the group velocity and n_μ is the phonon distribution function. In equilibrium, n_μ is equal to the Bose-Einstein distribution $n_{\mu,0}$, which means that every phonon propagation direction is equally populated. Hence, there is no net heat flux and the contribution of $n_{\mu,0}$ to Eq. (4.16) vanishes. This means that only deviations from the equilibrium distribution give a non-zero contribution to the heat flux. If we write the distribution function as $n_\mu = n_{\mu,0} + \delta n_\mu$, Eq. (4.16) becomes

$$\dot{\mathbf{Q}} = \frac{1}{V}\sum_\mu \hbar\omega \mathbf{v}_\mu \delta n_\mu \,. \tag{4.17}$$

As the phonons of type μ all travel with the same velocity, the distribution n_μ at position $\mathbf{r}$ must be the same as the distribution at place $\mathbf{r} - \mathbf{v}_\mu dt$ was some infinitesimal time step dt ago. If there is phonon decay in the system, part of the phonons will have decayed during time dt. This gives us the equality

$$n_\mu(\mathbf{r}, t) = n_\mu(\mathbf{r} - \mathbf{v}_\mu dt, t - dt) + \left(\frac{\partial n_\mu}{\partial t}\right)_{decay} dt \,. \tag{4.18}$$

Taylor expanding the left and right side up to first order, this becomes

$$0 = -\frac{\partial n_\mu}{\partial t} - \mathbf{v}_\mu \cdot \boldsymbol{\nabla} n_\mu + \left(\frac{\partial n_\mu}{\partial t}\right)_{decay} . \tag{4.19}$$

As we are only considering stationary situations, the partial time derivative of n_μ is zero. Furthermore, by introducing the relaxation time τ_μ, we can express the decay term as

$$\begin{aligned} \left(\frac{\partial n_\mu}{\partial t}\right)_{decay} &= -\frac{n_\mu - n_{\mu,0}}{\tau_\mu} \\ &= -\frac{\delta n_\mu}{\tau_\mu} \,, \end{aligned} \tag{4.20}$$

and thus get an expression for δn_μ,

$$\delta n_\mu = -\tau_\mu \mathbf{v}_\mu \frac{\partial n_{\mu,0}}{\partial T} \boldsymbol{\nabla} T \,. \tag{4.21}$$

Here we replaced n_μ with $n_{\mu,0}$, as we are only considering steady-state situations and small deviations from equilibrium. Inserting (4.21) into (4.17), we arrive at the final expression for the heat flux,

$$\dot{\mathbf{Q}} = -\frac{1}{V}\sum_\mu \hbar\omega_\mu \tau_\mu \frac{\partial n_\mu}{\partial T} \mathbf{v}_\mu \cdot (\mathbf{v}_\mu \cdot \boldsymbol{\nabla} T) \tag{4.22}$$

If, like for example in isotropic systems, no other quantities but $\mathbf{v}_\mu$ in Eq. (4.22) depend on the direction of the wave vector, the expression for the heat

flux reduces further, as the angle integration in (4.22) yields $\langle v_i v_j \rangle = \delta_{ij} v^2/3$ for 3D systems and $\delta_{ij} v^2/2$ for 2D systems. The expression for the heat flux then reads

$$\dot{\mathbf{Q}} = -\frac{1}{3V} \sum_{\mu} \hbar \omega_\mu \tau_\mu \frac{\partial n_\mu}{\partial T} v_\mu^2 \boldsymbol{\nabla} T \,. \tag{4.23}$$

Together with Eq. (4.15) we can then extract an expression for the heat conductivity κ. In Sections 4.4 and 4.5 we will use Eqs. (4.22) and (4.23) to calculate the heat conductivity in specific systems.

4.4 Heat transfer along narrow bridges

A common problem in experiments is to thermally insulate a nanoscale device that is mounted on top of a thin, dielectric membrane. To do this most efficiently, the membrane is often cut in such a way that the central part that carries the device is connected to the bulk by narrow bridges. A schematic drawing of such a structure and one of the bridges is shown in Fig. 4.4. The width w of these bridges can be as small as 4 µm [4, 8], while their lengths are of the order of 100 µm. We want to discuss this problem in a regime where the phonon mean free path in the uncut membrane is of the order of or bigger than w, while the dominant thermal phonon wavelength is much smaller than the width of the bridge, so that the phonon modes of the uncut membrane are still applicable.

As the width of the bridge becomes smaller than the phonon mean free path, the interaction of phonons with the edges of the bridge should become the main scattering mechanism. We assume the scattering at the edges to be diffusive, meaning that scattered phonons are uniformly distributed over the angles, branches and polarizations that correspond to the same angular frequency ω. This assumption is justified if the variance of the scattering surface is of the order of the phonon wavelength [4].

As indicated in Fig. 4.4, we assume the bridge for the following derivation to be oriented along the x direction. If we consider the heat flux through the cross-section $d \times w$ of the bridge of total length l, expression (4.23) becomes

$$\dot{Q}_x = -\frac{1}{l} \sum_{\mu} \hbar \omega_\mu \tau_\mu v_{\mu,x}^2 \frac{\partial n_\mu}{\partial T} \frac{\partial T}{\partial x} \,. \tag{4.24}$$

Here τ_μ is an effective scattering time, corresponding to many different scattering mechanisms. If we denote the scattering time of the uncut membrane by $\tau_{M,\mu}$ and the scattering time due to the scattering at the edges of the bridge by $\tau_{E,\mu}$, we can write the the effective scattering time as

$$\tau_\mu^{-1} = \tau_{M,\mu}^{-1} + \tau_{E,\mu}^{-1} \,. \tag{4.25}$$

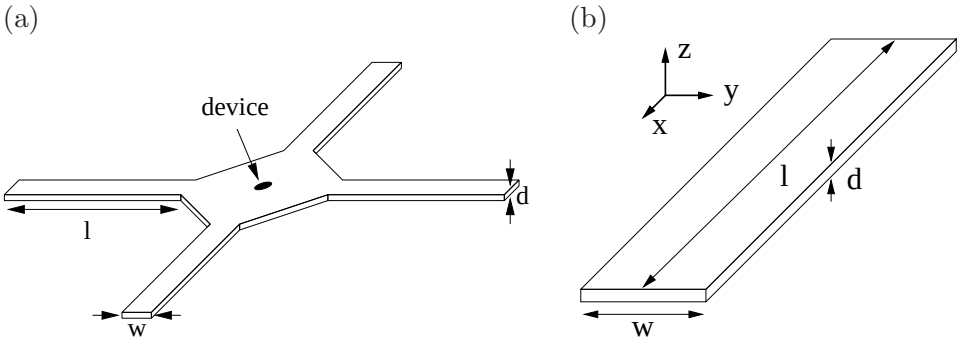

Figure 4.4: (a) Schematic drawing of a suspended nanostructure. The membrane is cut in such a way that the device is mounted on the wider central part, which itself is connected to the bulk by narrow bridges. (b) The geometry of a bridge as it is assumed in the calculations.

In our diffusive model, the scattering time $\tau_{E,\mu}$ can be approximated by the time that a phonon needs to travel from one edge to the other,

$$\tau_{E,\mu} = \frac{w}{v_\mu |\sin(\vartheta)|}, \tag{4.26}$$

where ϑ is the angle between $\mathbf{k}_\parallel$ and the x direction. We transform the summation over $\mathbf{k}_\parallel$ in Eq. (4.24) into an integral and use Eq. (4.23) with a one-dimensional temperature gradient to obtain an expression for the heat conductivity along the bridge,

$$\begin{aligned} \kappa &= \frac{w}{2\pi} \sum_{\sigma,m} \int_0^{2\pi} d\vartheta \int_0^{\infty} dk_\parallel \, k_\parallel \hbar\omega_\mu \frac{v_\mu^2 \cos^2(\vartheta)}{v_\mu |\sin(\vartheta)|/w + 1/\tau_{M,\mu}} \frac{\partial n_\mu}{\partial T} \\ &= \frac{w^2}{2\pi} \sum_{\sigma,m} \int_0^{\infty} dk_\parallel \, k_\parallel \hbar\omega_\mu \frac{\partial n_\mu}{\partial T} v \int_0^{2\pi} d\vartheta \, \frac{\cos^2(\vartheta)}{|\sin(\vartheta)| + w/l_{M,\mu}}, \end{aligned} \tag{4.27}$$

where we introduced the mean free path of the uncut membrane, $l_{M,\mu} \equiv v_\mu \tau_{M,\mu}$. Denoting $x \equiv w/l_{M,\mu}$, we can write the integral over the angle ϑ as

$$\begin{aligned} C(x) &\equiv \int_0^{2\pi} d\vartheta \, \frac{\cos^2(\vartheta)}{|\sin(\vartheta)| + x} \\ &= 4\left[\frac{x\pi}{2} - 1 + \sqrt{1-x^2} \ln\left(\frac{1}{x} + \sqrt{\frac{1}{x^2} + 1} \right) \right]. \end{aligned} \tag{4.28}$$

If edge scattering dominates, i.e. $x \ll 1$, the integral depends only logarithmically on x,

$$C(x) \approx 4 \log\left(\frac{2}{xe} \right). \tag{4.29}$$

Considering the small bandwidth of occupied phonon modes as well as the long mean free paths in the free membranes at low temperatures, we can consider $C(x) \approx C = \text{const}$ over the temperature range that we work in.

This effectively constant mean free path allows us to evaluate the heat conductivity along the bridge. In the low temperature limit, we can again derive an analytic expression, using the expansions (3.13), (3.15) and (3.17),

$$\begin{aligned} \kappa &= 3Cw^2 k_B \pi \left[\zeta(3) \left(\frac{1}{c_t} + \frac{1}{c_s} \right) \left(\frac{k_B T}{\pi \hbar} \right)^2 \right. \\ &\quad \left. + \sqrt{\frac{2m^\star}{\hbar}} \frac{5}{16} \zeta\left(\frac{5}{2} \right) \left(\frac{k_B T}{\pi \hbar} \right)^{3/2} \right] . \end{aligned} \tag{4.30}$$

This means that in the 2D limit at very low temperatures the heat conductivity along narrow bridges becomes proportional to $T^{3/2}$. In Ref. [4], the central part of the membrane of the geometry in Fig. 4.4a has been heated with an AC current. At low frequencies the temperature of the central part follows the signal, but becomes constant above the cutoff frequency f_c. This cutoff frequency is given by $f_c = \kappa l / c_V$, where c_V is the heat capacity of the membrane. Using expressions (4.3) and (4.30), we get that in the low temperature limit $f_c \propto T^{1/2}$. In Ref. [4] such an increase has been measured for narrow enough bridges.

4.5 Heat transfer in amorphous membranes

The SiN_x membranes that are usually used in experiments are grown by plasma-enhanced chemical vapour deposition (PECVD) on top of crystalline silicon, which is afterwards etched away. Due to this fabrication process, the membranes are amorphous with very little short-range structural ordering [21]. Amorphous materials differ significantly from crystals in many ways, especially at low temperatures. For 3D bulks for instance, the heat capacity is proportional to T rather than to T^3, while the heat conductivity is proportional to T^2 [9, 10]. To explain these temperature dependencies, the concept of dynamic defects was introduced. Due to the absence of a crystalline structure, the position and orientation of many atoms or groups of atoms is not fixed and they may tunnel between two close minima in configuration space, which is modeled by introducing an ensemble of two-level systems (TLS) [22, 23]. If the energy splitting between these minima is $\lesssim k_B T$, the TLS can be excited and thus contribute to the heat capacity. As TLSs are very sensitive to strain in the material, they provide a scattering mechanism for phonons, thus reducing the phonon mean free path and accordingly the heat conductivity.

An effective double-well potential and the tunneling of the atom between the two wells are depicted in Fig. 4.5 [22, 23]. Written in the 2D Hilbert space

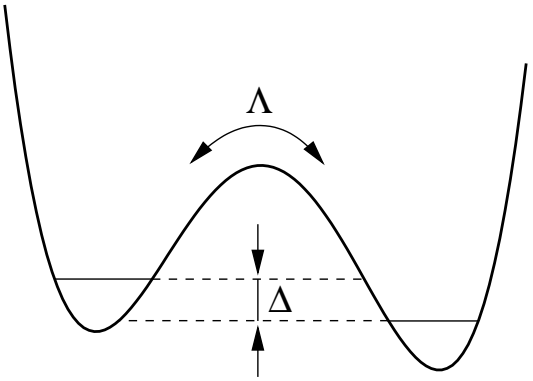

Figure 4.5: An atom or a group of atoms moves in an effective potential like this. The separation Δ between the ground states in the two wells is much smaller than the energy scale of the oscillation frequency ω_0 in the wells.

spanned by the ground states of the two wells, the effective Hamiltonian of this TLS reads

$$H_{\rm TLS} = \frac{\Delta}{2}\sigma_z - \frac{\Lambda}{2}\sigma_x\,, \tag{4.31}$$

where Δ is called the asymmetry of the potential and the tunnel splitting Λ describes the tunneling between the two wells. σ_x and σ_z are Pauli matrices.

The Hamiltonian (4.31) can be diagonalized by applying an orthogonal transformation O,

$$\begin{aligned} H'_{\rm TLS} &\equiv O^T H_{\rm TLS} O \\ &= \frac{\epsilon}{2}\sigma_z \end{aligned} \tag{4.32}$$

where $\epsilon \equiv \sqrt{\Delta^2 + \Lambda^2}$ is the excitation energy of this TLS.

The Hamiltonian parameters Δ and Λ are distributed with the density $P(\Delta, \Lambda)$. According to the standard tunneling model (STM), $P(\Delta, \Lambda)$ is assumed to have the form [9]

$$P(\Delta, \Lambda) = P_0/\Lambda\,, \tag{4.33}$$

where P_0 is a constant. In the later calculations however, it will prove more practical to express P in terms of the variables ϵ and $u \equiv \Lambda/\epsilon$, where [9]

$$P(\epsilon, u) = \frac{P_0}{u\sqrt{1-u^2}}\,. \tag{4.34}$$

The strain caused by the phonon field adds a perturbation to $H_{\rm TLS}$, which we denote by H_1. With the total Hamiltonian $H = H_{\rm TLS} + H_1 + H_{\rm ph}$

we can now describe the coupling between the phonon field and a TLS. In the STM, H_1 is assumed to be diagonal, i.e. the variation of the off-diagonal elements of $H_{\rm TLS}$ are neglected [22, 23, 24, 25, 9],

$$H_1 \;=\; \frac{1}{2}\delta\sigma_z\,. \tag{4.35}$$

The perturbation δ is linear in the strain field [25, 9] and in general may be written as

$$\delta \;=\; 2\gamma_{ij}\left((S_\mu)_{ij}b_\mu + (S_\mu^\star)_{ij}b_\mu^\dagger\right)\,, \tag{4.36}$$

where γ_{ij} is a general tensor that describes the coupling between the strain field and the TLS. $b_\mu^\dagger$ and b_μ are phonon creation and annihilation operators, as defined in Section 3.3. For the sake of simplicity, we will omit the dependence of δ on these operators at first, but will later write it out explicitly again. In the discussion of the perturbation H_1, we are not interested in static strains, as these would just slightly renormalize the eigenvalues of the Hamiltonian. Instead, since thermal and transport properties of insulators are determined by vibrations, we consider time-dependent strains like the ones caused by phonons. Such time-dependent perturbations cause transitions of the TLS between its two unperturbed eigenstates, which in turn contribute to phonon scattering and thus limit the phonon mean free path and ultimately the heat conductance. In order to calculate these phonon-induced transition rates of the TLS from one eigenstate to another, we have to write H_1 in the basis that diagonalizes $H_{\rm TLS}$,

$$\begin{aligned} H_1' \;&\equiv\; O^T H_1 O \\ &=\; \frac{\delta}{2\epsilon}\left(\Delta\sigma_z - \Lambda\sigma_x\right)\,. \end{aligned} \tag{4.37}$$

In the STM the TLS interacts with 3D, transversally or longitudinally polarized, plane waves, with all the components of the strain tensor being proportional to the absolute value k of the wave vector $\mathbf{k}$. A longitudinal wave will produce a compressional strain of the form $(S_{xx}, S_{yy}, S_{zz}, 0, 0, 0)^T$, while the shear strain that is produced by a transversal wave is of the form $(0, 0, 0, 2S_{yz}, 2S_{xz}, 2S_{xy})^T$. In this case, the expression for δ is always reduced to $\delta_\sigma = 2C_\sigma N_\sigma \gamma_\sigma k_\sigma$, where $\sigma = \{t, l\}$ denotes the polarization as usual. C_σ was given in (3.54) and the N_σ are the normalization constants of the phonon displacement field. γ_σ is called the deformation potential parameter or coupling constant. Since $C_\sigma N_\sigma$ has dimensions of length, $C_\sigma N_\sigma k_\sigma$ is dimensionless and γ_σ has dimensions of energy.

If the boundaries of a system are taken into account when calculating its phonon modes, the above simplifications are no longer valid, as transversal and longitudinal waves are coupled to each other and we can no longer speak

of *one* wave vector $\mathbf{k}$. To describe the TLS-phonon interaction in finite-sized systems correctly, we thus need to write the interaction Hamiltonian of the STM in a more general form. To do so, we will start from the full expression for δ of Eq. (4.36), $\delta = \gamma_{ij} S_{ij}$, where γ_{ij} are the components of the 3×3 tensor $[\gamma]$, and discuss the general properties of the $[\gamma]$ in more detail.

In general we can write $[\gamma]$ as a sum of a symmetric and an antisymmetric tensor, $[\gamma] \equiv [\gamma]_S + [\gamma]_A$. As the dyadic product between an antisymmetric and a symmetric tensor is zero and the strain tensor $[S]$ is a symmetric tensor, we have $\gamma_{ij} S_{ij} = (\gamma_S)_{ij} S_{ij}$. Hence the antisymmetric part of $[\gamma]$ has no physical implications and we postulate that $[\gamma] \equiv [\gamma]_S$ is symmetric. This in turn allows us to use abbreviated subscripts, since all tensors in our model are symmetric. In this notation, we can write δ as $\delta = 2\boldsymbol{\gamma}^T \cdot \mathbf{S}$, where we defined

$$\boldsymbol{\gamma} \quad = \quad (\gamma_{xx}, \gamma_{yy}, \gamma_{zz}, \gamma_{yz}, \gamma_{xz}, \gamma_{xy})^T \,. \tag{4.38}$$

As explained before, a TLS is imagined to be an atom or group of atoms that can tunnel between two potential wells. This can for instance be a translation or a rotation [26]. In either case, there is a direction associated to the TLS, which we denote by $\hat{\mathbf{t}}$. In the case of a translation, $\hat{\mathbf{t}}$ would point along the line that connects the two potential wells, while in the case of a rotation, $\hat{\mathbf{t}}$ would point along the rotational axis. Naturally one would expect that the orientation of the TLS relative to the phonon's propagation direction and polarization has an effect on the interaction strength. Without building a microscopic model of the TLS, we have no other quantities that describe the TLS apart from the three components of $\hat{\mathbf{t}}$. The simplest symmetric 3×3 tensor that can be constructed out of these components is of the form $T_{ij} \equiv t_i t_j$, which in abbreviated subscript notation reads

$$\mathbf{T} \quad = \quad (t_x^2, t_y^2, t_z^2, 2t_y t_z, 2t_x t_z, 2t_y t_z)^T \,. \tag{4.39}$$

As the vector $\boldsymbol{\gamma}$ should contain the information about the orientation of the TLS as well as its deformability in presence of a strain field, we construct $\boldsymbol{\gamma}$ in the most general way as $\gamma_{kl} \equiv R_{ijkl} T_{ij}$, where, because of the symmetry of $[\gamma]$, $R_{ijkl} = R_{ijlk}$. Because $[T]$ is a symmetric tensor as well, the sum $R_{ijkl} T_{ij}$ can be written as $T_{ij}(R_{ijkl} + R_{jikl})$, which allows us to also choose $R_{ijkl} = R_{jikl}$. With these symmetries we can write also $[R]$ in abbreviated subscript notations, where R_{ijkl} becomes R_{IJ}, similar to the tensor of elastic stiffness constants $[[c]]$, and we can write $\boldsymbol{\gamma}$ as

$$\boldsymbol{\gamma} \equiv [R]^T \cdot \mathbf{T} \,. \tag{4.40}$$

In Eq. (4.40), the tensor $[R]$ contains all the relevant deformation potential parameters. Still, $[R]$ cannot be taken arbitrary but is instead, like the tensor of elastic stiffness constants (2.6), restricted by the symmetry properties of

the material. How exactly a TLS responds to strain in the material depends on the atoms that surround it. As we do not want to build a microscopic model for the TLS, we make the simplest possible assumption about the atoms in the vicinity of the TLS, which is to assume that we have an isotropic mass distribution also in the microscopic surrounding of the TLS.

With this assumption, we can use the invariance of the scalar quantity $h_1 \equiv \mathbf{T}^T \cdot [R] \cdot \mathbf{S}$ under any coordinate rotation to derive the properties of $[R]$. We do this with the help of some simple transformations in specific settings regarding $[S]$ and $[T]$. The procedure of finding the properties of $[R]$ is given in Appendix C. There we deduce that $[R]$ can be written as $[R] = \tilde{\gamma}[r]$, with

$$[r] \;=\; \begin{pmatrix} 1 & \zeta & \zeta & 0 & 0 & 0 \\ \zeta & 1 & \zeta & 0 & 0 & 0 \\ \zeta & \zeta & 1 & 0 & 0 & 0 \\ 0 & 0 & 0 & \xi & 0 & 0 \\ 0 & 0 & 0 & 0 & \xi & 0 \\ 0 & 0 & 0 & 0 & 0 & \xi \end{pmatrix} \tag{4.41}$$

and the additional condition that $\zeta + 2\xi = 1$. This means that the matrix $[R]$ is, like the tensor of elastic stiffness constants $[c]$, given by only two parameters, $\tilde{\gamma}$ and either ζ or ξ. In the following we will use ξ as the second parameter.

Although the form of $[R]$ is very general, there may be more than one type of TLSs in any given material. For such different types, the values for $\tilde{\gamma}$ and ξ may very well vary. For example for the aforementioned translational and rotational types of TLSs [26], $[R]$ may be different. However, in experiments it may be difficult to distinguish between different types of TLSs and most likely only averages will be seen.

With these new definitions, we are now able to write out our generalized version of the interaction Hamiltonian. The new expression for δ is now

$$\delta = 2\tilde{\gamma}\mathbf{T}^T \cdot [r] \cdot \mathbf{S} \tag{4.42}$$

and we thus have all the ingredients we need. For calculations of physical quantities, we have to write H_1 in second quantization. The phonon field has already been quantized in Chapter 3. The second quantization of the TLSs is a simple matter. As TLSs have only two energy levels, they effectively behave like spins. We therefore denote the TLS ground state by $|\downarrow\rangle$ and the excited state by $|\uparrow\rangle$. The fermionic excitation and de-excitation operators $a^\dagger$ and a, respectively, are connected to the Pauli matrices as $\sigma_x = a^\dagger + a$ and $\sigma_z = (2a^\dagger a - 1)$. $a^\dagger$ and a obey fermionic commutation relations and thus $a^\dagger|\downarrow\rangle = |\uparrow\rangle$, $a^\dagger|\uparrow\rangle = 0$, $a|\downarrow\rangle = 0$ and $a|\uparrow\rangle = |\downarrow\rangle$. With these definitions and δ in the form (4.36), the full interaction Hamiltonian reads

in the basis that diagonalizes $H_{\rm TLS}$,

$$\tilde{H}_1 = \frac{\tilde{\gamma}\Delta}{\epsilon}\mathbf{T}^T\cdot[r]\cdot\sum_\mu\left[\mathbf{S}_\mu b_\mu+\mathbf{S}_\mu^\star b_\mu^\dagger\right]\Big((2a^\dagger a-1)-(a^\dagger+a)\Big)\,, \quad (4.43)$$

where we used the notation $\tilde{H}_1$ to distinguish this form from the one in Eq. (4.37). In first order perturbation theory, only the off-diagonal terms of $\tilde{H}_1$, which are given by the term $(a^\dagger + a)$ in Eq. (4.43), enter the expressions for the phonon emission and absorption rates. As we do not consider higher order processes here, the diagonal elements $(2a^\dagger a - 1)$ do not enter the description.

4.5.1 Scattering times

In order to calculate the heat conductivity that results from TLS-phonon scattering, we need to calculate the phonon scattering times. In first order perturbation theory the only allowed interaction processes are the excitation of an unexcited TLS through absorption of a phonon and the reverse process of a phonon emission by a TLS that at the same time relaxes into the ground state. We denote the TLS-phonon quantum states by $|n_\mu,\downarrow\rangle$ and $|n_\mu,\uparrow\rangle$, where, as in Section 4.3, n_μ denotes the population of phonons in state μ. Using Eq. (4.43) and defining $M_\mu \equiv \mathbf{T}^T\cdot[r]\cdot\mathbf{S}$, we write the absorption amplitude of a phonon by a TLS as

$$\langle n_\mu,\uparrow|\tilde{H}_1|n_\mu+1,\downarrow\rangle = -\frac{\tilde{\gamma}\Lambda}{\epsilon}\sqrt{\frac{\hbar n_\mu}{2\rho\omega_\mu}}M_\mu\,. \quad (4.44)$$

Applying Fermi's golden rule, we calculate the phonon absorption and emission rates, respectively

$$\Gamma^\mu_{abs} = \frac{\pi}{\rho\omega_\mu}\frac{\tilde{\gamma}^2\Lambda^2}{\epsilon^2}|M_\mu|^2 n_\mu\delta(\hbar\omega_\mu-\epsilon) \quad (4.45a)$$

$$\Gamma^\mu_{em} = \frac{\pi}{\rho\omega_\mu}\frac{\tilde{\gamma}^2\Lambda^2}{\epsilon^2}|M_\mu|^2 (n_\mu+1)\delta(\hbar\omega_\mu-\epsilon)\,, \quad (4.45b)$$

where ϵ is the excitation energy of the TLS as defined in (4.32) and ω_μ is the angular frequency of the phonon. The quantities Γ^μ_{abs} and Γ^μ_{em} describe the absorption and emission rates of an arbitrary phonon by a TLS with orientation $\hat{\mathbf{t}}$. In an amorphous solid the orientations of the TLSs are arbitrary and their distribution is uniform. The for us relevant quantities are thus the averages of Γ^μ_{abs} and Γ^μ_{em} over the directions $\hat{t}$. We denote these averages by $\langle\cdot\rangle$. As the only quantities in (4.45a) and (4.45b) are $|M_\mu|^2$, the averaged expressions for the absorption and emission rates become

$$\langle\Gamma^\mu_{abs}\rangle = \frac{\pi}{\rho\omega_\mu}\frac{\tilde{\gamma}^2\Lambda^2}{\epsilon^2}\langle|M_\mu|^2\rangle n_\mu\delta(\hbar\omega-\epsilon) \quad (4.46a)$$

$$\langle\Gamma^\mu_{em}\rangle = \frac{\pi}{\rho\omega_\mu}\frac{\tilde{\gamma}^2\Lambda^2}{\epsilon^2}\langle|M_\mu|^2\rangle (n_\mu+1)\delta(\hbar\omega-\epsilon)\,, \quad (4.46b)$$

The explicit form of $\langle|M_\mu|^2\rangle$ depends on the geometry of the system and will be given explicitly in the later sections. Note that for finite systems the amplitude of $\langle|M_\mu|^2\rangle$ also depends on position. As we assume a spatially uniform distribution of TLSs also in finite systems, the expressions $|M_\mu|^2$ are again the only quantity that depends on position and we will in such cases also include an average over position into the expressions $\langle|M_\mu|^2\rangle$.

Each TLS is characterized by the energy splitting ϵ and the ratio $u = \Lambda/\epsilon$. We denote the probability that such a TLS is excited by $f_{\epsilon,u}$, with $0 < f_{\epsilon,u} < 1$. In thermal equilibrium, $f_{\epsilon,u}$ equals the Fermi-Dirac distribution, which we denote by $f_{\epsilon,u,0}$. Similar as in Section 4.3, we denote the deviations of $f_{\epsilon,u}$ from $f_{\epsilon,u,0}$ by $\delta f_{\epsilon,u}$. Then the time variation of $\delta f_{\epsilon,u}$ is

$$\begin{aligned}\delta\dot{f}_{\epsilon,u} &= \sum_\mu \left(\langle\Gamma^\mu_{abs}\rangle(1-f_{\epsilon,u}) - \langle\Gamma^\mu_{em}\rangle f_{\epsilon,u}\right) \\ &= \frac{\pi}{\rho}\frac{\tilde{\gamma}^2\Lambda^2}{\epsilon^2}\sum_\mu \frac{1}{\omega}\langle|M_\mu|^2\rangle \\ &\quad\times\left(\delta n_\mu \tanh(\beta\epsilon/2) - \delta f_{\epsilon,u}\coth(\beta\epsilon/2)\right)\delta(\hbar\omega_\mu-\epsilon)\,, \quad (4.47)\end{aligned}$$

where we neglected the second order terms of the form $\delta n\delta f$ and used the equality $n_0(1-f_0)-(n_0+1)f_0 = 0$ in the case that $\hbar\omega = \epsilon$. For n_μ we use the same definition as in Section 4.3 and get for the time variation of δn_μ

$$\begin{aligned}\delta\dot{n}_\mu &= \sum_{u,\epsilon}\left(\langle\Gamma^\mu_{em}\rangle(f_{\epsilon,u}) - \langle\Gamma^\mu_{abs}\rangle(1-f_{\epsilon,u})\right) \\ &= \frac{\pi}{\rho}\frac{\tilde{\gamma}^2}{\omega}\sum_{\epsilon,u} u^2\langle|M_\mu|^2\rangle \\ &\quad\times\left(\delta f_{\epsilon,u}\coth(\beta\epsilon/2) - \delta n_\mu\tanh(\beta\epsilon/2)\right)\delta(\hbar\omega_\mu-\epsilon)\,. \quad (4.48)\end{aligned}$$

In order to use expression (4.23) for the calculation of the heat conductivity, we need to write Eqs. (4.47) and (4.48) in the relaxation time approximation, i.e. $\delta\dot{f}_{\epsilon,u} = -\delta f_{\epsilon,u}/\tau_{\epsilon,u}$ and $\delta\dot{n}_\mu = -\delta n_\mu/\tau_\mu$. To do so, we need to eliminate the respective first term on the right hand side of Eqs. (4.47) and (4.48). For this we make the usual assumption [27] that the deviation δn_μ has the form

$$\delta n_\mu = \mathbf{a}(k_\mu)\cdot\hat{\mathbf{k}}_\mu\,. \quad (4.49)$$

Here the vectors $\mathbf{a}(k_\mu)$ all point along the direction of the heat flow, while their amplitude may only depend on the phonon polarization and the absolute value of the wave vector, but not on its direction $\hat{\mathbf{k}}_\mu$. As $\langle|M_\mu|^2\rangle$ does not depend on $\hat{\mathbf{k}}_\mu$, the first term on the right hand side of Eq. (4.47) indeed cancels out and we can write $\delta\dot{f}_{\epsilon,u}$ in the relaxation time approximation, which gives

$$\tau_\epsilon^{-1} = \frac{\pi}{\rho}\frac{\tilde{\gamma}^2\Lambda^2}{\epsilon^2}\coth(\beta\epsilon/2)\sum_\mu\frac{1}{\omega_\mu}\langle|M_\mu|^2\rangle\delta(\hbar\omega_\mu-\epsilon)\,. \quad (4.50)$$

As, due to the assumption (4.49), the sum $\sum_{\hat{\mathbf{k}}} \delta n_\mu$ over the directions $\hat{\mathbf{k}}_\mu$ is zero for all energies, the average population of phonon energy levels is equal to the thermal population. The TLS distribution on the other hand can only be driven out of equilibrium due to interactions with the phonon gas. Since the average population of phonon modes at each energy level corresponds to the thermal distribution, we assume the same for the TLSs, i.e. $\sum_u \delta f_{\epsilon,u} = 0$. This leads to the cancellation of the first term on the right hand side of Eq. (4.48), which in turn allows us to use the relaxation time approximation also there, hence

$$\begin{aligned} \tau_\mu^{-1} &= \frac{\pi}{\rho}\frac{\tilde{\gamma}^2}{\omega_\mu}\sum_{\epsilon,u} u^2 \langle |M_\mu|^2 \rangle \tanh(\beta\epsilon/2)\delta(\hbar\omega_\mu - \epsilon) \\ &= \frac{\pi\tilde{\gamma}^2 V P_0}{\rho\omega_\mu}\langle |M_\mu|^2 \rangle \tanh(\beta\hbar\omega/2)\,. \end{aligned} \tag{4.51}$$

In the second step of Eq. (4.51) the summation over u and ϵ has been changed into an integral and we inserted the TLS density (4.34).

Inserting Eq. (4.51) into Eq. (4.23), we get the most general result for the heat conductivity in amorphous insulators that can be derived without entering the specific phonon modes of the system in question.

$$\kappa = \frac{\hbar\rho}{3\pi V^2}\frac{1}{\tilde{\gamma}^2 P_0}\sum_\mu \frac{\omega_\mu^2 v_\mu^2}{\langle |M_\mu|^2 \rangle}\coth(\beta\hbar\omega/2)\frac{\partial n_\mu}{\partial T} \tag{4.52}$$

In Sections 4.5.2 and 4.5.3 we will explicitly calculate the expressions $\langle |M_\mu|^2 \rangle$ for 3D bulk phonons and for the phonon modes of thin membranes, respectively.

4.5.2 3D phonons

As stated earlier, the phonon modes of 3D bulk systems are either transversally or longitudinally polarized plane waves and the quantities $\langle |M_\mu|^2 \rangle$, where $\mu = \sigma, \mathbf{k}$ and $\sigma = l$ or t, are easily calculated. If we assume the phonon wave vector to be parallel to the z axis and the transversal phonons to be polarized along the x and y axes, we get

$$M_{t,1} = 2ikt_x t_z \xi/\sqrt{V} \tag{4.53}$$

$$M_{t,2} = 2ikt_y t_z \xi/\sqrt{V} \tag{4.54}$$

$$M_l = ik(1 - 2(t_x^2 + t_y^2)\xi)/\sqrt{V} \tag{4.55}$$

where the $\hat{t} = (t_x, t_y, t_z)^T$ describes the orientation of the TLS. Averaging the absolute square of M_t and M_l over all TLS orientations, we get

$$\langle |M_\sigma|^2 \rangle = \frac{k^2}{V} C_\sigma\,, \tag{4.56}$$

where we defined the constants C_t and C_l as

$$C_t = \frac{4}{15}\xi^2 . \tag{4.57}$$

$$C_l = \frac{1}{15}(15 - 40\xi + 32\xi^2) \tag{4.58}$$

Even though we are not able to make any statement about the range of values of ξ, we can still make the interesting prediction that

$$C_l > C_t \geq 0 \text{ for any } \xi . \tag{4.59}$$

Entering the expression for $\langle |M_\sigma|^2 \rangle$ into the expression for the heat conductivity (4.52), we get

$$\kappa = \frac{\rho k_B^3}{6\pi\hbar^2}\left(\frac{2c_t}{\tilde{\gamma}^2 C_t P_0} + \frac{c_l}{\tilde{\gamma}^2 C_l P_0}\right) T^2 . \tag{4.60}$$

This is exactly the result that one obtains from the STM [28], with γ_σ^2 replaced by $\tilde{\gamma}^2 C_\sigma$. But with Eq. (4.59) this means that we have shown for the STM parameters γ_t and γ_l that $\gamma_l > \gamma_t$, which is in agreement with the experimental data we know of [28, 9, 29, 30].

The TLS relaxation and phonon absorption times can now be calculated by Eqs. (4.50) and (4.51). Therefore, $C_t\tilde{\gamma}^2$ and $C_l\tilde{\gamma}^2$ can be calculated from unsaturated ultrasonic sound attenuation or sound velocity shift experiments. Once the values $C_t\tilde{\gamma}^2$ and $C_l\tilde{\gamma}^2$ are obtained, the ratio

$$\frac{4C_l}{C_t} = \frac{15}{\xi^2} - \frac{40}{\xi} + 32 \tag{4.61}$$

gives us the value of ξ, which further enables us to calculate ζ. If the value of $\tilde{\gamma}$ can be extracted from phonon echo experiments [31], then all the elements of the displacement potential tensor $[R]$ are known.

At the end of this section, we give a numerical example for the values of ξ and $P_0\tilde{\gamma}^2$. Black collected in Ref. [28] a range of values for $P_0\gamma_t^2$ and $P_0\gamma_l^2$ from various experiments. Unfortunately, few of the experiments provided data for both values at the same time. Nevertheless, two sets are given, the first one with $P_0\gamma_l^2 = 1.4 \times 10^7$ J/m^3 and $P_0\gamma_t^2 = 0.63 \times 10^7$ J/m^3 [29] and the second one with $P_0\gamma_l^2 = 2.0 \times 10^7$ J/m^3 and $P_0\gamma_t^2 = 0.89 \times 10^7$ J/m^3 [30]. Solving Eq. (4.61), we get two values of ξ for each set of data. For a better overview, we put the results into a table,

	Ref. [29]	Ref. [30]
$P_0\gamma_l^2$	1.4×10^7 J/m^3	2.0×10^7 J/m^3
$P_0\gamma_t^2$	0.63×10^7 J/m^3	0.89×10^7 J/m^3
ξ_1	0.55	0.55
$(P_0\tilde{\gamma}^2)_1$	7.8×10^7 J/m^3	11×10^7 J/m^3
ξ_2	1.2	1.2
$(P_0\tilde{\gamma}^2)_2$	1.7×10^7 J/m^3	2.4×10^7 J/m^3

Here the two values for ξ are denoted ξ_1 and ξ_2 and the according values for $P_0\tilde{\gamma}^2$ are marked by the same subscript. Remarkable is that although the values for $P_0\tilde{\gamma}^2$ are quite different for different experiments, the values for the parameter ξ are very similar. The reason for this is that the ratio $P_0\gamma_t^2/P_0\gamma_l^2$ does not change very much from one experiment to the other.

4.5.3 Membrane phonons

For the membrane geometry, the expressions $\langle|M_\mu|^2\rangle$ are considerably more difficult to calculate. Like in the case of 3D bulk systems, we assume a uniform distribution of the TLS orientations $\hat{\mathbf{t}}$ and average over them. We further assume a uniform spatial distribution of TLSs in the medium and average the expression $|M_\sigma|^2$ over the direction perpendicular to the membrane (here the z direction). This is a somewhat strong assumption, as one can easily imagine the TLS distribution to be a function of the distance from the sample surfaces, but taking this dependence into account would only add a numerical factor to the expressions for the scattering times, rather than qualitatively change the result. We give the expressions for $\langle|M_\mu|^2\rangle$ explicitly in Eqs. (B.4), (B.17) and (B.18) in Appendix B. Entering $\langle|M_\mu|^2\rangle$ into (4.52), we can in principle calculate the heat conductivity in an amorphous membrane. Due to the complexity of the expressions however, this is in general a numerical task. For the 2D limit, however, at temperatures far below the cross-over temperature T_C, we can derive an analytic expression.

Low temperature limit

We use the low-energy expansions (3.13), (3.15) and (3.17) for the lowest branch of the dispersion relation of each polarization and get for the scattering times in this limit

$$\tau_{h,0,k_\parallel} = \frac{\hbar\rho c_t^2}{\pi\tilde{\gamma}^2 P_0}\frac{1}{C_t}\frac{\coth(\beta\hbar\omega/2)}{\hbar\omega} \tag{4.62}$$

$$\tau_{s,0,k_\parallel} = \frac{\hbar\rho c_t^2}{\pi\tilde{\gamma}^2 P_0}\frac{1}{C_s}\frac{\coth(\beta\hbar\omega/2)}{\hbar\omega}\,. \tag{4.63}$$

$$\tau_{a,0,k_\parallel} = \frac{\hbar\rho c_t^2}{\pi\tilde{\gamma}^2 P_0}\frac{1}{C_a}\frac{\coth(\beta\hbar\omega/2)}{\hbar\omega}\,, \tag{4.64}$$

where the constants C_a and C_s are given by

$$\frac{1}{C_a} = \frac{1}{4C_s} = \frac{c_l^2(c_l^2-c_t^2)}{C_l c_t^4 + C_t c_l^2(c_l^2-2c_t^2)} \tag{4.65}$$

and C_t and C_l are given by the equations (4.57) and (4.58), respectively. Inserting these expressions into Eq. (4.52), we get an expression for the heat

conductivity in amorphous membranes at low temperatures ($T \ll T_C$),

$$\kappa = \frac{k_B \rho c_t^2}{16\pi d\tilde{\gamma}^2 P_0}\left(\frac{1}{C_t}+\frac{1}{C_s}+\frac{2}{C_a}\right)\left(\frac{k_B T}{\pi\hbar}\right)\int_0^\infty dx\,\frac{x^2\coth(x/2)}{\sinh^2(x/2)}\,. \quad (4.66)$$

Even though the dispersion relations for the s and the a modes have different $k_\parallel$ dependencies, their scattering rates have the same functional dependence, save for a factor of four. As also the expression $k_\parallel(\partial\omega/\partial k_\parallel) \propto \omega$ for the h, s and a mode, the integrand in Eq. (4.66) becomes common to all three modes. Apparently the heat conductivity κ is linear in T in the 2D limit, but the integral in Eq. (4.66) diverges, because the integrand becomes proportional to $1/x$ for $x \ll 1$. Since this is an unphysical result, we have to analyse the problem further.

First we note that the primitive of the integrand in (4.66),

$$\begin{aligned} I(x) &\equiv \int dx\,\frac{x^2\coth(x/2)}{\sinh^2(x/2)} \\ &= -\frac{x^2}{\sinh^2(x/2)} - 4x\coth(x/2) + 8\ln(\sinh(x/2))\,, \end{aligned} \quad (4.67)$$

has a logarithmic divergence in $x = 0$. Hence, as already stated, κ is divergent as well. This could explain the apparent radiative nature of the heat transport in SiN_x membranes, that is observed in some experiments [7, 19].

On the other hand, there are several reasons for which the heat conductivity could be finite in some membranes. One is that the phonons may scatter on other defects or impurities besides the TLSs. Another possible mechanism is roughness-induced scattering against the membrane surfaces. If we denote the partial mean free path that results from scattering on the TLSs by $l^{\mathrm{TLS}}_{\sigma,0,k_\parallel}$ and the one resulting from all other scattering mechanisms by $l^{\mathrm{imp}}_{\sigma,0,k_\parallel}$, the total mean free path is given by

$$\frac{1}{l^{\mathrm{tot}}_{\sigma,0,k_\parallel}} = \frac{1}{l^{\mathrm{TLS}}_{\sigma,0,k_\parallel}} + \frac{1}{l^{\mathrm{imp}}_{\sigma,0,k_\parallel}}\,. \quad (4.68)$$

Using the definition of the mean free path, $l = v\tau$, where v is the phonon group velocity, we can rewrite Eq. (4.52) as

$$\kappa = \frac{\hbar^2}{16\pi k_B T^2}\sum_\sigma \int_0^\infty d\omega\,\frac{k_{\parallel,\sigma,0}(\omega) l^{\mathrm{tot}}_{\sigma,0,k_\parallel}\omega^2}{\sinh^2(\beta\hbar\omega/2)}\,. \quad (4.69)$$

In the following discussion we will restrict ourselves to a simplified model, where $l^{\mathrm{imp}}_{\sigma,0,k_\parallel}$ in Eq. (4.68) is replaced by some $k_\parallel$-independent cut-off l^c_σ. If

$l^{\rm TLS}_{\sigma,0,k_\parallel} \gg l^c_\sigma$, the scattering at the cut-off dominates and $l^{\rm tot}_{\sigma,0,k_\parallel} = l^c_\sigma$ is a good approximation. Then the heat conductivity (4.69) becomes

$$\begin{aligned}\kappa &= \frac{k_B}{16\pi\hbar^2}\left[12\Gamma(3)\zeta(3)\left(\frac{l^c_h}{c_t}+\frac{l^c_s}{c_s}\right)(k_BT)^2\right.\\ &\qquad\left.+\,10\Gamma\left(\frac{5}{2}\right)\zeta\left(\frac{5}{2}\right)l^c_a\sqrt{2m^\star}(k_BT)^{3/2}\right]. \qquad (4.70)\end{aligned}$$

This result is similar to Eq. (4.30), where we also assumed a constant mean free path. Since $l^{\rm TLS}_{\sigma,0,k_\parallel}$ increases with decreasing $k_\parallel$, we can find the cross-over frequencies $\omega^c_{\sigma,0} \ll k_BT/\hbar$ such that $l_{\sigma,0}(\omega^c_{\sigma,0}) = l^c_\sigma$. This provides us with a low frequency cut-off in Eq. (4.69) and the heat conductivity can be expressed as

$$\begin{aligned}\kappa &= \frac{\hbar^2}{16\pi k_BT^2}\sum_\sigma\left\{l^c_\sigma\int_0^{\omega^c_{\sigma,0}}d\omega\,\frac{k_{\parallel,\sigma,0}(\omega)\omega^2}{\sinh^2(\beta\hbar\omega/2)}\right.\\ &\qquad\left.+\int_{\omega^c_{\sigma,0}}^{\infty}d\omega\,\frac{k_{\parallel,\sigma,0}(\omega)l^{\rm TLS}_{\sigma,0,k_\parallel}\omega^2}{\sinh^2(\beta\hbar\omega/2)}\right\} \qquad (4.71)\end{aligned}$$

Because of the smallness of $\omega^c_{\sigma,0}$, we approximate

$$\int_0^{\omega^c_{\sigma,0}}d\omega\,\frac{(\beta\hbar\omega)^n}{\sinh^2(\beta\hbar\omega/2)} \approx 4\frac{(\beta\hbar\omega^c_{\sigma,0})^{n-1}}{n-1} \qquad (4.72)$$

and

$$\int_{\omega^c_{\sigma,0}}^{\infty}d\omega\,\frac{k_{\parallel,\sigma,0}(\omega)l^{\rm TLS}_{\sigma,0,k_\parallel}\omega^2}{\sinh^2(\beta\hbar\omega/2)} \approx 12\beta\hbar\omega^c_{\sigma,0} - 8\ln(\beta\hbar\omega^c_{\sigma,0})\,. \qquad (4.73)$$

For small enough $\omega^c_{\sigma,0}$, the integral (4.72) can be neglected compared to integral (4.73) and we can write Eq. 4.71 as

$$\begin{aligned}\kappa &= \frac{k_B\rho c_t^2}{4\pi d\tilde{\gamma}^2P_0}\left(\frac{k_BT}{\pi\hbar}\right)\left\{\frac{3\beta\hbar\omega^c_{h,0}-2\ln(\beta\hbar\omega^c_{h,0})}{C_h}\right.\\ &\qquad\left.+\frac{3\beta\hbar\omega^c_{s,0}-2\ln(\beta\hbar\omega^c_{s,0})}{C_s}+\frac{2(3\beta\hbar\omega^c_{a,0}-2\ln(\beta\hbar\omega^c_{a,0}))}{C_a}\right\}, \qquad (4.74)\end{aligned}$$

where the first, second and third terms in the curly brackets above respectively give the contributions of the h, s and a modes to the heat conductivity. Equation (4.74) leads to the temperature dependence $\kappa \propto T(a + b\ln(T))$. For a numerical estimate, we use the finite size of the membrane for the cut-off. Then the cut-off wave vectors are estimated as $2\pi/\sqrt{A}$, where A is the

area of the membrane, and the cut-off frequencies become $\omega^c_{h,0} = 2\pi c_t/\sqrt{A}$, $\omega_{s,0} = 2\pi c_s/\sqrt{A}$ and $\omega_{a,0} = (\hbar/2m^\star)(2\pi)^2/A$. Typical experimental values are $T = 0.1$ K, $A = 400 \times 400$ μm^2 and $d = 200$ nm. The bulk sound velocities in SiN_x are $c_t = 6200$ m/s and $c_l = 10300$ m/s. With these values we get $\ln(\beta\hbar\omega^c_{h,0}) \approx -4.9$, $\ln(\beta\hbar\omega^c_{s,0}) \approx -4.4$ and $\ln(\beta\hbar\omega^c_{a,0}) \approx -11.4$, but since $C_a = 4C_s$, the contributions of all the phonon polarizations to the heat conductivity are of the same order.

Another crucial factor in the calculation of the heat conductivity is the TLS distribution $P(\epsilon, u)$ that enters the expressions for the phonon relaxation times (4.51). Following the STM, we assumed that the TLS distribution has the form (4.34). This may however change in the presence of boundaries. If for example an extra energy dependence is introduced, i.e. $P'(\epsilon, u) = P'_0/(\epsilon^\alpha u\sqrt{1-u^2})$, with $\alpha > 0$, an extra factor x^α would enter the integral in Eq. (4.66) and the divergence would disappear, leaving κ proportional to $T^{1+\alpha}$, even if no additional scattering mechanisms would be considered.

Comparison of the scattering rates and mean free paths

As already remarked, the scattering times for the low energy s and the a phonons are connected by the simple relation $\tau_{s,0,k_\parallel} = 4\tau_{a,0,k_\parallel}$, in other words, the scattering rate for the s phonons is 4 times smaller than the scattering rate of the a phonons.

To compare the the scattering rates for the a and the h phonons, we write the ratio of the scattering rates $\tau_{a,0,k_\parallel}$ and $\tau_{h,0,k_\parallel}$,

$$\begin{aligned}\frac{\tau_{h,0,k_\parallel}}{\tau_{a,0,k_\parallel}} &= \frac{C_l c_t^4 + C_t c_l^2(c_l^2 - 2c_t^2)}{C_t c_l^2(c_l^2 - c_t^2)} \\ &= 1 - (c_t/c_l)^2 \frac{1 - (C_l/C_t)(c_t/c_l)^2}{1 - (c_t/c_l)^2}\,. \end{aligned} \tag{4.75}$$

We know from Eq. (2.14) that in any normal material (i.e. with positive Poisson ratio), the ratio c_t^2/c_l^2 is restricted to $0 < c_t^2/c_l^2 \leq 1/2$ and for C_l/C_t we have from Eq. (4.61) $C_l/C_t \geq 4/3$.

A plot of the ratio $\tau_{h,0,k_\parallel}/\tau_{a,0,k_\parallel}$ as function of c_t^2/c_l^2 for different values of C_l/C_t is shown in Fig. 4.6. In the limit $c_t^2/c_l^2 \to 0$, $\tau_{h,0,k_\parallel}/\tau_{a,0,k_\parallel} = 1$, independent of the value for C_l/C_t. Increasing $(c_t/c_l)^2$ will result in a decrease of $\tau_{h,0,k_\parallel}/\tau_{a,0,k_\parallel}$, until a minimum is reached at $(c_t/c_l)^2 = 1 - \sqrt{1-(C_l/C_t)^{-1}}$, which lies between 0 and 1/2. Afterwards $\tau_{h,0,k_\parallel}/\tau_{a,0,k_\parallel}$ increases monotonically until it reaches the value $(C_l/C_t)/2$ for $(c_t/c_l)^2 = 1/2$. As $\tau_{h,0,k_\parallel}/\tau_{a,0,k_\parallel}$ increases monotonically with C_l/C_t, we conclude that $\tau_{h,0,k_\parallel} < \tau_{a,0,k_\parallel}$ for any c_t/c_l, as long as $C_l/C_t < 2$. For $C_l/C_t \geq 2$, $\tau_{h,0,k_\parallel}$ can be either smaller or greater than $\tau_{a,0,k_\parallel}$, depending on whether $(c_t/c_l)^2$

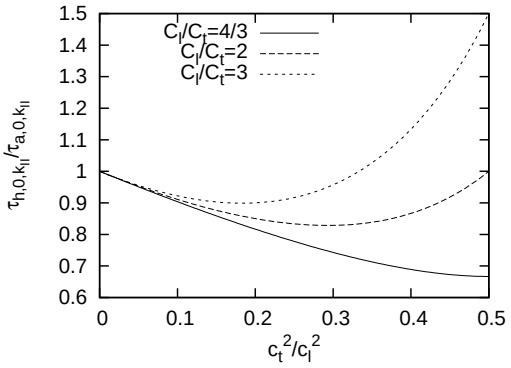

Figure 4.6: The ratios $\tau_{h,0,k_\parallel}/\tau_{a,0,k_\parallel}$ (left) and $\tau_{h,0,k_\parallel}/\tau_{s,0,k_\parallel}$ (right) as function of the ratio c_t^2/c_l^2.

is smaller or greater than C_t/C_l, respectively. A typical value for $(c_t/c_l)^2$ in SiN_x is 0.36, which means that $\tau_{h,0,k_\parallel} < \tau_{a,0,k_\parallel}$ as long as C_l/C_t is smaller than 2.78.

When comparing the scattering rates of the s and the h phonons, we encounter a similar situation. As $\tau_{s,0,k_\parallel} = 4\tau_{a,0,k_\parallel}$ the ratio $\tau_{h,0,k_\parallel}/\tau_{s,0,k_\parallel}$ has the same features as the ratio $\tau_{h,0,k_\parallel}/\tau_{a,0,k_\parallel}$, except for the fact that the critical value for C_l/C_t is 8, i.e. $\tau_{h,0,k_\parallel}$ is always smaller than $\tau_{s,0,k_\parallel}$, if $C_l/C_t < 8$, and can be either smaller or greater than $\tau_{s,0,k_\parallel}$ for $C_l/C_t \geq 8$. For the SiN_x typical value, $(c_t/c_l)^2 = 0.36$, we have $\tau_{h,0,k_\parallel} \leq \tau_{s,0,k_\parallel}$ as long as $C_l/C_t \leq 17.6$.

More interesting than the scattering rates, is to compare the phonon mean free paths, since these can be directly measured experimentally. A straightforward way to determine the mean free path of phonons is to measure the attenuation of ultrasound, propagating along the membrane. We use the dispersion relations (3.13), (3.15) and (3.17) and the identity $l_\mu = (d\omega_\mu/dk_\parallel)\tau_\mu$ to write the expressions for the mean free paths,

$$l_{h,0,k_\parallel} = \frac{\hbar\rho c_t^3}{\pi\tilde{\gamma}^2 P_0}\frac{1}{C_t}\frac{\coth(\beta\hbar\omega/2)}{\hbar\omega} \tag{4.76}$$

$$l_{s,0,k_\parallel} = \frac{\hbar\rho c_t^3}{\pi\tilde{\gamma}^2 P_0}\frac{2\sqrt{1-c_t^2/c_l^2}}{C_s}\frac{\coth(\beta\hbar\omega/2)}{\hbar\omega} \tag{4.77}$$

$$l_{a,0,k_\parallel} = \frac{\hbar\rho c_t^3}{\pi\tilde{\gamma}^2 P_0}\frac{2(1-c_t^2/c_l^2)^{1/4}}{3^{1/4}C_a}\sqrt{\frac{\omega d}{c_t}}\frac{\coth(\beta\hbar\omega/2)}{\hbar\omega} \tag{4.78}$$

If the elastic modes of different polarizations are produced with the same ω, then we can directly compare the mean free paths as given by the expressions (4.76), (4.77), and (4.78). To indicate that the angular frequency is the same in all expressions, we change the notation to $l_{\sigma,0,\omega}$.

$l_{h,0,\omega}/l_{s,0,\omega} = (\tau_{h,0,\omega}/\tau_{s,0,\omega})(c_t/c_s)$ for instance is smaller than $(\tau_{h,0,\omega}/\tau_{s,0,\omega})$ in any material. The discussion we made above about $\tau_{h,0,\omega}/\tau_{s,0,\omega}$ applies here, too. The ratios $l_{a,0,\omega}/l_{h,0,\omega}$ and $l_{a,0,\omega}/l_{s,0,\omega}$ are both proportional to $\sqrt{\omega}$, which means that for low enough frequencies, the antisymmetric Lamb modes have the shortest mean free path as function of frequency. This is a consequence of the fact that the group velocity of the a modes decreases to zero, as $k_\parallel$ decreases.

Next we compare the mean free paths as functions of $k_\parallel$. For this we rewrite Eqs. (4.76), (4.77), and (4.78) as

$$l_{h,0,k_\parallel} = \frac{\hbar\rho c_t^2}{\pi\tilde{\gamma}^2 P_0}\frac{1}{C_t}\frac{\coth(\beta\hbar c_t k_\parallel/2)}{\hbar k_\parallel}\,, \tag{4.79}$$

$$l_{s,0,k_\parallel} = \frac{\hbar\rho c_t^2}{\pi\tilde{\gamma}^2 P_0}\frac{1}{C_s}\frac{\coth(\beta\hbar c_s k_\parallel/2)}{\hbar k_\parallel}\,, \tag{4.80}$$

$$l_{a,0,k_\parallel} = \frac{\hbar\rho c_t^2}{\pi\tilde{\gamma}^2 P_0}\frac{2}{C_a}\frac{\coth\left(\frac{\beta\hbar d c_t}{2\sqrt{3}}\sqrt{1-c_t^2/c_l^2}k_\parallel^2\right)}{\hbar k_\parallel}\,. \tag{4.81}$$

First we compare again the mean free paths of the h and s phonons. There we have $l_{h,0,k_\parallel}/l_{s,0,k_\parallel} = (\tau_{h,0,k_\parallel}/\tau_{s,0,k_\parallel}) \times (\coth(\beta\hbar c_t k_\parallel/2)/\coth(\beta\hbar c_s k_\parallel/2))$, which is bigger than $\tau_{h,0,k_\parallel}/\tau_{s,0,k_\parallel}$, since $c_t < c_s$ implies $\coth(\beta\hbar c_t k_\parallel/2) > \coth(\beta\hbar c_s k_\parallel/2)$.

If we compare $l_{a,0,k_\parallel}$ with the expressions (4.79) and (4.80), we get $l_{a,0,k_\parallel}/l_{\sigma,0,k_\parallel} \propto \coth(\beta\hbar^2 k_\parallel^2/4m^\star)/\coth(\beta\hbar c_\sigma k_\parallel/2)$, with $\sigma = h$ or s. For small enough values of $k_\parallel$ this expression becomes proportional to $1/k_\parallel$, so as function of $k_\parallel$ the a phonons have the longest mean free path.

Chapter 5

An example of application: the TES

Superconducting transition-edge sensors (TES) are frequently used as microcalorimeters and microbolometers. Their trademarks are a very high energy resolution, low noise, high speed and the wide frequency range they can be operated in. To achieve an even better performance, the TESs are often mounted on a thin dielectric membrane. In this chapter we will show that the TES parameters are very sensitive functions of the operating temperature and the membrane thickness and can thus be optimized through careful tuning of the setup.

5.1 Introduction

A micro- (or quantum) calorimeter is a device that measures the energy of single photons. If the calorimeter is hit by a photon, its temperature increases, which enables us to determine the energy of the absorbed photon. A microbolometer is basically the same device, but instead of detecting single photons, it rather measures the power of a flux of photons that hit the detector in rapid succession.

Figure 5.1 shows a very simple schematic diagram of a microcalorimeter. The detector is weakly coupled to a heat bath (the substrate), which is held at temperature T_S. Due to the measurement and other effects, like for instance background radiation, there is a constant power flow P_{in} into the detector and through the weak link to the substrate there is a power flow P_{out} out of the detector. In steady state $P_{\text{in}} = P_{\text{out}}$ and the detector stays at the temperature T_D, which is higher than T_S. If a photon of energy E_γ is absorbed by the detector, its temperature rises by $\Delta T = E_\gamma / C$, where C is the heat capacity of the detector. By measuring the temperature rise ΔT, the photon energy can be determined.

A TES is a superconducting metal film that is biased at its supercon-

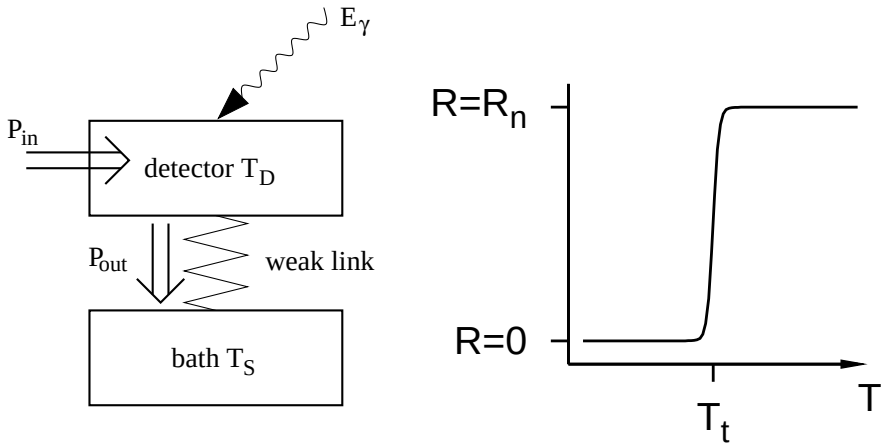

Figure 5.1: Left: Schematic diagram of the functionality of a microcalorimeter. The detector is coupled through a weak thermal link to the heat bath. In steady state, the input and output powers are equal ($P_{\rm in} = P_{\rm out}$) and the detector has the temperature T_D. If a photon of energy E_γ hits the detector, its temperature rises by $\Delta T = E_\gamma/C$ and the energy of the photon can be determined. Right: Schematic plot of the transition of a superconducting film. In the superconducting state, the resistance of the film is zero, in the normal state it is R_n. The transition happens in a very small temperature range around the transition temperature T_t.

ducting transition. There the electrical resistance of the metal is a very strong function of the temperature. In Fig. 5.1 we show a schematic plot of the TES resistance as function of temperature. In the superconducting state, where its temperature is smaller than the transition temperature T_t, the electrical resistance is zero. In the normal metal state, where $T > T_t$, the electrical resistance is almost constant $R = R_n > 0$. The transition between the two states happens in a very small temperature interval around T_t. As a measure of the sharpness of the transition, we define the parameter α, which is the logarithmic slope of the TES resistance $R(T)$,

$$\alpha \equiv \frac{d\ln(R)}{d\ln(T)} = \frac{T}{R}\frac{dR}{dT}. \tag{5.1}$$

By voltage biasing the detector, the TES is stabilized at the steady state temperature T_D. The input power $P_{\rm in}$ due to the bias is given by

$$P_{\rm in} = \frac{V^2}{R(T)}. \tag{5.2}$$

When a photon is absorbed by the detector, the temperature and thus $R(T)$ rise, effectively decreasing $P_{\rm in}$. This in turn results in a cool down of the detector until the steady state temperature T_D is reached. This way a

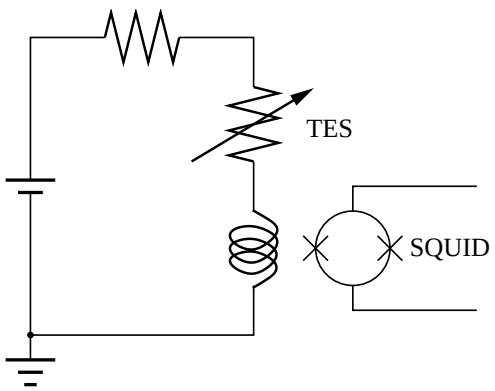

Figure 5.2: Voltage biased TES with a SQUID ammeter for signal read-out.

current pulse is generated in the circuit, which is measured with a sensitive SQUID ammeter [32]. The pulse height is a measure of the photon energy E_γ. Figure 5.2 shows a simplified version of the TES bias and read out circuit.

The effective time constant $\tau_{\rm eff}$ is a measure of how quickly a detector returns to steady state after an absorption event. To determine $\tau_{\rm eff}$, we write the thermal equation for the detector [33]

$$C\dot{T}(t) \;=\; P_{\rm in} - P_{\rm out} + E_\gamma \delta(t - t_\gamma)\,, \tag{5.3}$$

where by the δ-function we indicate the photon absorption event. To solve this differential equation, we linearize it by expanding the time dependent detector temperature $T(t)$ to first order around the steady state temperature T_D, i.e. $T(t) = T_D + \Delta T(t)$. Then Eq. (5.3) becomes

$$\begin{aligned} C\Delta\dot{T}(t) \;&=\; P_{\rm in}(T_D) - P_{\rm out}(T_D) \\ &\quad + \left(\frac{dP_{\rm in}}{dT}(T_D) - \frac{dP_{\rm out}}{dT}(T_D)\right)\Delta T(t) + E_\gamma\delta(t-t_\gamma) \end{aligned} \tag{5.4}$$

From the discussion above we know that the steady state powers in the first line of Eq. (5.4) cancel each other out. With Eqs. (5.2) and (5.1) we can rewrite Eq. (5.4) as

$$\Delta\dot{T}(t) \;=\; -\left(\alpha\frac{P_{\rm out}(T_D)}{CT_D} + \frac{g_{\rm out}(T_D)}{C}\right)\Delta T(t) + E_\gamma\delta(t-t_\gamma)\,, \tag{5.5}$$

where we used the usual definition of the thermal conductance, $g = dP/dT$ and the steady state condition $P_{\rm in}(T_D) = P_{\rm out}(T_D)$. Equation (5.5) is easily

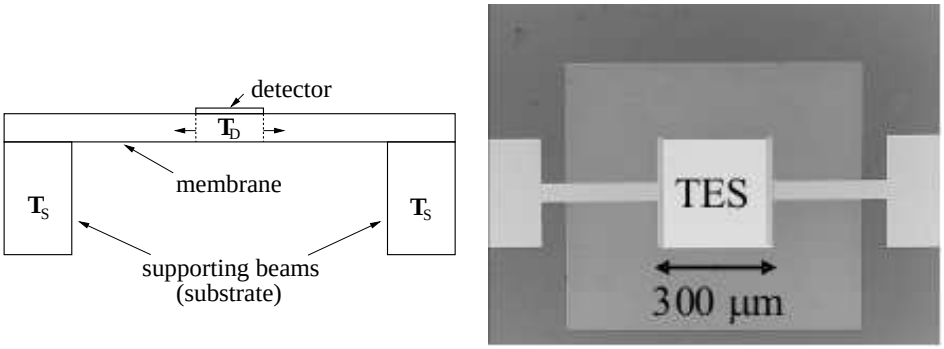

Figure 5.3: Left: Basic TES detector setup. The TES is carried by a thin dielectric membrane (usually amorphous low-stress SiN_x), which is itself supported by thicker beams (usually crystalline silicon). Right: Picture of a typical TES (sample by Antti Nuottajärvi, picture by Kimmo Kinnunen)

solvable. The result is an exponentially decaying function with the effective time constant

$$\tau_{\text{eff}} = \frac{C/g_{\text{out}}(T_D)}{1+\alpha\frac{P_{\text{out}}(T_D)}{T_D g_{\text{out}}(T_D)}}\,. \tag{5.6}$$

Note that without the temperature dependent input power, the time constant would only be given by $\tau_{\text{eff}} = \tau_0 \equiv C/g_{\text{out}}$ [33] and the detector cool down could only be sped up by increasing the heat conductance into the substrate. But this would also affect other parameters of the detector. For example the thermal noise in the detector increases with g_{out}. Through the voltage bias of the detector, we gain the additional variable α. By manipulating α, τ_{eff} can be decreased to a much smaller value. The thermal noise on the other hand is independent of α, allowing for an over all better detector performance.

In the next section we will calculate the operating parameters of the TES for the case in which it is mounted on a thin membrane.

5.2 Membrane mounted TES

In many applications, the TES detector is mounted on a thin dielectric membrane, which is connected to the substrate (see Fig. 5.3). Making the assumptions of Section 4.2, i.e. assuming radiative heat transfer and a thermal distribution of the phonons that are emitted by the detector, we can give numerical values of the detector parameters for different combinations of detector and substrate temperatures, membrane thickness and the parameter α.

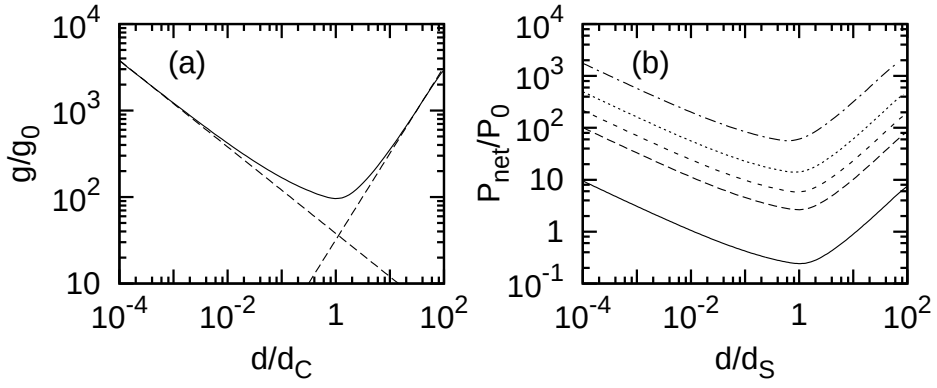

Figure 5.4: (a) Heat conductance as function of the membrane thickness in a system where membrane phonons are ballistically radiated from a hot spot. The normalization constant g_0 is given by $g_0 \equiv (k_B l c_t/8\pi^2)(k_B T/\hbar c_t)^2$. (b) Net cooling power of the detector as function of the membrane thickness for $T_D/T_S = 1.01$, 1.1, 1.2, 1.4 and 2.0, where curves with higher T_D/T_S lie above the curves with lower T_D/T_S. The position of the minimum slightly shifts with T_D/T_S. The normalization constant is $P_0 \equiv (\hbar l c_t^2/2\pi)(k_B T_S/\hbar c_t)^3$

5.2.1 Conductance

As the radiative heat conductance enters many of the following expressions directly, we will give an explicit expression. Using Eq. (4.11) and the definition of conductance, $g = dP/dT$, we have

$$g(T) \;=\; \frac{l}{8\pi^2}\frac{1}{k_B T^2}\sum_{\sigma,m}\int_0^\infty dk_\parallel \left|\frac{\partial\omega_\mu}{\partial k_\parallel}\right| \frac{k_\parallel(\hbar\omega_\mu)^2}{\sinh^2(\beta\hbar\omega_\mu)}\,. \tag{5.7}$$

In Fig. 5.4a we plot the conductance as function of the membrane thickness. It behaves qualitatively similar to the radiated phonon power, i.e. it is proportional to the membrane thickness d in the 3D limit, has a minimum at about $d_C = \hbar c_t/2k_B T$ and is proportional to $1/\sqrt{d}$ in the 2D limit.

5.2.2 Net power

In Section 4.2 we only considered phononic heat flow out of the detector. In a more realistic situation, there will also be phononic heat flow into the detector, originating from other radiators and/or the background. For our simple model, we only consider the radiation that comes from the substrate. Then the net phononic cooling power of the detector is given as

$$P_{\rm net} \;=\; P(T_D) - P(T_S)\,, \tag{5.8}$$

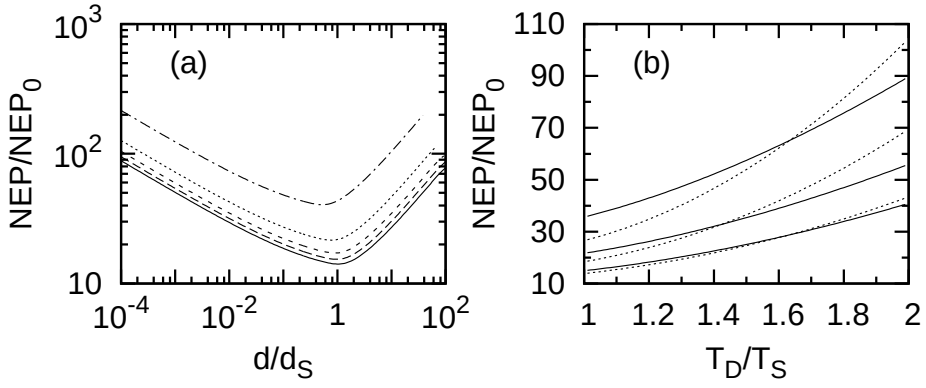

Figure 5.5: Phonon NEP (a) as function of membrane thickness for the ratios $T_D/T_S = 1.0$, 1.1, 1.2, 1.4 and 2.0, ordered from bottom to top and (b) as function of T_D/T_S for the values $d/d_S = 0.004$, 0.04 and 0.4 (solid lines, ordered top to bottom) and $d/d_S = 1$, 4 and 40 (dotted lines, ordered bottom to top). In other words, the solid curves in (b) lie left of the minimum in (a) and the dotted curves in (b) lie right of the minimum in (a). The normalization constant is $\mathrm{NEP}_0 \equiv \sqrt{l/c_t}(k_B T_S)^2/(2\pi\hbar)$

where we used the definition (4.11) for the expressions $P(T)$. As the temperatures of the detector and the substrate are in general different, the phonon distributions of the detector and the substrate also have different cross-over thicknesses d_C. In the following we will base all discussion on the cross-over thickness of the substrate phonons. To emphasize this, we denote this quantity by d_S,

$$d_S \;=\; \frac{\hbar c_t}{2k_B T_S}\,. \tag{5.9}$$

The minimum of P_{net} is no longer fixed to one value, but depends on the ratio T_D/T_S. In Fig. 5.4b we plot P_{net} for different values of T_D/T_S. The higher T_D gets compared to T_S, the more the minimum is shifted to smaller values of d.

5.2.3 Noise equivalent power

The noise equivalent power (NEP) tells how strong a signal has to be in order to stand out from the noise in the detector and thus be measurable. Conduction of heat causes energy fluctuations and thus gives a contribution to the NEP of the detector. As we consider two phonon sources, the detector and the substrate, we have two terms entering the phonon NEP, the first is caused by the phonon flow out of the detector at temperature T_D into the substrate and the second is caused by the reverse process. The phonon NEP

is then given by [34, 35]

$$\mathrm{NEP}_{\mathrm{ph}} = \sqrt{2k_B(T_D^2 g(T_D) + T_S^2 g(T_S))}\,. \tag{5.10}$$

Different NEP terms are combined by the relation $\mathrm{NEP}_{\mathrm{tot}}^2 = \mathrm{NEP}_1^2 + \mathrm{NEP}_2^2 + \ldots$.

With the help of Eq. (5.7), we can calculate the phonon NEP that is caused in the membrane. In Fig. 5.5 we show the NEP as function of membrane thickness as well as function of the ratio T_D/T_S. As function of thickness the NEP has unsurprisingly a minimum at about d_S, just like the conductance itself. Like in the case of the net cooling power, the position of the minimum shifts slightly with T_D/T_S. The asymptotic behaviours are $\mathrm{NEP} \propto \sqrt{d}$ in the 3D limit ($d \gg d_S$) and $\mathrm{NEP} \propto 1/d^{1/4}$ in the 2D limit ($d \ll d_S$).

As function of T_D/T_S, the NEP does not follow a power law, as the second term in Eq. (5.10) is held constant. However, if the first term in (5.10) dominates, the NEP becomes roughly proportional to $T_D^{5/2}$ in the 3D limit and in the 2D limit to $\sqrt{AT_D^{7/2} + BT_D^4}$, where A and B are constants. Note that if we aim at a specific NEP for a given ratio of T_D/T_S, we have always two membrane thicknesses to choose from when designing the detector.

5.2.4 Effective time constant

The effective time constant τ_{eff} has been given in Eq. (5.6). In Fig. 5.6a we plot τ_{eff} as function of membrane thickness. Contrary to all other detector parameters, τ_{eff} has a maximum at the cross-over thickness d_S and decreases for both $d > d_S$ and $d < d_S$. This means that there will always be a trade-off between detector speed and signal quality. However, as discussed in Section 5.1, the effective time constant can also be modified with the help of the parameter α, which is an attribute of the superconducting metal film alone, not of the underlying membrane. The behaviour of τ_{eff} far away from the cross-over region is described by $\tau_{\mathrm{eff}} \propto \sqrt{d}$ in the 2D limit and $\tau_{\mathrm{eff}} \propto 1/d$ in the 3D limit.

5.2.5 Energy resolution

The energy resolution tells how much two detected signals must be separated in energy to be recognized as absorbed photons of different energies. The optimal obtainable spectral peak has a Gaussian shape [32] and we use the width of this optimal Gaussian at half its maximum height (FWHM) as measure of the energy resolution. ΔE_{FWHM} is given as [32]

$$\Delta E_{\mathrm{FWHM}} = 2\sqrt{2\ln(2)}\sqrt{k_B T_D^2 C_{\mathrm{el}}}\frac{2}{\sqrt{\alpha_{\mathrm{I}}}}\left(\frac{\mathrm{NEP}^2}{4k_B T_D P_{\mathrm{net}}}\right)^{1/4}, \tag{5.11}$$

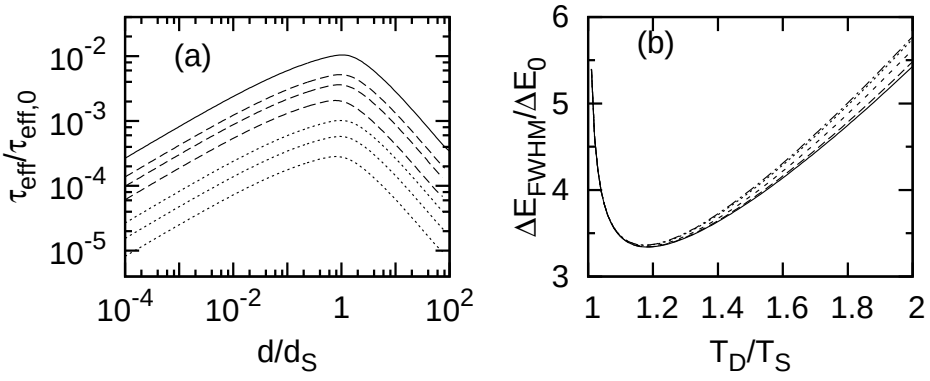

Figure 5.6: a) Effective time constant τ_{eff} as function of the membrane thickness for $\alpha = 0$ and/or $T_D = T_S$ (solid curve), $\alpha = 10$ (dashed curves) and $\alpha = 100$ (dotted curves), for the values $T_D/T_S = 1.1$, 1.2 and 1.5, the curves with greater T_D/T_S lie below the curves with smaller T_D/T_S. b) Energy resolution ΔE_{FWHM} of the detector as function of the ratio T_D/T_S for $d/d_S = 0.04$, 0.4, 1, 4 and 40, ordered bottom to top. It is immediately visible that ΔE_{FWHM} is a weak function of the membrane thickness. As function of T_D/T_S there is a pronounced minimum between 1.1 and 1.2.

where α_{I} is, contrary to Eq. (5.1), a partial derivative, $\alpha_{\text{I}} = \partial \ln(R)/\partial \ln(T)$. We take only the phonon noise into account, and use Eq. (5.10) for a numerical treatment. In Fig. 5.6b we show ΔE_{FWHM} as function of the ratio T_D/T_S. It has a pronounced minimum between 1.1 and 1.2, similar to the 3D case [36]. The exact place of the minimum depends on the membrane thickness. As function of the membrane thickness, ΔE_{FWHM} does not change very significantly, which means that we can optimize the membrane thickness either for low noise or fast read-out, without having to care much about the energy resolution, which in turn is tuned with the parameter T_D/T_S.

Chapter 6

Summary

After a short introduction to elasticity theory in Chapter 2, we introduced the acoustics eigenmodes of thin membranes in Chapter 3. These modes are called horizontal shear and Lamb waves and are superpositions of transversal and longitudinal 3D bulk plane waves. As the partial waves of these superpositions have different sound velocities, the resulting waves have non-linear dispersion relations, which are, due to the finite thickness of the membrane, split into branches. In general these dispersion relations can only be calculated numerically, but in the low frequency limit analytical expression can be derived. In Section 3.3 we proved that the given modes form a complete, orthonormal set of functions, which is essential for a correct quantum mechanical description. We then formally quantized the elastic field of the membrane. We show that the horizontal shear modes together with the Lamb modes form a complete set of functions for the displacement field in the membrane. Using this set, we then write the elastic Hamiltonian of the membrane as a sum of harmonic oscillators, which are the phonon modes of the membrane.

In Chapter 4, we investigated the thermal properties of thin dielectric membranes. As the dispersion relations of the membrane phonons are split into branches, the phonon gas becomes two dimensional below the cross-over condition $Td \approx \hbar c_t/2k_B$. This dimensionality cross-over becomes visible through a change in the temperature dependence of quantities like the heat capacity and conductance of the membrane. In the low temperature limit we found that the heat capacity becomes linear in T. We also found that the same quantities do not become independent of the membrane thickness in the 2D limit. Instead the heat capacity and conductance have a global minimum in the cross-over region and increase afterwards as $d^{-1/2}$.

In Sections 4.2 to 4.5 we discussed the heat transfer in the membrane in the ballistic as well as in the diffusive limit. For the ballistic case the radiated power of an emitting source becomes proportional to $T^{5/2}$ at very low temperatures. For the diffusive case we treated two different scattering

mechanisms. In Section 4.4 we considered a setup where the membrane is cut in such a way that a wider central part is supported by long narrow bridges. The heat conductivity along these bridges is dominated by the phonon scattering at the edges of the bridge and is in the low temperature limit proportional to $T^{3/2}$. Together with the temperature dependence of the heat capacity in this limit, the AC heating cut-off frequency $f_c \propto \kappa/c_V$ becomes proportional to $T^{1/2}$, which qualitatively agrees with the experiment.

In Section 4.5 we investigated the heat transfer in amorphous membranes. There the phonons are scattered by two-level systems (TLS). To be able to carry out this discussion, we had to generalize the interaction Hamiltonian of the standard tunneling model (STM), as there only plane wave phonons are treated. With this generalized Hamiltonian we were able to show that 3D longitudinal phonons are scattered stronger by TLSs than transversal phonons, which agrees with the experiment. For the membrane phonons it turned out that TLSs are inefficient phonon scatterers at low temperatures. The phonon mean free path is thus limited by other defects and impurities or the finite size of the membrane. The latter case might indicate that the heat transfer in the membrane is indeed ballistic.

In Chapter 5 we calculate how the operating parameters of a membrane mounted transition-edge sensor (TES) depend on the operating temperature and membrane thickness. While the effective time constant and the noise-equivalent power (NEP) are strong functions of the membrane thickness, with a global maximum or minimum, respectively, the energy resolution is almost unaffected by the choice of the membrane thickness. Instead it can be optimized by tuning the detector temperature relative to the substrate temperature. It is therefore possible to find an optimal combination of membrane thickness and detector and substrate temperatures for both calorimeter and bolometer applications.

Appendix A

Normalization constants of the Lamb modes

We calculate the normalization constants of the Lamb modes of Section 3.1, applying the norm (3.20) to the expressions of the Lamb modes, (3.11) and (3.12). We use the general wave vector components $\bar{k}_t = k_t + i\kappa_t$ and $\bar{k}_l = k_l + i\kappa_l$, where $k_{t,l}$ and $\kappa_{t,l}$ are real and positive. Furthermore we demand a real $k_\parallel$, which results in both $\bar{k}_t$ and $\bar{k}_l$ being either real or imaginary, i.e. if for example $k_t > 0$, $\kappa_t = 0$ and vice versa.

For the s mode we have

$$1 = \int_{-\infty}^{\infty} d\mathbf{r}\, |\mathbf{u}_s|^2 \tag{A.1}$$

$$= AN_s^2 \int_{-\infty}^{\infty} dz \Big(|\bar{k}_t|^2 \left| 2k_\parallel^2 \cos(\bar{k}_t d/2)\cos(\bar{k}_l z) + (\bar{k}_t^2 - k_\parallel^2)\cos(\bar{k}_l d/2)\cos(\bar{k}_t z) \right|^2 + k_\parallel^2 \left| 2\bar{k}_l \bar{k}_t \cos(\bar{k}_t d/2)\cos(\bar{k}_l z) - (\bar{k}_t^2 - k_\parallel^2)\cos(\bar{k}_l d/2)\cos(\bar{k}_t z) \right|^2 \Big) \tag{A.2}$$

$$\begin{aligned} = {} & AN_s^2 4|\bar{k}_t|^2 k_\parallel^2 |\cos(\bar{k}_t d/2)|^2 \Big((|\bar{k}_l|^2 + k_\parallel^2)\frac{\sinh(\kappa_l d)}{2\kappa_l} - (|\bar{k}_l|^2 - k_\parallel^2)\frac{\sin(k_l d)}{2k_l} \Big) \\ & + |\bar{k}_t^2 - k_\parallel^2|^2 |\cos(\bar{k}_l d/2)|^2 \Big((|\bar{k}_t|^2 + k_\parallel^2)\frac{\sinh(\kappa_t d)}{2\kappa_t} + (|\bar{k}_t|^2 - k_\parallel^2)\frac{\sin(k_t d)}{2k_t} \Big) \\ & + 4\bar{k}_t k_\parallel^2 ((\bar{k}_t^\star)^2 - k_\parallel^2) |\cos(\bar{k}_l d/2)|^2 \cos(\bar{k}_t d/2)\sin(\bar{k}_t^\star d/2) \\ & + 4\bar{k}_t^\star k_\parallel^2 (\bar{k}_t^2 - k_\parallel^2) |\cos(\bar{k}_l d/2)|^2 \cos(\bar{k}_t^\star d/2)\sin(\bar{k}_t d/2)\,. \end{aligned} \tag{A.3}$$

In step (A.2) we calculated the trivial integral over the x and y directions, assuming that the membrane is of rectangular shape with the area $A = l_x \times l_y$. Combining the last two lines of (A.3), we arrive at

$$\frac{1}{N_s^2} = A \Big\{ 4|\bar{k}_t|^2 k_\parallel^2 |\cos(\bar{k}_t d/2)|^2 \Big((|\bar{k}_l|^2 + k_\parallel^2)\frac{\sinh(\kappa_l d)}{2\kappa_l} - (|\bar{k}_l|^2 - k_\parallel^2)\frac{\sin(k_l d)}{2k_l} \Big)$$

$$+|\bar{k}_t^2 - k_\parallel^2|^2|\cos(\bar{k}_l d/2)|^2\Big((|\bar{k}_t|^2 + k_\parallel^2)\frac{\sinh(\kappa_t d)}{2\kappa_t} + (|\bar{k}_t|^2 - k_\parallel^2)\frac{\sin(k_t d)}{2k_t}\Big)$$
$$-4k_\parallel^2|\cos(\bar{k}_l d/2)|^2\Big(\kappa_t(|\bar{k}_t|^2 + k_\parallel^2)\sinh(\kappa_t d) - k_t(|\bar{k}_t|^2 - k_\parallel^2)\sin(k_t d)\Big)\Big\}\,. \tag{A.4}$$

Similarly we get for the a modes

$$\frac{1}{N_a^2} = A\Big\{4|\bar{k}_t|^2 k_\parallel^2|\sin(\bar{k}_t d/2)|^2\Big((|\bar{k}_l|^2 + k_\parallel^2)\frac{\sinh(\kappa_l d)}{2\kappa_l} + (|\bar{k}_l|^2 - k_\parallel^2)\frac{\sin(k_l d)}{2k_l}\Big)$$
$$+|\bar{k}_t^2 - k_\parallel^2|^2|\sin(\bar{k}_l d/2)|^2\Big((|\bar{k}_t|^2 + k_\parallel^2)\frac{\sinh(\kappa_t d)}{2\kappa_t} - (|\bar{k}_t|^2 - k_\parallel^2)\frac{\sin(k_t d)}{2k_t}\Big)$$
$$-4k_\parallel^2|\sin(\bar{k}_l d/2)|^2\Big(\kappa_t(|\bar{k}_t|^2 + k_\parallel^2)\sinh(\kappa_t d) + k_t(|\bar{k}_t|^2 - k_\parallel^2)\sin(k_t d)\Big)\Big\}\,. \tag{A.5}$$

These are the general normalization constants for complex $\bar{k}_t$ and $\bar{k}_l$ and real $k_\parallel$. From expressions (A.4) and (A.5) one can obtain the normalization constants in each quadrant of Fig. 3.4 by taking the limit of the redundant components of $\overline{k}_t$ and $\overline{k}_l$ being zero. As this might not be very clear, we will give the normalization constants for the three relevant quadrants defined in Section 3.1.

In the first quadrant both $\bar{k}_t$ and $\bar{k}_l$ are real, which means that we have to take the limits $\kappa_t \to 0$ and $\kappa_l \to 0$ in the expressions for the normalization constants. This results in the expressions

$$\begin{aligned}\frac{1}{(N_s^I)^2} &= A\Big\{4k_t^2k_\parallel^2\cos^2(k_t d/2)\Big((k_l^2 + k_\parallel^2)\frac{d}{2} - (k_l^2 - k_\parallel^2)\frac{\sin(k_l d)}{2k_l}\Big)\\ &\quad +(k_t^2 - k_\parallel^2)^2\cos^2(k_l d/2)\Big((k_t^2 + k_\parallel^2)\frac{d}{2} + (k_t^2 - k_\parallel^2)\frac{\sin(k_t d)}{2k_t}\Big)\\ &\quad +4k_t k_\parallel^2(k_t^2 - k_\parallel^2)\cos^2(k_l d/2)\sin(k_t d)\Big\} \qquad \text{(A.6)}\\ \frac{1}{(N_a^I)^2} &= A\Big\{4k_t^2k_\parallel^2\sin^2(k_t d/2)\Big((k_l^2 + k_\parallel^2)\frac{d}{2} + (k_l^2 - k_\parallel^2)\frac{\sin(k_l d)}{2k_l}\Big)\\ &\quad +(k_t^2 - k_\parallel^2)^2\sin^2(k_l d/2)\Big((k_t^2 + k_\parallel^2)\frac{d}{2} - (k_t^2 - k_\parallel^2)\frac{\sin(k_t d)}{2k_t}\Big)\\ &\quad -4k_t k_\parallel^2(k_t^2 - k_\parallel^2)\sin^2(k_l d/2)\sin(k_t d)\Big\}\,. \qquad \text{(A.7)}\end{aligned}$$

Note that the expressions of the type $\sin(\kappa_x d)/(2\kappa_x)$ go to $d/2$ in the limit of $\kappa_x \to 0$. For the second quadrant, where $\bar{k}_t$ is real and $\bar{k}_l$ is imaginary, we get

$$\frac{1}{(N_s^{II})^2} = A\Big\{4k_t^2k_\parallel^2\cos^2(k_t d/2)\Big((\kappa_l^2 + k_\parallel^2)\frac{\sinh(\kappa_l d)}{2\kappa_l} - (\kappa_l^2 - k_\parallel^2)\frac{d}{2}\Big)$$

$$
\begin{aligned}
&+(k_t^2-k_\parallel^2)^2\cosh^2(\kappa_l d/2)\left((k_t^2+k_\parallel^2)\frac{d}{2}+(k_t^2-k_\parallel^2)\frac{\sin(k_t d)}{2k_t}\right)\\
&+4k_t k_\parallel^2(k_t^2-k_\parallel^2)\cosh^2(\kappa_l d/2)\sin(k_t d)\Big\} \qquad \text{(A.8)}\\
\frac{1}{(N_a^{II})^2} &= A\Big\{4k_t^2k_\parallel^2\sin^2(k_t d/2)\left((\kappa_l^2+k_\parallel^2)\frac{\sinh(\kappa_l d)}{2\kappa_l}+(\kappa_l^2-k_\parallel^2)\frac{d}{2}\right)\\
&+(k_t^2-k_\parallel^2)^2\sinh^2(\kappa_l d/2)\left((k_t^2+k_\parallel^2)\frac{d}{2}-(k_t^2-k_\parallel^2)\frac{\sin(k_t d)}{2k_t}\right)\\
&-4k_t k_\parallel^2(k_t^2-k_\parallel^2)\sinh^2(\kappa_l d/2)\sin(k_t d)\Big\}\,. \qquad \text{(A.9)}
\end{aligned}
$$

Here the trigonometric functions have been replaced by hyperbolic functions, if they had an imaginary argument. In the third quadrant both $\bar{k}_t$ and $\bar{k}_l$ are imaginary. Then we get for the normalization constants

$$
\begin{aligned}
\frac{1}{(N_s^{III})^2} &= A\Big\{4\kappa_t^2k_\parallel^2\cosh^2(\kappa_t d/2)\left((\kappa_l^2+k_\parallel^2)\frac{\sinh(\kappa_l d)}{2\kappa_l}-(\kappa_l^2-k_\parallel^2)\frac{d}{2}\right)\\
&+(\kappa_t^2+k_\parallel^2)^2\cosh^2(\kappa_l d/2)\left((\kappa_t^2+k_\parallel^2)\frac{\sinh(\kappa_t d)}{2\kappa_t}+(\kappa_t^2-k_\parallel^2)\frac{d}{2}\right)\\
&-4k_\parallel^2\cosh^2(\kappa_l d/2)\left(\kappa_t(-\kappa_t^2+k_\parallel^2)\sinh(\kappa_t d)\right)\Big\} \qquad \text{(A.10)}\\
\frac{1}{(N_a^{III})^2} &= A\Big\{4\kappa_t^2k_\parallel^2\sinh^2(\kappa_t d/2)\left((\kappa_l^2+k_\parallel^2)\frac{\sinh(\kappa_l d)}{2\kappa_l}+(\kappa_l^2-k_\parallel^2)\frac{d}{2}\right)\\
&+(\kappa_t^2+k_\parallel^2)^2\sinh^2(\kappa_l d/2)\left((\kappa_t^2+k_\parallel^2)\frac{\sinh(\kappa_t d)}{2\kappa_t}-(\kappa_t^2-k_\parallel^2)\frac{d}{2}\right)\\
&-4k_\parallel^2\sinh^2(\kappa_l d/2)\left(\kappa_t(\kappa_t^2+k_\parallel^2)\sinh(\kappa_t d)\right)\Big\}\,. \qquad \text{(A.11)}
\end{aligned}
$$

Appendix B

Expressions for $\langle |M|^2 \rangle$

In Section 4.5.3 we discuss the interaction between the TLSs and the phonon modes of thin membranes. The coupling is basically described by the quantities $M_\mu = \mathbf{T}^T \cdot [R] \cdot \mathbf{S}$, where $\mu = \sigma, m, \mathbf{k}_\parallel$. In this appendix we show details of the calculations of $\langle |M_\mu|^2 \rangle$, where the brackets $\langle \cdot \rangle$ indicate an average over the TLS orientations $\hat{\mathbf{t}}$ and the z coordinate. For simplicity we assume in this appendix that the phonons propagate along the x direction.

B.1 h modes

The strain of the h modes is given by $\mathbf{S}_h = (0, 0, 0, S_4, 0, S_6)^T$, with

$$S_4 = N_h i k_\parallel \cos(k_h(z - d/2)), \tag{B.1}$$

$$S_6 = -N_h k_h \sin(k_h(z - d/2)), \tag{B.2}$$

where we omitted the x and t dependence of the mode for brevity. With this, M_h becomes

$$M_h = 2N_h \xi (i t_y t_z k_\parallel \cos(k_h(z - d/2)) - t_x t_y k_h \sin(k_h(z - d/2))), \tag{B.3}$$

where we further omitted the quantum numbers m and $\mathbf{k}_\parallel$ in the subscript of $\langle |M_\mu|^2 \rangle$. Averaging over the TLS directions $\hat{\mathbf{t}}$ and the z-coordinate, we arrive at the expression for $\langle |M_h|^2 \rangle$,

$$\langle |M_h|^2 \rangle = \frac{C_t}{V}(k_\parallel^2 + k_h^2), \tag{B.4}$$

where C_t was defined in Eq. (4.57).

B.2 Lamb modes

The strain fields of the Lamb modes have the form $\mathbf{S} = (S_1, 0, S_3, 0, S_5, 0)^T$, with

$$S_1 = -N_s \bar{k}_t k_\parallel \left(2k_\parallel^2 \cos(\bar{k}_t d/2) \cos(\bar{k}_l z) + (\bar{k}_t^2 - k_\parallel^2) \cos(\bar{k}_l d/2) \cos(\bar{k}_t z)\right), \tag{B.5}$$

$$S_3 = N_s \bar{k}_t k_\parallel \left(-2\bar{k}_l^2 \cos(\bar{k}_t d/2)\cos(\bar{k}_l z) + (\bar{k}_t^2 - k_\parallel^2)\cos(\bar{k}_l d/2)\cos(\bar{k}_t z)\right), \quad \text{(B.6)}$$

$$S_5 = -iN_s \left(4\bar{k}_t \bar{k}_l k_\parallel^2 \cos(\bar{k}_t d/2)\sin(\bar{k}_l z) + (\bar{k}_t^2 - k_\parallel^2)^2 \cos(\bar{k}_l d/2)\sin(\bar{k}_t z)\right) \quad \text{(B.7)}$$

for the s modes and

$$S_1 = N_a \bar{k}_t k_\parallel \left(2k_\parallel^2 \sin(\bar{k}_t d/2)\sin(\bar{k}_l z) + (\bar{k}_t^2 - k_\parallel^2)\sin(\bar{k}_l d/2)\sin(\bar{k}_t z)\right), \quad \text{(B.8)}$$

$$S_3 = N_a \bar{k}_t k_\parallel \left(2\bar{k}_l^2 \sin(\bar{k}_t d/2)\sin(\bar{k}_l z) - (\bar{k}_t^2 - k_\parallel^2)\sin(\bar{k}_l d/2)\sin(\bar{k}_t z)\right), \quad \text{(B.9)}$$

$$S_5 = -iN_a \left(4\bar{k}_t \bar{k}_l k_\parallel^2 \sin(\bar{k}_t d/2)\cos(\bar{k}_l z) + (\bar{k}_t^2 - k_\parallel^2)^2 \sin(\bar{k}_l d/2)\cos(\bar{k}_t z)\right) \quad \text{(B.10)}$$

for the a modes. For both, the s and the a modes, M_μ has the form

$$M_{s,a} \;=\; (1 - 2\xi(1-t_x^2))S_1 + (1 - 2\xi(1-t_z^2))S_3 + 2\xi t_x t_z S_5\,, \quad \text{(B.11)}$$

from which we get

$$\begin{aligned} M_s \;=\; & -N_s \Big\{ \bar{k}_t k_\parallel (\bar{k}_t^2 - k_\parallel^2)\cos(\bar{k}_l d/2)\cos(\bar{k}_t z) 2\xi(t_x^2 - t_z^2) \\ & + 2\bar{k}_t k_\parallel \cos(\bar{k}_t d/2)\cos(\bar{k}_l z)(k_\parallel^2(1 - 2\xi(1-t_x^2)) + \bar{k}_l^2(1 - 2\xi(1-t_z^2))) \\ & + 4i\bar{k}_t \bar{k}_l k_\parallel^2 \cos(\bar{k}_t d/2)\sin(\bar{k}_l z) 2\xi t_x t_z \\ & + i(\bar{k}_t^2 - k_\parallel^2)^2 \cos(\bar{k}_l d/2)\sin(\bar{k}_t z) 2\xi t_x t_z\,, \end{aligned} \quad \text{(B.12)}$$

$$\begin{aligned} M_a \;=\; & N_a \Big\{ \bar{k}_t k_\parallel (\bar{k}_t^2 - k_\parallel^2)\sin(\bar{k}_l d/2)\sin(\bar{k}_t z) 2\xi(t_x^2 - t_z^2) \\ & + 2\bar{k}_t k_\parallel \sin(\bar{k}_t d/2)\sin(\bar{k}_l z)(k_\parallel^2(1 - 2\xi(1-t_x^2)) + \bar{k}_l^2(1 - 2\xi(1-t_z^2))) \\ & - 4i\bar{k}_t \bar{k}_l k_\parallel^2 \sin(\bar{k}_t d/2)\cos(\bar{k}_l z) 2\xi t_x t_z \\ & - i(\bar{k}_t^2 - k_\parallel^2)^2 \sin(\bar{k}_l d/2)\cos(\bar{k}_t z) 2\xi t_x t_z \Big\}\,. \end{aligned} \quad \text{(B.13)}$$

Taking the absolute square of Eq. (B.11) and averaging over $\hat{\mathbf{t}}$, we get

$$\langle |M_{s,a}|^2 \rangle_{\hat{\mathbf{t}}} \;=\; C_l |S_1 + S_3|^2 + C_t(|S_5|^2 - 2(S_1 \bar{S}_3 + \bar{S}_1 S_3))\,, \quad \text{(B.14)}$$

where by the subscript $\hat{\mathbf{t}}$ we indicate that expression (B.14) is not yet averaged over the z direction. The constants C_t and C_l are given in Eqs. (4.57) and (4.58), respectively. The average over the z direction has to be done separately for each mode. For the s mode we get

$$\begin{aligned} \frac{\langle |M_s|^2 \rangle}{N_s^2} \;=\; & \frac{C_l}{d} 4|\bar{k}_t|^2 k^2 |k^2 + \bar{k}_l^2|^2 |\cos(\bar{k}_t d/2)|^2 \left(\frac{\sinh(\kappa_l d)}{2\kappa_l} + \frac{\sin(k_l d)}{2k_l}\right) \\ & + \frac{C_t}{d} \Big\{ 16|\bar{k}_t|^2 k^4 |\cos(\bar{k}_t d/2)|^2 (\kappa_l \sinh(\kappa_l d) - k_l \sin(k_l d)) \\ & + |\bar{k}_t^2 - k^2|^2 |\cos(\bar{k}_l d/2)|^2 \left(((|\bar{k}_t|^2 + k^2)^2 + 4\kappa_t^2 k^2) \frac{\sinh(\kappa_t d)}{2\kappa_t} \right. \\ & \left. - ((|\bar{k}_t|^2 - k^2)^2 - 4k_t^2 k^2) \frac{\sin(k_t d)}{2k_t} \right) \end{aligned}$$

$$
\begin{aligned}
&-8|\bar{k}_t|^2\bar{k}_l k^2((\bar{k}_t^\star)^2-k^2)|\cos(\bar{k}_t d/2)|^2\cos(\bar{k}_l^\star d/2)\sin(\bar{k}_l d/2)\\
&+8\bar{k}_t k^4((\bar{k}_t^\star)^2-k^2)|\cos(\bar{k}_l d/2)|^2\cos(\bar{k}_t d/2)\sin(\bar{k}_t^\star d/2)\\
&-8|\bar{k}_t|^2\bar{k}_l^\star k^2(\bar{k}_t^2-k^2)|\cos(\bar{k}_t d/2)|^2\cos(\bar{k}_l d/2)\sin(\bar{k}_l^\star d/2)\\
&+8\bar{k}_t^\star k^4(\bar{k}_t^2-k^2)|\cos(\bar{k}_l d/2)|^2\cos(\bar{k}_t^\star d/2)\sin(\bar{k}_t d/2)\ \}\ , \qquad \text{(B.15)}
\end{aligned}
$$

which after some manipulation becomes

$$
\begin{aligned}
\frac{\langle|M_s|^2\rangle}{N_s^2} \;=\;& \frac{C_l}{d}4|\bar{k}_t|^2k^2|k^2+\bar{k}_l^2|^2|\cos(\bar{k}_t d/2)|^2\left(\frac{\sinh(\kappa_l d)}{2\kappa_l}+\frac{\sin(k_l d)}{2k_l}\right)\\
&+\frac{C_t}{d}|\bar{k}_t^2-k^2|^2|\cos(\bar{k}_l d/2)|^2\\
&\quad\times\left((|\bar{k}_t|^2+k^2)^2\frac{\sinh(\kappa_t d)}{2\kappa_t}-(|\bar{k}_t|^2-k^2)^2\frac{\sin(k_t d)}{2k_t}\right)\\
&+\frac{C_t}{d}\Big\{2\bar{k}_t k^2|\bar{k}_t^2-k^2|^2|\cos(\bar{k}_l d/2)|^2\cos(\bar{k}_t d/2)\sin(\bar{k}_t^\star d/2)\\
&\quad+2\bar{k}_t^\star k^2|\bar{k}_t^2-k^2|^2|\cos(\bar{k}_l d/2)|^2\cos(\bar{k}_t^\star d/2)\sin(\bar{k}_t d/2)\\
&\quad-8|\bar{k}_t|^2\bar{k}_l k^2((\bar{k}_t^\star)^2+k^2)|\cos(\bar{k}_t d/2)|^2\cos(\bar{k}_l^\star d/2)\sin(\bar{k}_l d/2)\\
&\quad-8|\bar{k}_t|^2\bar{k}_l^\star k^2(\bar{k}_t^2+k^2)|\cos(\bar{k}_t d/2)|^2\cos(\bar{k}_l d/2)\sin(\bar{k}_l^\star d/2)\\
&\quad+8\bar{k}_t k^4((\bar{k}_t^\star)^2-k^2)|\cos(\bar{k}_l d/2)|^2\cos(\bar{k}_t d/2)\sin(\bar{k}_t^\star d/2)\\
&\quad+8\bar{k}_t^\star k^4(\bar{k}_t^2-k^2)|\cos(\bar{k}_l d/2)|^2\cos(\bar{k}_t^\star d/2)\sin(\bar{k}_t d/2)\ \Big\}\,. \qquad \text{(B.16)}
\end{aligned}
$$

Applying the dispersion relation (3.7) to the sixth and seventh line and doing some more simplifications, we finally arrive at

$$
\begin{aligned}
\langle|M_s|^2\rangle \;=\;& \frac{N_s^2}{d}\Big\{4C_l|\bar{k}_t|^2k_\parallel^2|k_\parallel^2+\bar{k}_l^2|^2|\cos(\bar{k}_t d/2)|^2\left(\frac{\sinh(\kappa_l d)}{2\kappa_l}+\frac{\sin(k_l d)}{2k_l}\right)\\
&+C_t|\bar{k}_t^2-k_\parallel^2|^2|\cos(\bar{k}_l d/2)|^2\left((|\bar{k}_t|^2+k_\parallel^2)^2\frac{\sinh(\kappa_t d)}{2\kappa_t}-(|\bar{k}_t|^2-k_\parallel^2)^2\frac{\sin(k_t d)}{2k_t}\right)\\
&-2C_t k_t(2k_\parallel^6-k_\parallel^4k_t^2-k_t^6)|\cos(\bar{k}_l d/2)|^2\sin(k_t d)\\
&-2C_t\kappa_t(2k_\parallel^6+k_\parallel^4\kappa_t^2+\kappa_t^6)\cos(\bar{k}_l d/2)|^2\sinh(\kappa_t d)\ \Big\}\,. \qquad \text{(B.17)}
\end{aligned}
$$

For the a modes, a similar calculation leads to

$$
\begin{aligned}
\langle|M_a|^2\rangle \;=\;& \frac{N_a^2}{d}\Big\{4C_l|\bar{k}_t|^2k_\parallel^2|k_\parallel^2+\bar{k}_l^2|^2|\sin(\bar{k}_t d/2)|^2\left(\frac{\sinh(\kappa_l d)}{2\kappa_l}-\frac{\sin(k_l d)}{2k_l}\right)\\
&+C_t|\bar{k}_t^2-k_\parallel^2|^2|\sin(\bar{k}_l d/2)|^2\left((|\bar{k}_t|^2+k_\parallel^2)^2\frac{\sinh(\kappa_t d)}{2\kappa_t}+(|\bar{k}_t|^2-k_\parallel^2)^2\frac{\sin(k_t d)}{2k_t}\right)\\
&-2C_t k_t(-2k_\parallel^6+k_\parallel^4k_t^2+k_t^6)|\sin(\bar{k}_l d/2)|^2\sin(k_t d)\\
&-2C_t\kappa_t(2k_\parallel^6+k_\parallel^4\kappa_t^2+\kappa_t^6)|\sin(\bar{k}_l d/2)|^2\sinh(\kappa_t d)\ \Big\}\,. \qquad \text{(B.18)}
\end{aligned}
$$

Like in the case of the normalization constants for the Lamb modes, to obtain the expressions of $\langle|M_{s,a}|^2\rangle$ for the different quadrants defined in

Section 3.1, one has to take the limit to zero of the vanishing components of $\bar{k}_t$ and $\bar{k}_l$. How this is done is explained in Appendix A.

Appendix C

Properties of the matrix $[R]$

In Section 4.5 we generalize the standard model of TLS-phonon interaction by taking the orientation of the TLS relative to the phonon polarization and wave vector explicitly into account. In this generalization, the coupling of a phonon to a TLS is basically given by the scalar $h_1 = \mathbf{T}^T \cdot [R] \cdot \mathbf{S}$. If we assume that the material we consider is isotropic both in the macroscopic scale and the microscopic scale that is defined by the size of the TLS, h_1 becomes invariant under coordinate rotations. In this appendix we use this invariance of h_1 to derive the properties of the matrix $[R]$ with the help of some simple transformations.

Let us start with assuming that S_4 is the only non-zero strain component, while the TLS is oriented along the x direction, which means that $h_1 = R_{14} t_x^2 S_4$. Rotating the coordinate system through π about the z axis will result in $S_4' = -S_4$, while $\mathbf{T}$ remains unchanged. Hence, $h_1' = -R_{14} t_x^2 S_4$ can only be equal to h_1 if $R_{14} = 0$. Similar rotations about the other axes, with properly chosen $\mathbf{T}$ and $\mathbf{S}$ will lead to

$$R_{IJ} \;=\; 0 \quad \text{for any} \quad I = 1,2,3 \quad \text{and} \quad J = 4,5,6\,, \tag{C.1}$$

and $[R]$ has now the form

$$[R] = \begin{pmatrix} R_{11} & R_{12} & R_{13} & 0 & 0 & 0 \\ R_{21} & R_{22} & R_{23} & 0 & 0 & 0 \\ R_{31} & R_{32} & R_{33} & 0 & 0 & 0 \\ R_{41} & R_{42} & R_{43} & R_{44} & R_{45} & R_{46} \\ R_{51} & R_{52} & R_{53} & R_{54} & R_{55} & R_{56} \\ R_{61} & R_{62} & R_{62} & R_{64} & R_{65} & R_{66} \end{pmatrix}. \tag{C.2}$$

Next, we shall let S_1 be the only non-zero strain component and $\mathbf{T} = (0, t_y^2, t_z^2, 2t_y t_z, 0, 0)^T$. Then we get that $h_1 = S_1(R_{21} t_y^2 + R_{31} t_z^2 + R_{41} 2 t_y t_z)$. Again we rotate the system through π about the z axis. Here, S_1 and t_z are invariant to the rotation, while $t_y' = -t_y$, which leads to $h_1' = S_1(R_{21} t_y^2 +$

$R_{31}t_z^2 - R_{41}2t_yt_z$). Then $h_1' = h_1$ implies that $R_{41} = 0$. Again, by performing similar coordinate rotations about the other axes one can show that

$$R_{IJ} \;=\; 0 \quad \text{for any} \quad I = 4,5,6 \quad \text{and} \quad J = 1,2,3\,. \tag{C.3}$$

This leaves $[R]$ block-diagonal,

$$[R] = \begin{pmatrix} R_{11} & R_{12} & R_{13} & 0 & 0 & 0 \\ R_{21} & R_{22} & R_{23} & 0 & 0 & 0 \\ R_{31} & R_{32} & R_{33} & 0 & 0 & 0 \\ 0 & 0 & 0 & R_{44} & R_{45} & R_{46} \\ 0 & 0 & 0 & R_{54} & R_{55} & R_{56} \\ 0 & 0 & 0 & R_{64} & R_{65} & R_{66} \end{pmatrix}, \tag{C.4}$$

but it can be simplified even further.

Now we assume that $\mathbf{T} = (0, t_y^2, t_z^2, 2t_yt_z, 0, 0)^T$, while of the strain vector components only S_5 is different from zero. A rotation through π about the x axis leaves $\mathbf{T}$ unchanged, while $S_5' = -S_5$. From the invariance of h_1 we get the equality $h_1' = -R_{45}2t_yt_zS_5 = R_{45}2t_yt_zS_5 = h_1$, which can only be fulfilled if $R_{45} = 0$. Similarly we get

$$R_{IJ} = 0 \quad \text{for any} \quad I,J = 4,5,6 \quad \text{if} \quad I \neq J \tag{C.5}$$

Furthermore, $[R]$ cannot depend on the notation of axes, which means that

$$\begin{array}{l} R_{11} = R_{22} = R_{33}, \\ R_{44} = R_{55} = R_{66}, \\ R_{12} = R_{13} = R_{23}, \\ R_{21} = R_{31} = R_{32}, \end{array}, \tag{C.6}$$

which leaves $[R]$ in the form

$$[R] = \begin{pmatrix} R_{11} & R_{12} & R_{12} & 0 & 0 & 0 \\ R_{21} & R_{11} & R_{12} & 0 & 0 & 0 \\ R_{21} & R_{21} & R_{11} & 0 & 0 & 0 \\ 0 & 0 & 0 & R_{44} & 0 & 0 \\ 0 & 0 & 0 & 0 & R_{44} & 0 \\ 0 & 0 & 0 & 0 & 0 & R_{44} \end{pmatrix}, \tag{C.7}$$

At the end, we are going to perform some arbitrary rotations on the system. From elasticity theory we know that arbitrary coordinate transformations can be performed directly in abbreviated subscript notation with the help of the Bond method for transforming stiffness and compliance [11]. According to this method, the vectors $\mathbf{S}$ and $\mathbf{T}$ transform under coordinate transformations as $\mathbf{S}' = [N] \cdot \mathbf{S}$ and $\mathbf{T}' = [N] \cdot \mathbf{T}$, where $[N]$ is the 6×6

component Bond strain transformation matrix. For a rotation about the z axis through an arbitrary angle α for instance, $[N]$ is

$$[N] = \begin{pmatrix} \cos^2(\alpha) & \sin^2(\alpha) & 0 & 0 & 0 & \sin(2\alpha)/2 \\ \sin^2(\alpha) & \cos^2(\alpha) & 0 & 0 & 0 & -\sin(2\alpha)/2 \\ 0 & 0 & 1 & 0 & 0 & 0 \\ 0 & 0 & 0 & \cos(\alpha) & -\sin(\alpha) & 0 \\ 0 & 0 & 0 & \sin(\alpha) & \cos(\alpha) & 0 \\ -\sin(2\alpha) & \sin(2\alpha) & 0 & 0 & 0 & \cos(2\alpha) \end{pmatrix}. \quad \text{(C.8)}$$

As in isotropic systems both h_1 and $[R]$ are invariant under rotations we have that $h_1 = \mathbf{T}^T \cdot [R] \cdot \mathbf{S} = \mathbf{T}^T \cdot [N]^T \cdot [R] \cdot [N] \cdot \mathbf{S}$, or

$$[R] \;=\; [N]^T \cdot [R] \cdot [N]\,. \quad \text{(C.9)}$$

Applying arbitrary rotations about each of the coordinate axes, we find that $R_{21} = R_{12} = R_{11} - 2R_{44}$. We thus define $R_{11} \equiv \tilde{\gamma}$, $R_{12} \equiv \tilde{\gamma}\xi$ and $R_{44} \equiv \tilde{\gamma}\zeta$ whereby $[R]$ becomes

$$\begin{aligned} [R] &= \tilde{\gamma}[r] \\ &\equiv \tilde{\gamma} \begin{pmatrix} 1 & \zeta & \zeta & 0 & 0 & 0 \\ \zeta & 1 & \zeta & 0 & 0 & 0 \\ \zeta & \zeta & 1 & 0 & 0 & 0 \\ 0 & 0 & 0 & \xi & 0 & 0 \\ 0 & 0 & 0 & 0 & \xi & 0 \\ 0 & 0 & 0 & 0 & 0 & \xi \end{pmatrix}, \end{aligned} \quad \text{(C.10)}$$

with $\zeta + 2\xi = 1$. This means that the matrix $[R]$ has the same functional form as the matrix of elastic stiffness constants $[c]$ for isotropic media.

Bibliography

[I] T. Kühn, D. V. Anghel, J. P. Pekola, M. Manninen, and Y. M. Galperin, *Heat transport in ultrathin dielectric membranes and bridges*, Phys. Rev. B, **70**, 125425 (2004).

[II] T. Kühn and I. J. Maasilta, *Ballistic phonon transport in dielectric membranes*, Nucl. Instr. and Meth. A **559**, 724 (2006).

[III] D. V. Anghel, T. Kühn, Y. M. Galperin, and M. Manninen, *Interaction of two-level systems in amorphous materials with arbitrary phonon fields*, Phys. Rev. B, **75**, 064202 (2007).

[IV] D. V. Anghel and T. Kühn, *Quantization of the elastic modes in an isotropic plate*, (submitted) cond-mat/0611528 (2006).

[V] T. Kühn, D. V. Anghel, and Y. M. Galperin, *Interaction of two-level systems with phonons in amorphous nanoscopic membranes*, (to be submitted) (2007).

[VI] T. Kühn and I. J. Maasilta, *Optimal operation of transition-edge sensors on ballistic membranes*, (submitted) cond-mat/0702542 (2007).

[1] D. V. Anghel, J. P. Pekola, M. M. Leivo, J. K. Suoknuuti, and M. Manninen, *Properties of the phonon gas in ultrathin membranes at low temperature*, Phys. Rev. Lett., **81**, 2958–2961 (1998).

[2] D. V. Anghel and M. Manninen, *Behavior of the phonon gas in restricted geometries*, Phys. Rev. B, **59**, 9854 (1999).

[3] M. Leivo, *On-chip Cooling by Quasiparticle Tunneling Below 1 Kelvin*, PhD thesis, University of Jyväskylä (1999),

[4] M. M. Leivo and J. P. Pekola, *Thermal characteristics of silicon nitride membranes at sub-kelvin temperatures*, Appl. Phys. Lett., **72**, 1305 (1998).

[5] W. Holmes, J. M. Gildemeister, P. L. Richards, and V. Kotsubo, *Measurements of thermal transport in low stress silicon nitride films*, Appl. Phys. Lett., **72**, 2250 (1998).

[6] A. L. Woodcraft, R. V. Sudiwalaa, E. Wakui, R. S. Bhatia, J. J. Bock, and A. D. Turner, *Thermal conductance measurements of a silicon nitride membrane at low temperatures*, Physica B: Cond. Matt., **284**, 1968 (2000).

[7] H. F. C. Hoevers, M. L. Ridder, A. Germeau, M. P. Bruijn, P. A. J. de Korte, and R. J. Wiegerink, *Radiative ballistic phonon transport in silicon-nitride membranes at low temperatures*, Appl. Phys. Lett., **86**, 251903 (2005).

[8] J. P. Pekola, A. J. Manninen, M. M. Leivo, K. Arutyunov, J. K. Suoknuuti, T. I. Suppula, and B. Collaudin, *Microrefrigeration by quasiparticle tunnelling in NIS and SIS junctions*, Physica B, **280**, 485 (2000).

[9] P. Esquinazi, *Tunneling systems in amorphous and crystalline solids*, Springer (1998).

[10] R. C. Zeller and R. O. Pohl, *Thermal conductivity and specific heat of noncrystalline solids*, Phys. Rev. B, **4**, 2029 (1971).

[11] B. A. Auld, *Acoustic Fields and Waves in Solids, 2nd Ed.*, Robert E. Krieger Publishing Company (1990).

[12] H. Ezawa, *Phonons in a half space*, Ann. Phys., NY, **67**, 438 (1971).

[13] L. D. Landau and E. M. Lifschitz, *Lehrbuch der theoretischen Physik – Band VII: Elastizitätstheorie*, Akademie-Verlag Berlin (1965).

[14] M. Grimsditch, R. Bhadra and Ivan K. Schuller, *Lamb Waves in Unsupported Thin Films: A Brilluin-Scattering Study*, Phys. Rev. Lett., **58**, 1216 (1987).

[15] T. Kühn, *Phonons in nanoscopic films*, masters thesis, University of Karlsruhe (2002).

[16] F. Riesz and B. Sz. Nagy, *Functional Analysis (Translated from the 2nd French edition by Leo F. Boron*, Dover Publication, inc. (1956).

[17] C. Kittel, *Introduction to Solid State Physics, 7th Ed.*, John Wiley and Sons, Inc. (1996).

[18] T. Fließbach, *Statistische Physik, Lehrbuch zur theoretischen Physik IV, 2. überarbeitete Auflage*, Spektrum Akademischer Verlag (1995).

[19] K. M. Kinnunen, J. T. Karvonen, and I. J. Maasilta, (unpublished results).

[20] Harald Ibach and Hans Lüth, *Solid-State physics, An Introduction to Principles of Materials Science, 2nd Ed.*, Springer (1995).

[21] R. Williams, *Modern GaAs Processing Methods, 2nd Ed.*, Artich House, Inc. (1990).

[22] W. A. Philips, *Tunneling states in amorphous solids*, J. Low Temp. Phys., **7**, 351 (1972).

[23] P. W. Anderson, B. I. Halperin, and C. M. Varma, *Anomalous low-temperature thermal properties of glasses and spin glasses*, Phil. Mag., **25**, 1 (1972).

[24] J. Jäckle, *On the ultrasonic attenuation in glasses at low temperatures*, Z. Phys., **257**, 212 (1972).

[25] A. J. Leggett, S. Chakravarty, A. T. Dorsey, Matthew P. A. Fisher, Anupam Garg, and W. Zwerger, *Dynamics of the dissipative two-state system*, Rev. Mod. Phys., **59**, 1–85 (1987).

[26] Yu. M. Galperin, V. G. Karpov, and V. I. Kozub, *Localized states in glasses*, Advances in Physics, **38**, 669 (1989).

[27] N. W. Ashcroft and N. D. Mermin, *Solid State Physics*, Harcourt College Publishers (1976).

[28] J. L. Black, *Relationship between the time-dependent specific heat and the ultrasonic properties of glasses at low temperatures*, Phys. Rev. B, **17**, 2740 (1978).

[29] Brage Golding, John E. Graebner, and R. J. Schutz, *Intrinsic decay lengths of quasimonochromatic phonons in a glass below 1 K*, Phys. Rev. B, **14**, 1660–1662 (1976).

[30] Brage Golding, John E. Graebner, and Anne B. Kane, *Phase velocity of high-frequency phonons in glass below 1 K*, Phys. Rev. Lett., **37**, 1248–1250, (1976).

[31] Brage Golding and John E. Graebner, *Phonon echoes in glass*, Phys. Rev. Lett., **37**, 852–855, (1976).

[32] C. Enss, editor, *Cryogenic Particle Detection*, Springer (2005).

[33] E. Figueroa-Feliciano, *Theory and Development of Position-sensitive Quantum Calorimeters*, PhD thesis, Stanford University (2001).

[34] W. S. Boyle and Jr. K. F. Rodgers, *Performance characteristics of a new low-temperature bolometer*, J. Opt. Soc. Am., **49**, 66, 1959.

[35] I. J. Maasilta, (unpublished results).

[36] I. J. Maasilta, *Optimizing the operating temperature of a transition edge sensor* Nucl. Instr. Meth. Phys. Res. A, **559**, 706 (2006).